Report USAFSAM TR-83-36

12

RADIOFREQUENCY RADIATION EFFECTS ON EXCITABLE TISSUES

Ronald L. Seaman, Ph.D.

Georgia Institute of Technology
Atlanta, Georgia 30332

Robert L. DeHaan, Ph.D.

Emory University School of Medicine
Atlanta, Georgia 30322

AD A137772

DTIC
ELECTE
D

November 1983

Final Report for Period 1 June 1981 - 30 October 1982

DTIC FILE COPY

REPORT DOCUMENTATION PAGE		READ INSTRUCTIONS BEFORE COMPLETING FORM
1. REPORT NUMBER USAFSAM-TR-83-36	2. GOVT ACCESSION NO. *A.*	3. RECIPIENT'S CATALOG NUMBER
4. TITLE *(and Subtitle)* RADIOFREQUENCY RADIATION EFFECTS ON EXCITABLE TISSUES		5. TYPE OF REPORT & PERIOD COVERED Final Report 1 June 1981 – 30 Oct 1982
		6. PERFORMING ORG. REPORT NUMBER A-2974
7. AUTHOR(s) Ronald L. Seaman, Ph.D. Robert L. DeHaan, Ph.D.*		8. CONTRACT OR GRANT NUMBER(s) F-33615-81-K-0618
9. PERFORMING ORGANIZATION NAME AND ADDRESS Biomedical Research Division Engineering Experiment Station Georgia Institute of Technology Atlanta, Georgia 30332		10. PROGRAM ELEMENT, PROJECT, TASK AREA & WORK UNIT NUMBERS 61102F 2312-V7-04
11. CONTROLLING OFFICE NAME AND ADDRESS USAF School of Aerospace Medicine (RZP) Aerospace Medical Division (AFSC) Brooks Air Force Base, Texas 78235		12. REPORT DATE November 1983
		13. NUMBER OF PAGES 108
14. MONITORING AGENCY NAME & ADDRESS(*if different from Controlling Office*)		15. SECURITY CLASS. *(of this report)* Unclassified
		15a. DECLASSIFICATION/DOWNGRADING SCHEDULE

16. DISTRIBUTION STATEMENT *(of this Report)*

Approved for public release; distribution unlimited

17. DISTRIBUTION STATEMENT *(of the abstract entered in Block 20, if different from Report)*

18. SUPPLEMENTARY NOTES

*Department of Anatomy
Emory University School of Medicine
Atlanta, Georgia 30322

19. KEY WORDS *(Continue on reverse side if necessary and identify by block number)*

Electromagnetic fields	Cardiac-cell aggregates
Continuous wave	Membrane voltage noise
Pulse-modulation	Membrane impedance
Excitable tissues	Open-ended coaxial exposure device

20. ABSTRACT *(Continue on reverse side if necessary and identify by block number)*

Spheroidal aggregates of cultured chick cardiac cells were used to study effects of 2450-MHz radiofrequency radiation (RFR) on excitable membranes. Membrane voltage noise was recorded simultaneously with two microelectrodes. Preparation bulk temperature was $37 \pm 0.2°C$, and temperature at the aggregate was less than $0.9°C$ above this during RFR exposures of 2- and 3-min durations. Specific absorption rate (SAR) was between 1 and 231 mW/g, and both continuous-wave (CW) and pulse-modulated (PW, 5 μs at 100 pps) RFR were applied

(cont'd)

DD $\begin{smallmatrix} \text{FORM} \\ \text{1 JAN 73} \end{smallmatrix}$ 1473   EDITION OF 1 NOV 65 IS OBSOLETE

20. ABSTRACT (continued)

using an open-ended coaxial exposure device. Membrane voltage fluctuations, in the form of "noise" and microspike events, and membrane impedance were observed before, during, and after RFR exposures. No RFR effect was seen on membrane impedance viewed as parallel resistance and capacitance. The relation of membrane voltage noise power (0.1-1.0 Hz) to membrane potential was significantly altered during the first half of 3-min exposures to 1-5 and 15-30 mW/g CW RFR. This was found by using two-tailed t-tests to test the difference in slopes between least-squares linear regression fits of data from different RFR conditions with the significance level set at P<0.05. Although microspikes seemed to contribute to this RFR effect on noise, there was no significant difference (two-tailed t-test, P<0.05) in frequency of occurrence of microspikes greater than 0.2 mV for any RFR exposure condition.

FOREWORD

Accession For	
NTIS GRA&I	☒
DTIC TAB	☐
Unannounced	☐
Justification	
By	
Distribution/	
Availability Codes	
Dist	Avail and/or Special
A/1	

1

TABLE OF CONTENTS

LIST OF FIGURES

3

4

RADIOFREQUENCY RADIATION EFFECTS ON EXCITABLE TISSUES

I. INTRODUCTION

A. Background

Over the past several decades, the use of radiofrequency radiation (RFR) for military, industrial, and consumer applications has increased dramatically. Because RFR can penetrate and heat tissue, the concern that this type of electromagnetic radiation might adversely affect biological systems has correspondingly increased. Animal research has conclusively shown various adverse effects with RFR exposure levels that are high enough to induce significant heat loads, but conflicting results are seen for lower exposure levels.

Interest in RFR effects on biological systems has existed for some time. In many cases, interest has focused on these effects on excitable tissues, namely, nerve and muscle. The normal function of these tissues involves changing electric fields and ionic currents which can be altered by applied static and slowly changing electric fields. It is conceivable that higher frequency fields, such as those associated with RFR, could also interact with the naturally occurring fields or the voltage-sensitive membrane components of these tissues. This section presents a brief review of the literature on RFR effects on nerve and cardiac muscle and of literature on other topics relevant to the subject of this report.

Some of the earlier research on cardiovascular effects was reported in the Soviet literature [28, pp. 117-122; 46, pp. 116-124] and reflected the researchers' emphasis on central nervous system (CNS) control of the cardiovascular system. In these studies, rabbits were exposed to pulsed and continuous wave (CW) 2400- or 3000-MHz radiation at incident power densities of 3-5 and 7-12 mW/cm^2. Small increases and decreases observed in heart rate depended on the body region exposed. Decreases in heart rate were attributed to stimulation of the peripheral nervous system because they were absent when exposed skin was anesthetized. Increases in heart rate were attributed to effects on the CNS and were dominant when only the head was exposed. It was also concluded that pulsed radiation had a stronger effect than did CW radiation.

These studies have been repeated using 2400-MHz CW and pulsed radiation [10,14,28]. With CW energy applied only to a rabbit's head, 10 mW/cm^2 incident power density did not significantly change the heart rate; only the highest level used, 100 mW/cm^2, effected an increase. With 20 mW/cm^2 applied to the entire dorsal surface of the rabbit, no difference in heart rate was seen. In fact, respiration rate was more sensitive than heart rate in these studies. These results led to the conclusion that previously reported changes in heart rate were most likely due to chance variations.

Isolated heart preparations have been used in attempts to delineate direct effects on cardiac tissue. For denervated frog hearts in an early Soviet study, heart rate did not change in response to an incident field of 0.06 mW/cm^2; exposure of intact frogs, however, produced effects similar to those that had been observed in rabbits [46, p. 122]. In a later study, 1425-MHz radiation pulsed at low repetition rates caused arrhythmias in isolated frog hearts but only when delivery was delayed until after the P wave of the electrocardiogram [25]. Pulses were delivered coincident with the P wave, 100 ms after the P wave, and 200 ms after the P wave. Arrhythmias were observed in 50% of the irradiated cases with the longer delay, a much higher incidence than for other cases. However, these effects were not seen when other investigators repeated the experiment [17,33].

Some interesting results have been obtained from isolated hearts wher 'W radiation at 960 MHz was applied with a capacitor irradiator. For t   le hearts, specific absorption rate (SAR) in the range of 2-10 mW/g cau   a decrease in heart rate, but larger SARs and generalized heating cause   an increase [34,53]. Results from drug studies suggested that the decreases   en at small SARs were due to neurotransmitter release from nerve remnants i   .' hearts. Similar decreases in heart rate have been found in isolated   . hearts for SARs of 1.3-2.1 mW/g [43,47], and drug studies again indicated an interaction with nerve remnants. These apparent interactions of low-level RFR with remnant nerve components suggested that other than purely thermal mechanisms were involved.

Other isolated preparations of excitable tissue have been used to try to identify mechanisms for RFR interaction with excitable membranes. Much of this work was triggered by early Russian investigations using frog sciatic nerves, which showed not only apparent increases in excitability and conduction velocity with RFR but differences in effects produced by CW and pulsed 2400-MHz RFR [27]. This research and related work has been reviewed recently [37;46, pp. 157-159]. Researchers conducting replicates of these experiments, using 2450-MHz RFR at SARs of 0.3-1500 mW/g CW and 0.3-220 mW/g pulsed RFR, attributed all effects to heating of the nerve [15]. With RFR typically applied for several minutes, other nerve and muscle preparations revealed no microwave effect beyond that of heating [15,20]. When RFR was applied longer than 20-30 min, however, an accelerated rundown of frog sciatic nerves was measured by decreased amplitude of the stimulated compound action potential [37]. The accelerated decrease in vitality seemed to be a RFR interaction with a Na-K pump since ouabain eliminated the microwave effect [38]. The threshold for this effect was between 5 and 10 mW/g, and the illustrated data indicate that the effect can occur without changes in conduction velocity.

Invertebrate neurons have also been studied to obtain information on RFR effects at the cellular level. In one preparation, Aplysia pacemaker neurons were exposed to 1500- and 2450-MHz RFR in a stripline exposure device, and their transmembrane potentials were recorded during exposure [49,54]. The firing rate both decreased and increased, with some changes occurring for SARs as low as 2 mW/g. Not all RFR-induced slow changes in firing rate were reproduced by warming the preparation; also, rapid changes, seen most often for pulsed RFR, were not reproduced by heating the preparation. These findings pointed to RFR processes other than thermal ones and to possible

8

different mechanisms operative for pulsed RFR. Helix neurons showed a 22% decrease in membrane resistance after an hour of exposure to 2450-MHz CW RFR at 15.5 mW/g SAR in a slotted line [2]. A study using the birefringence of crab nerve indicated larger and more persistent changes caused by pulsed RFR than by CW RFR or equivalent heating [11].

Several possible mechanisms have been proposed to explain RFR interaction with excitable membranes. Directly induced transmembrane potential has been estimated to be on the order of a few hundred microvolts in the CNS of animals exposed to an incident-field power density of 10 mW/cm^2 [35]. Rectification of induced microwave currents to produce effective direct currents has been proposed [54] and can be predicted on the basis of nonlinear conductance [4] or capacitance [8] in the membrane. Studies of Chara and Nitella plant cells have shown rectification for frequencies between 1 and 10 MHz [5,44], but at higher frequencies only a shift in potential presumed to be thermally induced [6,44]. These results are in good agreement with the prediction that rectification cannot be effective at frequencies above an estimated 32 MHz because of transit time effects, and that effects on individual membrane particles are probably more significant than rectification at higher frequencies [45]. Models of RFR effects on membranes include one based on the Hodgkin-Huxley equations [13] and one based on quantum mechanics [51].

With previous Air Force sponsorship, we studied the beat rates of individual heart cells [12,50]. The research reported here was an outgrowth of that program and used the same preparation, which is described in Section II. Briefly, clusters of cultured chick embryo cardiac cells were exposed to pulsed (10.9 μs at 10,000 pps) and CW RFR at 2450 MHz for 3-min periods. An open-ended coaxial exposure device developed on the program was used. Contraction, or beat, rates (recorded with extracellular electrodes) were faster during exposure, but only by a few percent for levels up to 85 mW/g SAR. Most changes in mean beat rate and in variation were attributed to small temperature changes of less than 1°C during exposure. Because of the large scatter in beat rate variables, small changes opposite from predictable thermal effects at small SARs were attributed to chance occurrence. Results from this previous program will be referred to in this report as "previous FTR" [50].

B. Research Objectives

The overall objective of this program was to investigate the effects of pulsed and CW RFR on the electrical properties of cardiac-cell membranes. The specific research objectives as originally proposed are summarized as follows:

1. Measure voltage noise and small-signal membrane impedance of non-beating cardiac-cell aggregates from 7-day chick embryos for different RFR SARs

2. Calculate the variance of membrane current noise for different SARs, using voltage noise and impedance

9

3. Determine the magnitude of potassium current and the probability that a single potassium channel is open, using voltage-clamp analysis at different SARs

4. Derive potassium channel density and single channel density, using the current noise variance, and the probability, using a known relationship for different SARs

The above analysis was proposed for CW and pulsed (11 µs at 10,000 pps) RFR at 2450 MHz. However, after voltage noise was recorded and membrane impedance measured for a few aggregates, it became obvious that data relevant to the proposed research objectives could not be obtained. A voltage noise that showed a peak at around 1 Hz would have been required. This frequency is similar to beat frequency and contains information on potassium channels [21-24]. Also, an oscillatory response of membrane voltage to injected current pulses--related to channel dynamics [18-22]--was expected. Initial experiments and analysis showed neither the 1-Hz voltage noise peak nor the oscillatory response.

Despite the inability to investigate the membrane properties as proposed, data were gathered and analyzed as a function of RFR SAR and modulation. Comparisons between data for different RFR conditions described here provide information on RFR interaction with the cardiac-cell excitable membrane. Various aspects of these data and their interpretation are discussed in appropriate sections of this report.

II. TECHNICAL APPROACH

A. Cardiac-Cell Aggregate Preparation

The multicellular nature of heart tissue, and other tissues as well, can severely limit an investigation of its electrical and molecular properties. In 1972, the spheroidal heart-cell aggregate was introduced as a tissue culture model for studies of the electrical properties of the heart-cell membrane [36,48]. These aggregates offer the following advantages over more traditional cardiac preparations:

1. All cells within an aggregate are closely coupled by low-resistance junctions, but the nonjunctional myocyte membrane exhibits large resistive, capacitive, and inductive elements [18]. For spheroids of 200-µm diameter or smaller, signals in the frequency range 0-20 Hz are essentially experienced simultaneously throughout the entire membrane [21,23,24]. Thus, each aggregate approximates an isopotential system for both spontaneous and imposed signals.

2. Because of these properties, the aggregate action potential approximates a true nonpropagated membrane potential, whose electric field builds and collapses with each beat. For this situation, the time derivation of transmembrane potential is equal to the transmembrane current divided by the membrane capacitance.

3. Aggregates can be prepared in any size within a 30- to 300-μm-diameter range, from a few cells to several thousand cells, containing 10^{-7} to 10^{-2} cm^2 of membrane.

4. Aggregates are "sticky" and adhere to glass and to plastic culture dishes. They can also be formed into pairs, chains, or clusters in which electrical coupling junctions are quickly established at points of contact. Such multiaggregate systems soon take on a coordinated, synchronized beat [16,55,56].

5. Aggregates can be prepared from chick hearts at any desired embryonic age, from stages prior to the time the organ begins to beat to hatching or shortly thereafter. Such spheroids reflect the physiological and pharmacological properties of the intact donor tissue.

6. Aggregates can be maintained in healthy condition—exhibiting spontaneous, rhythmic beating—for many days in culture.

7. Because they are naturally "space clamped" (virtually isopotential over a reasonable range of frequencies), aggregates can be subjected to voltage-clamp analysis of their current-voltage relationship [42].

For the investigations described in this report, we made measurements on spheroidal aggregates of chick heart cells maintained in tissue culture. The cells were derived from embryos of white Leghorn chickens by procedures standard in Dr. DeHaan's laboratory. After incubation for 7 days at $37.5^{\circ}C$, embryos were harvested in amniotic fluid and decapitated. Their hearts were dissected free and trimmed of extraneous tissue; the ventricles were dissociated with trypsin by techniques previously reported [42,48]. Standard procedures called for aggregates to be prepared by placing an inoculum of 5 x 10^5 to 8 x 10^5 cells in 3 ml of 818A culture medium on a gyratory shaker. Cells were allowed to aggregate during gyration at 62 rpm and $37.5^{\circ}C$ in an atmosphere containing 5% carbon dioxide, 10% oxygen, and 85% nitrogen. In some cases, aggregates were prepared by using serum-enriched culture medium with 8% (ml/100 ml) fetal bovine serum and 4% and 2% concentrations in 818A. When enriched medium was used, ionic concentrations were also increased; the resulting medium was designated as E818A. A comparison of these two media shows the following:

	818A	E818A
Serum	6%	12%
Sodium (mM)	116	136
Potassium (mM)	1.3	3.3
Calcium (mM)	1.8	3.6

To optimize recording conditions, we used aggregates that had been gyrated either 48 or 72 hours. In Section III, type of culture medium and gyration duration are used to specify the aggregate preparation methods.

11

At the end of a 48-hour gyration period, each aggregation flask typically contained up to 200 spheroidal clusters which ranged in diameter from 60 to 250 μm and contained 10^2-10^4 cells each. At the end of a 72-hour gyration period, aggregate size was larger, ranging up to 300 μm. The several hundred individual cells in each aggregate were beating spontaneously and rhythmically in a coordinated fashion. For experiments, aggregates and their 3 ml of culture medium were poured into a 35-mm plastic culture dish and the volume was brought to 4 ml with the same medium (either 818A or E818A). The plastic dish was placed under a microscope, on a heating plate modified for RF exposure described in Section IIB. Temperature, pH, gaseous atmosphere, and evaporation were controlled and mechanical vibration was minimized.

B. Radiofrequency Radiation Exposure

The open-ended coaxial exposure device used in this program was described in the previous FTR [50] and became the subject of an Air Force application for a U.S. Letters Patent. Figure 1 is an isometric projection of this exposure device. A 1/4-in. (6.35 mm) semirigid cable opened into the circular brass heating plate, with its cut end flush with the plate's upper surface. A hubbed circular plate, used to mate the open-ended coax with existing heating plates, insured structural strength and electrical continuity of the ground plane. The other end of the cable was attached to RFR sources through appropriate connectors and cables. Figure 2 shows a top and side view of the configuration of aggregate generally used, along with microelectrodes and a temperature sensor. Since an RFR-insensitive temperature probe was not available until the end of this program, the YSI temperature probe used was placed farther away from the RFR fields than shown in Figure 2.

The RFR fields within the bathing medium in a culture dish placed on this exposure device were characterized by electric-field measurements and temperature changes [50]. The solid points in Figure 3 show the normalized SAR distribution at the bottom of the culture dish (the location of all aggregates studied in this program) as previously determined [50]. The SAR was normalized to net power (forward minus reflected) to the exposure device and is shown as a function of radial distance from the center of the coax's center conductor. Net power was determined for each RFR exposure by using the power meter reading of forward power for that exposure and readings of forward and reflected powers obtained at the end of an experiment for each RFR frequency and modulation. The distance of the aggregate from the coax center was measured within the microscope eyepiece micrometer to within 10-μm resolution. Net power and aggregate position were used to calculate SAR by equations for the straight-line portions of the distribution.

During this program, we checked that SAR distribution by using a Vitek model 101 Electrothermia Monitor. This RFR-transparent temperature probe has a diameter of about 1 mm. The rate of temperature rise at the onset of RFR at 2450 MHz was used to compute an SAR for each location of the probe. Figure 4 shows the temperature record for each of three bottom locations: at the center (R = 0), at 1/3 of coax dielectric distance from the center conductor (R = 1.55 mm), and at 1/2 of coax dielectric distance from the center conductor (R = 1.88 mm). Note the absence of a sudden jump in signal with RFR, which
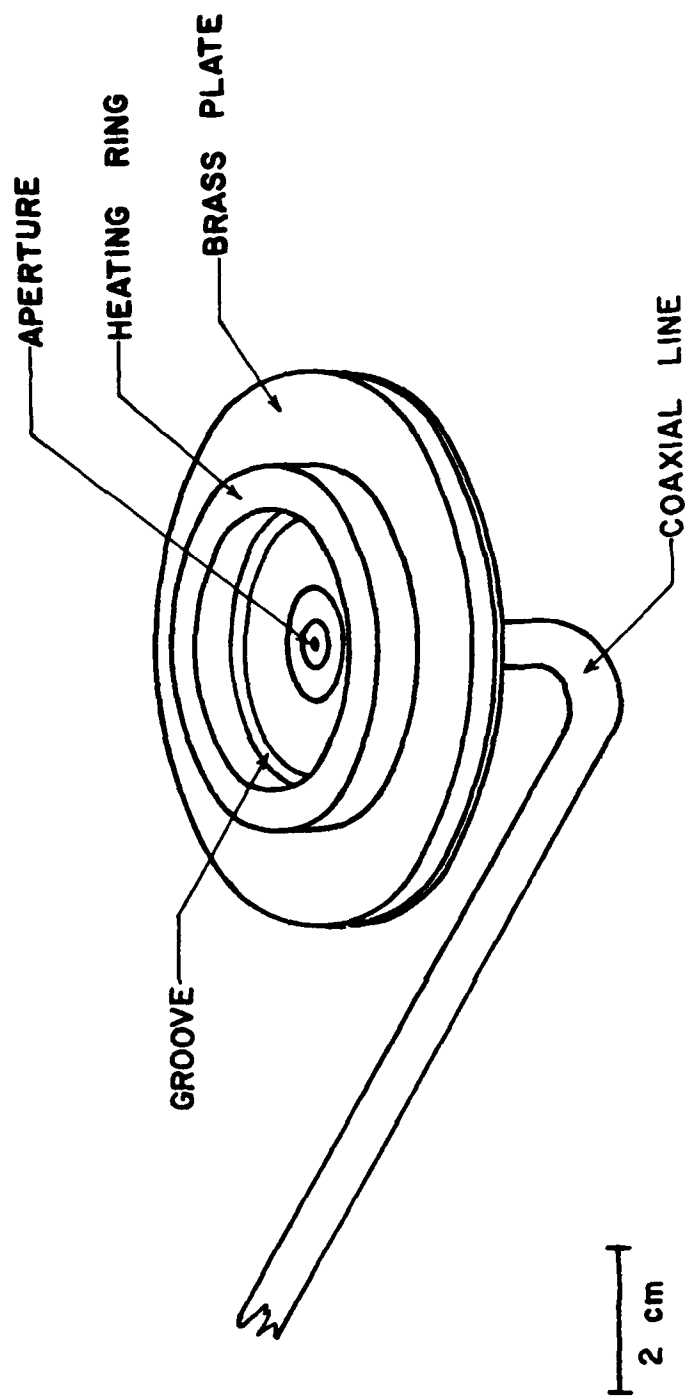
Figure 1. Isometric projection of open-ended coaxial exposure device. The bottom rim of a 35-mm culture dish is fitted into the groove for mechanical stability and direct contact of dish with the coaxial line's aperture.

APERTURE

HEATING RING

BRASS PLATE

COAXIAL LINE

GROOVE

2 cm

13
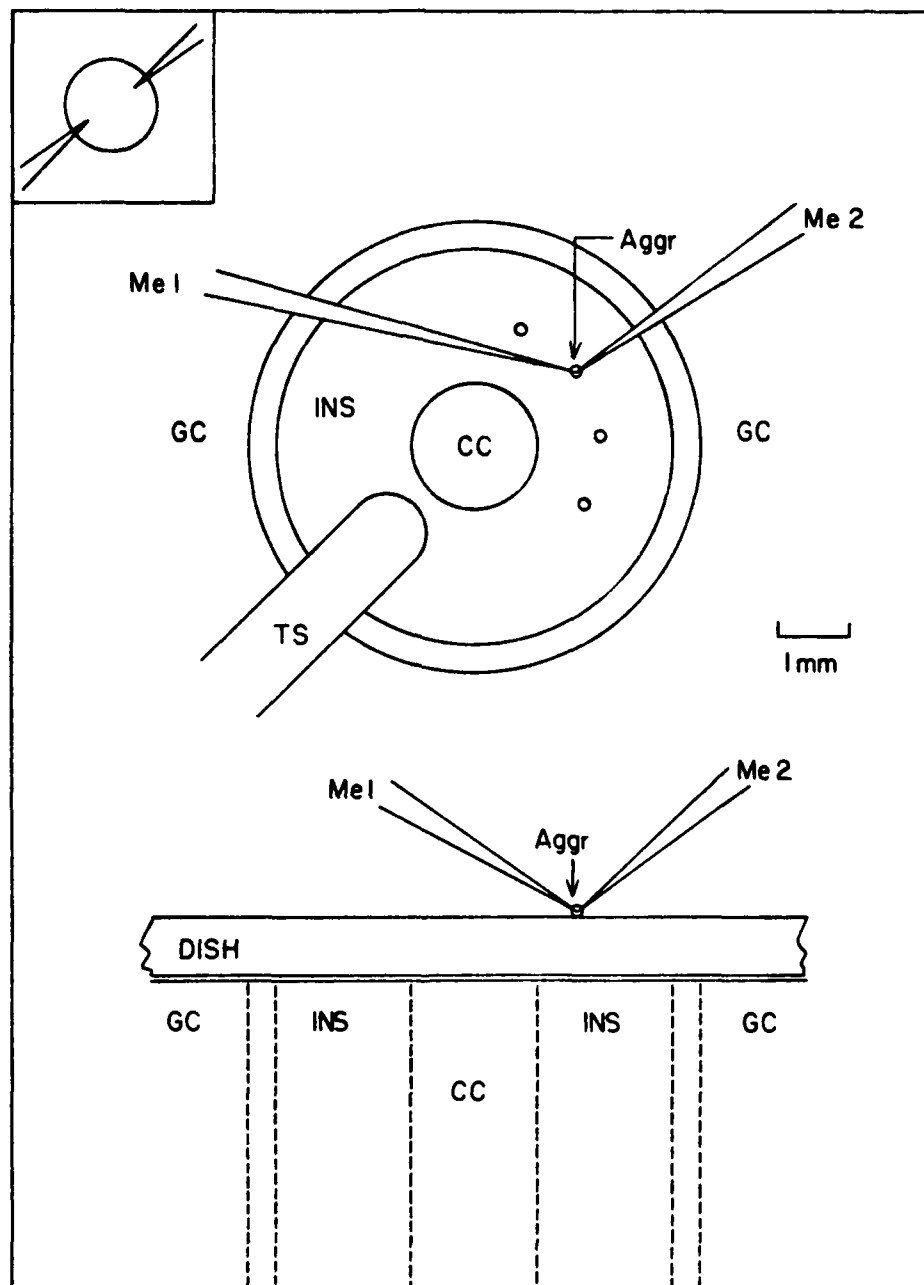
Figure 2. Typical cardiac-cell aggregate configuration during RFR exposure. Top and side views are seen at the top and bottom of figure. aggregate-microelectrode arrangement, in the inset. Aggr, aggregate; CC, center conductor; GC, ground conductor; INS, insulator (coax dielectric); Me, microelectrode: TS, temperature sensor.

14
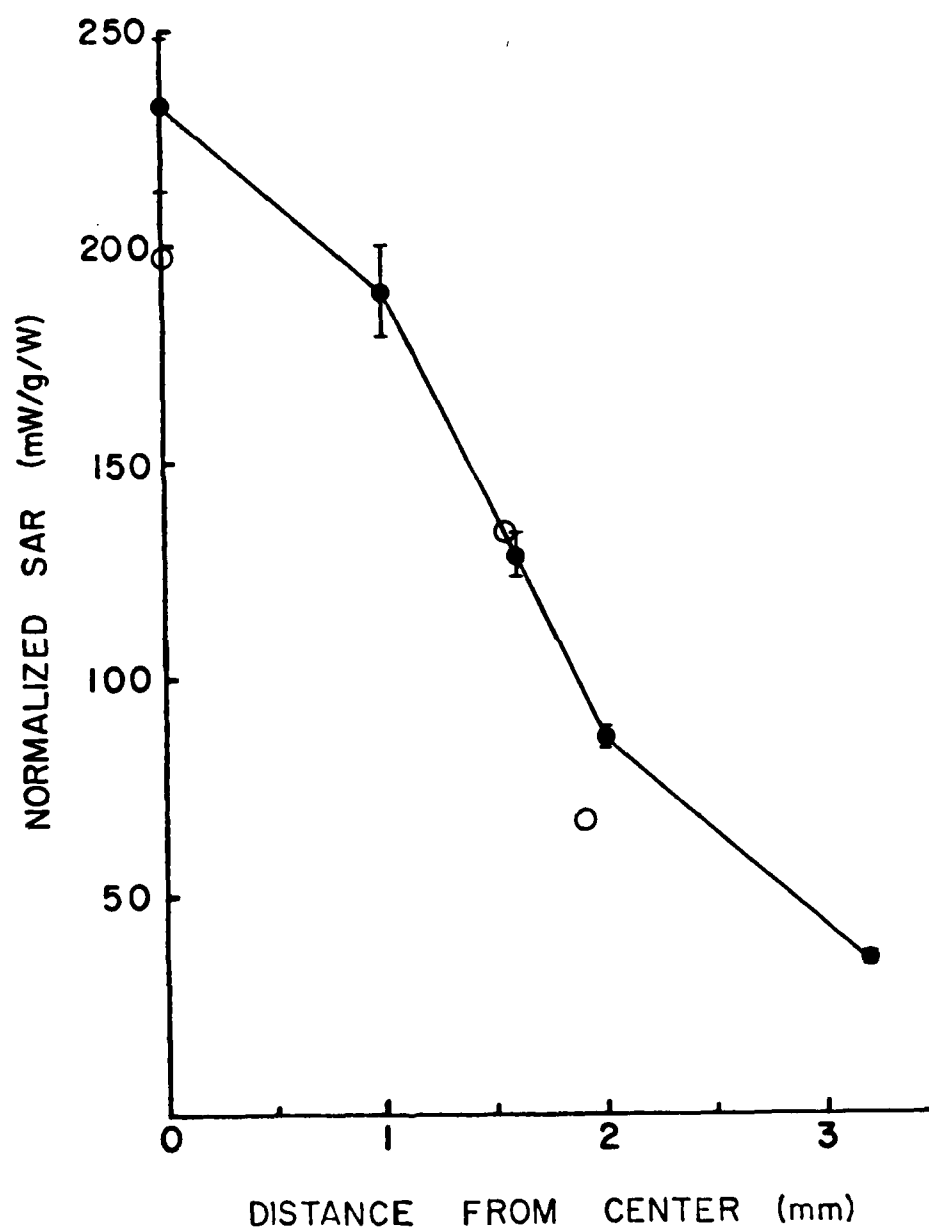
Figure 3. SAR as a function of radial distance at bottom of culture dish; normalized to watts of net input power to exposure device. Solid circles represent data obtained and reported in a previous FTR, [50]; open circles, data obtained during the current research program.

15
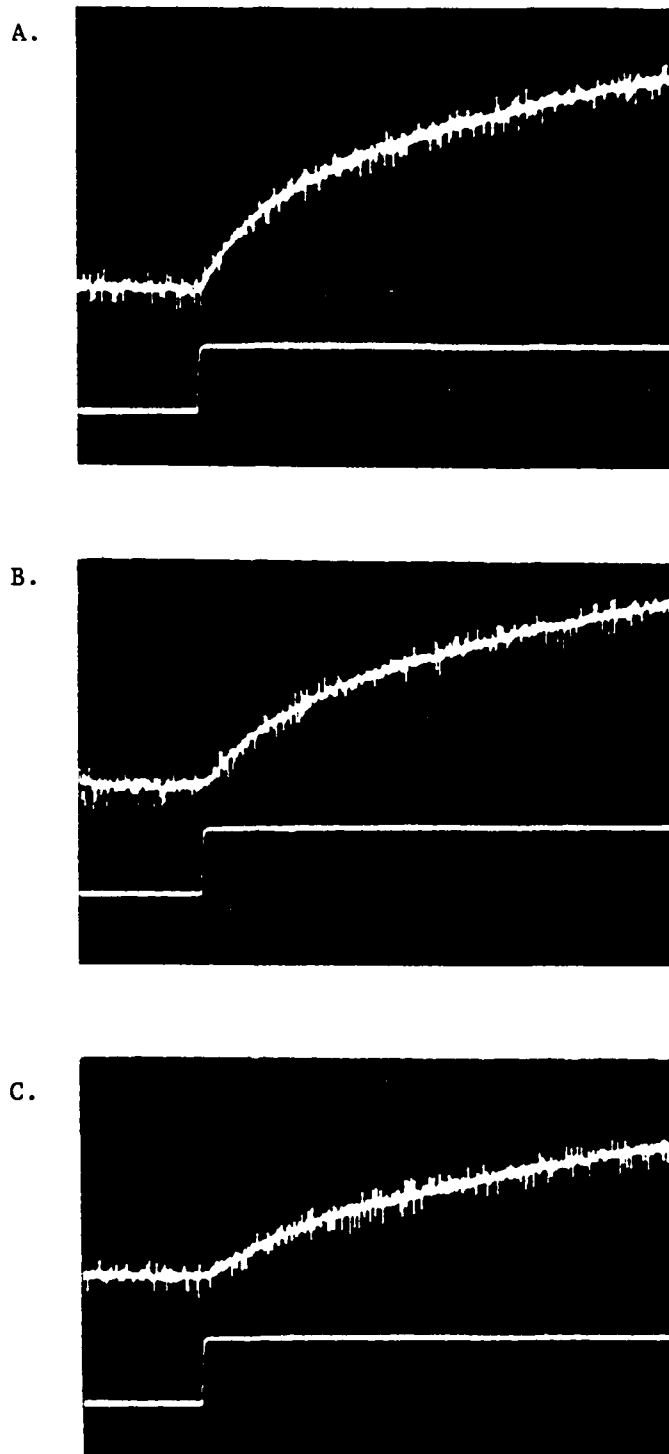
Figure 4. Temperature changes (upper traces) at the onset of 2450-MHz CW RFR (lower traces) at the culture dish bottom. A, Center; B, one-third of coax dielectric distance from center conductor; C, one-half of coax dielectric distance from center conductor. Calibrations: upper traces, 0.2°C per division; lower traces, 5 W forward power per division; time, 5 s per horizontal division.

16

would have indicated direct RFR pickup by the sensor. The SARs computed from these data, shown as the open circles in Figure 3, are in reasonably good agreement with the previously determined distribution. Possible sources of differences include positioning errors, inaccuracies in determining rate of temperature rise, and spatial averaging by the different probes. With respect to the last point, a published theoretical analysis of SAR in tissue in contact with an open-ended coaxial antenna showed that there is a peak at the edge of the center conductor [52]. Our measurements showed no peak SAR at the center-conductor edge (R = 0.9 mm), and its absence can be attributed to the spatial averaging of temperature by the probes used.

The open-ended coaxial exposure device was connected to appropriate RFR sources and measuring instruments to provide a system that could expose cardiac-cell aggregates to a variety of SARs and modulations. Our exposure and recording setup (Fig. 5) was very similar to that used in the previous program [50]. A signal source with a maximum output of 1 mW provided CW RFR. This power was amplified by a Hughes model 1177H S-band TWT Amplifier equipped with an isolator to protect its output from reflected power. For some experiments, an HP model 8731B PIN Modulator was placed between the source and this amplifier to obtain a 1.2-Hz sinewave modulation. The TWT amplifier output was connected by coaxial cable to the exposure device through a Narda 20-dB bidirectional coupler which sampled powers transmitted to and reflected from the exposure device. The difference of these powers was the net input power to the exposure device, which was used to calculate SAR values. Reflected power was measured at least once for each experiment to assure consistent operation of the exposure device.

Toward the end of this program, the acquisition of an Epsco model PG5KB High Power Pulsed Signal Source with a model 5238H/B8 RF Oscillator operating at 2450 MHz enabled us to expose aggregates to pulsed RFR. This source was connected to the bidirectional coupler through the same long cable connected to the TWT isolator for CW exposures. The source worked satisfactorily in this configuration without benefit of an isolator or matching network. Both CW and pulsed RFR could be alternately applied to the preparation during an experiment by connecting the cable to the appropriate source. Pulse modulation, designated as PW, consisted of 5-μs pulses at 100 pps which gave a 0.0005 duty cycle. Pulse duration was checked at the beginning of an experiment; repetition rate was continuously monitored with a frequency counter.

C. Experimental Procedures

The transmembrane potentials of individual-cell aggregates on the bottom of a culture dish were recorded to obtain data. After the medium volume was brought to 4 ml, the dish was placed on the heated open-ended coaxial exposure device on the epi-illumination microscope stage. Mineral oil was placed on the medium to prevent evaporation, a ring providing a gaseous atmosphere to control pH was put in place, and a YSI thermistor was inserted into the medium (away from concentrated RFR fields) to monitor bulk temperature. The culture medium was referenced to electrical ground through an agar bridge inserted at this time. If necessary, aggregates were moved so that several rested over a
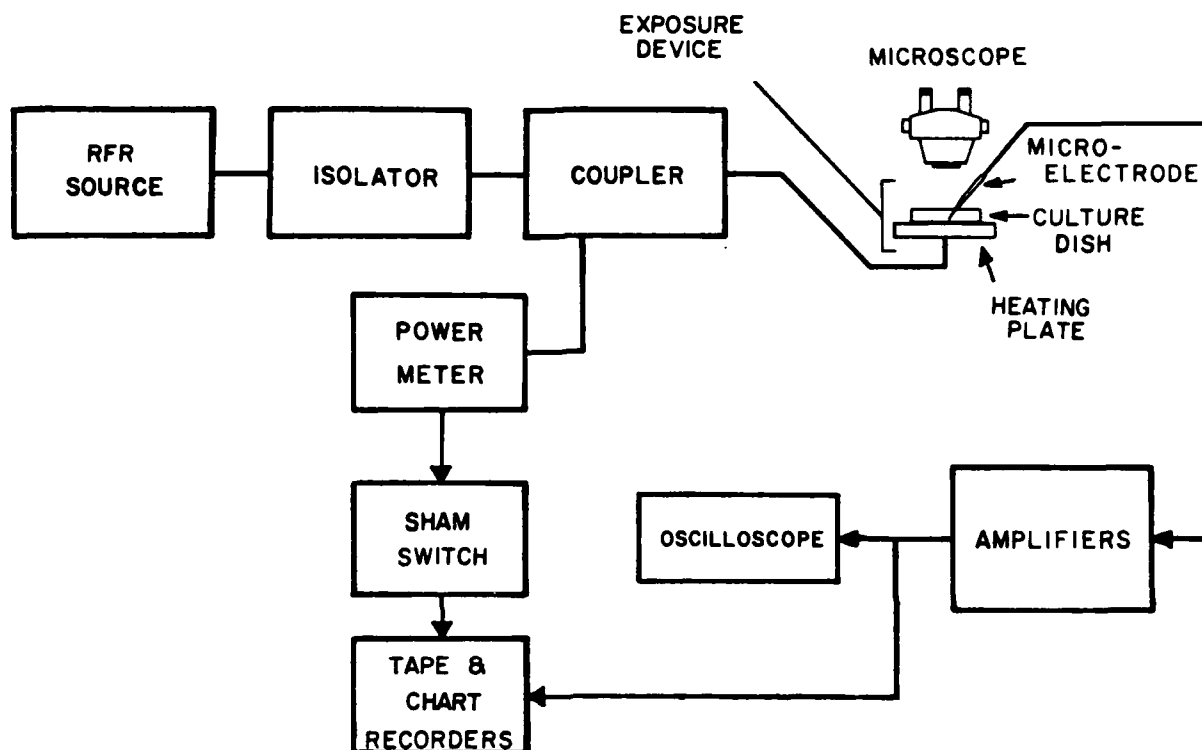
Figure 5. Block diagram of experimental setup. The RFR source consisted either
of a low-level signal generator and a TWT amplifier for CW exposure
or a high power pulsed-signal source for PW exposure. The power
meter and sham switch provided the RFR signal which was recorded
on FM magnetic tape. The microelectrode signal line represents low-
and high-gain channels for both microelectrodes.

region, about halfway between the coax conductors, where the RFR electric field was oriented almost horizontally. Tetrodotoxin (TTX) at 10^{-6}g/ml was usually added at this time to block fast sodium currents and thus suppress spontaneous production of action potentials and contractions. The preparation was then left for 2-4 h to allow temperature equilibration of 37°C (actual range was 37 ± 0.2°C) and aggregate adhesion to the dish. For some experiments, TTX was added after this equilibration period but 10-30 min before recording began. If an aggregate resumed activity in a long experiment, an additional dose of TTX was added to the preparaςion.

Microelectrodes were drawn from 1.1-mm glass capillary tubing with internal glass fibers. Each microelectrode was filled with 2.5 M KCl by pressure injection from a small metal tube inserted into the electrode's open end. These procedures resulted in microelectrodes with DC resistance between 10 and 80 MΩ. The tips of two microelectrodes with acceptable DC resistance of greater than 20 MΩ were positioned over an aggregate with micromanipulators. Gentle tapping and fine positioning of a micromanipulator were used to obtain an intracellular penetration to give a transmembrane potential. Several trial experiments were required to develop techniques that gave stable penetrations lasting more than a few minutes.

Microelectrode signals were amplified and recorded on FM magnetic tape for later analysis. Each signal was recorded at 10X DC-coupled and at 1000X AC-coupled, using a high-pass filter with a cutoff at 0.1 Hz. The low-gain signals, a signal proportional to RFR forward power, and a signal proportional to injected current were displayed on a four-channel strip chart. This display was useful for observing trends and making decisions on experimental manipulations. The chart record and notes taken during an experiment formed a permanent record. Signal flow for one microelectrode is shown in Figure 4.

After preliminary experiments to refine experimental techniques, RFR exposures were 3 min long (180- to 195-s range) with a similar, sometimes longer, period between exposures. Timing was accomplished initially with an experiment clock described previously [50], and later with a digital stopwatch. Figure 6 shows the designation of noise-analysis epochs to RFR exposures. Exposure and no-exposure periods consisted of two parts indicated in Figure 6 by the experiment-clock signal. The half-period interval just before an exposure was designated PRE; the interval just after an exposure, POST. The POST interval was followed by a POSTPOST interval which was usually the PRE interval for the next exposure. The exposure period itself was divided into the intervals BEG (for beginning) and END. In Section III, experimental results for membrane voltage noise are described in terms of these intervals. (Analysis epochs for microspike frequency of occurrence were similar except the exposure was divided into three 1-min intervals called BEG, MID, and END.) In some experiments, 2-min exposures were used to maximize the number of exposures during a stable dual penetration; for these, intervals were a nominal 1 min long (instead of the nominal 1.5 min for the 3-min exposures).
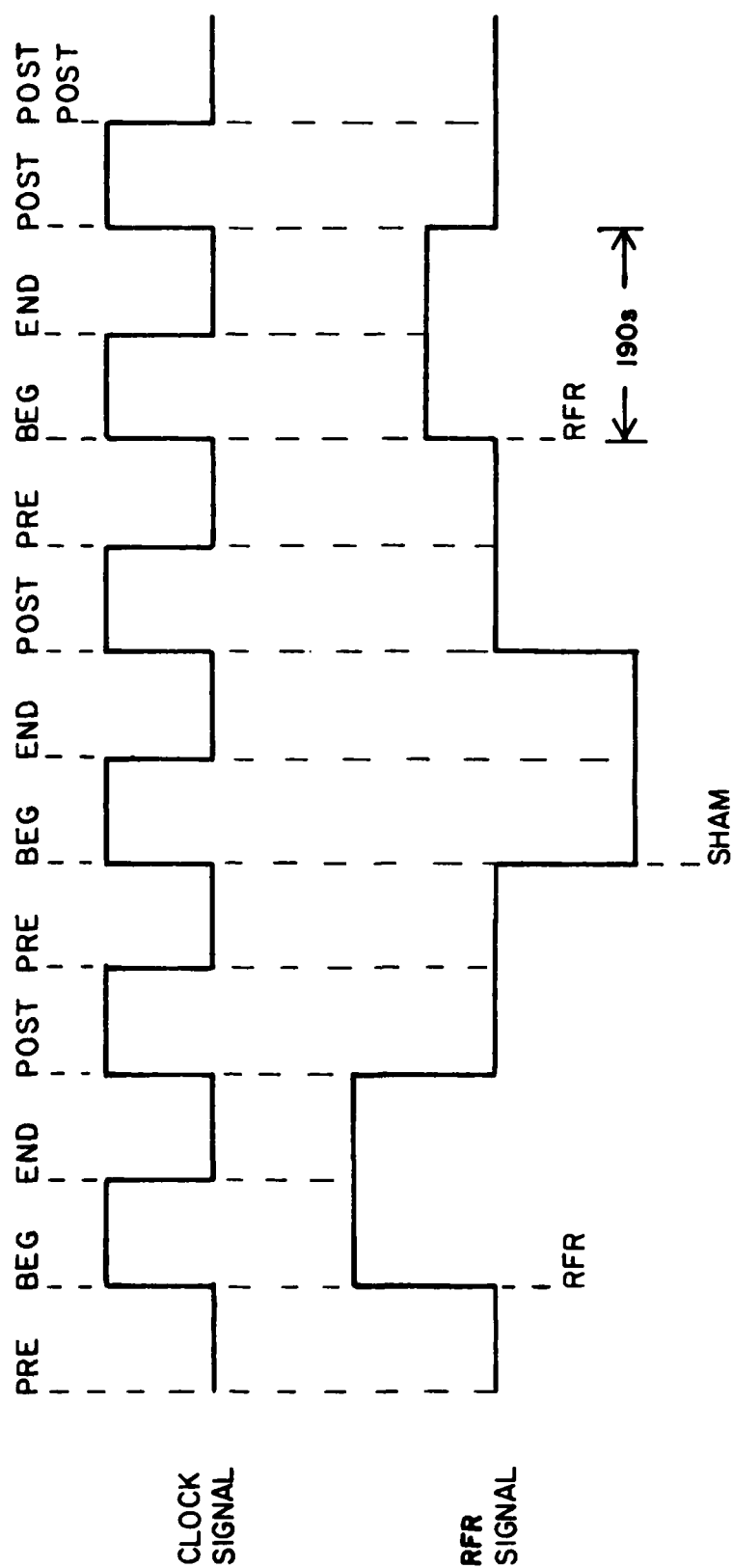
19

Figure 6. Experiment-clock and RFR signals for exposure intervals and analysis epochs (2-min exposures were also performed, with correspondingly shorter analysis epochs assigned). The latter signal was recorded on magnetic tape and strip chart to facilitate data analysis.

20

III. EXPERIMENTAL RESULTS

Cardiac-cell data collected during this program can be placed into three major types: membrane impedance, membrane voltage noise, and microspikes. Since each type was studied during different RFR exposure conditions, results are presented separately.

A. Membrane Impedance

The membrane impedance for the cardiac cells of an aggregate was measured by injecting a nominal 1- to 3-nA current through one microelectrode and recording the membrane voltage response with the other microelectrode. Based on previous studies [18,22], an oscillatory or near-oscillatory response to these step currents was expected. However, responses showed either no overshoot or a critically damped overshoot of steady-state value.

Figures 7 through 11 show the averaged responses to hyperpolarizing current pulses under different CW RFR levels in one aggregate. Each figure has four panels, and each panel represents a time-averaging analysis, on an HP 5420 Digital Signal Analyzer, of recorded data. The analyzer was triggered at time zero by the recorded current-pulse signal either at onset or offset of each 4.5-s pulse. The two top panels are the on- and off-responses over 4 s. The recorded low-gain DC signal, used to provide an accurate representation of slow variations in potential, gave a relatively high noise level. The voltage scale includes microelectrode offset potential and is 2-mV full scale in all figures. The two bottom panels show the recorded high-gain signal for the first 160 ms of on- and off-responses. The voltage scale for these panels is also 2-mV full scale.

For the low-gain signal recordings (top panels Figs. 7-11), analyzer cursors were set to measure steady-state voltage difference in each panel. This difference divided by the 0.95 nA of injected current is the membrane DC-resistance R_m, an average value of which is included in each figure. Although R_m ranged between 0.758 and 0.881 MΩ, no specific effect could be assigned to the RFR that ranged between 2.03 and 141.6 mW/g. The observed changes in R_m and the variations in membrane potential in this experiment were attributed to variability in the quality of the microelectrode penetrations. The slope (dV/dt) of the high-gain response onsets and offsets (bottom panels, Figs. 7-11) is equal to I/C_m, where I is the injected current and C_m is the membrane capacitance, for the isopotential aggregates. Since I was the same in all cases in these figures, the slope provides a measure of C_m. No differences were seen in slope (thus C_m) for the range of SARs applied.

Figure 12 shows voltage responses of an aggregate in another experiment. The average of 10 response onsets before and the average of 10 response onsets during 139-mW/g CW RFR are shown for the first 3 s of the responses. The decrease in overshoot with RFR was seen in both onset and offset of the voltage response. This example illustrates the only case in which a change in the overshoot of steady-state potential was seen. Because there was no overshoot in subsequently tested aggregates, the effect on overshoot was not pursued.
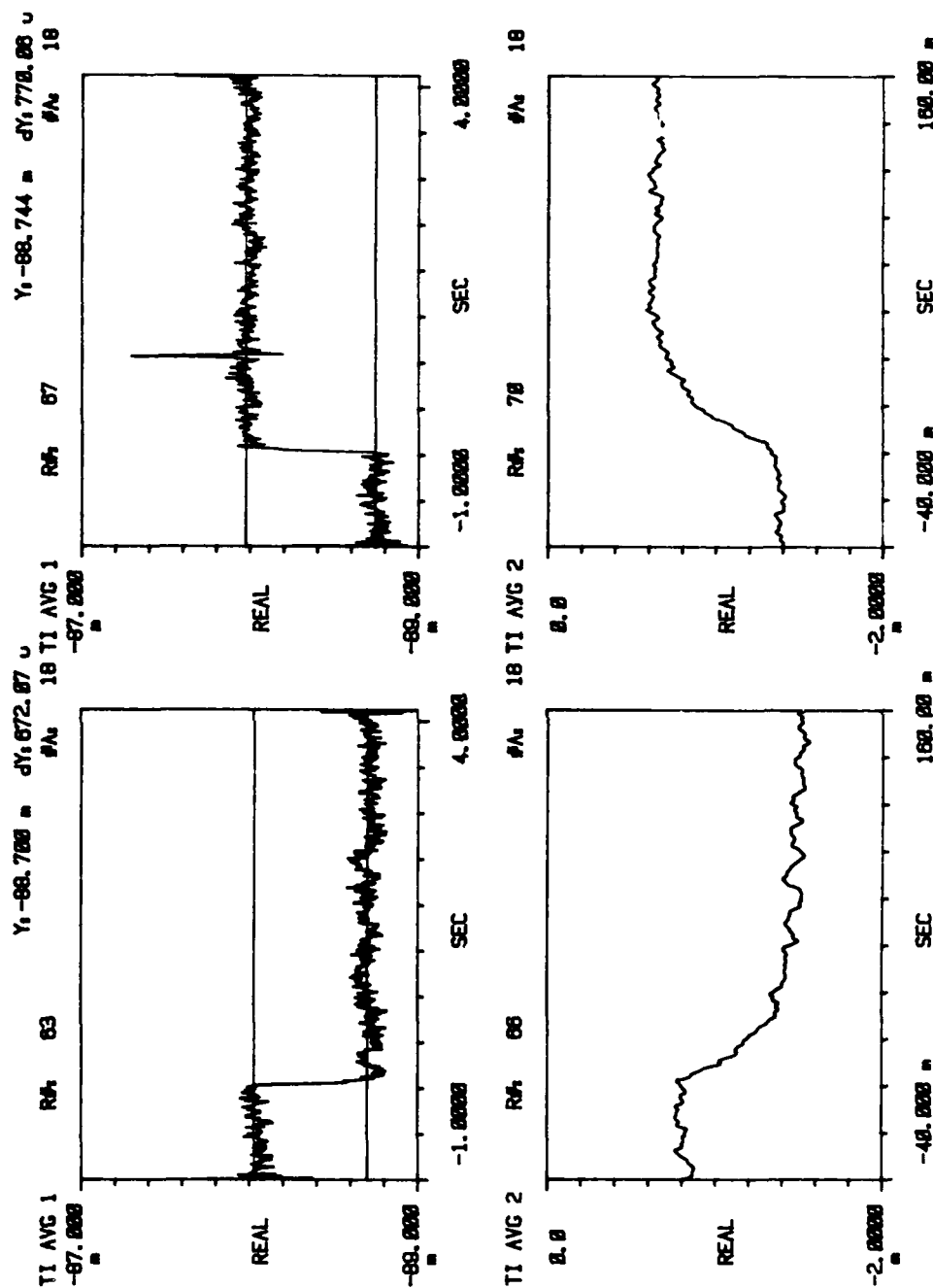
Figure 7. Average of 18 PRE-period membrane impedance measurements. Top panels: on-and off-responses, low-gain signal; bottom panels, high-gain signal. SAR = 0, R_m = 0.758 MΩ.
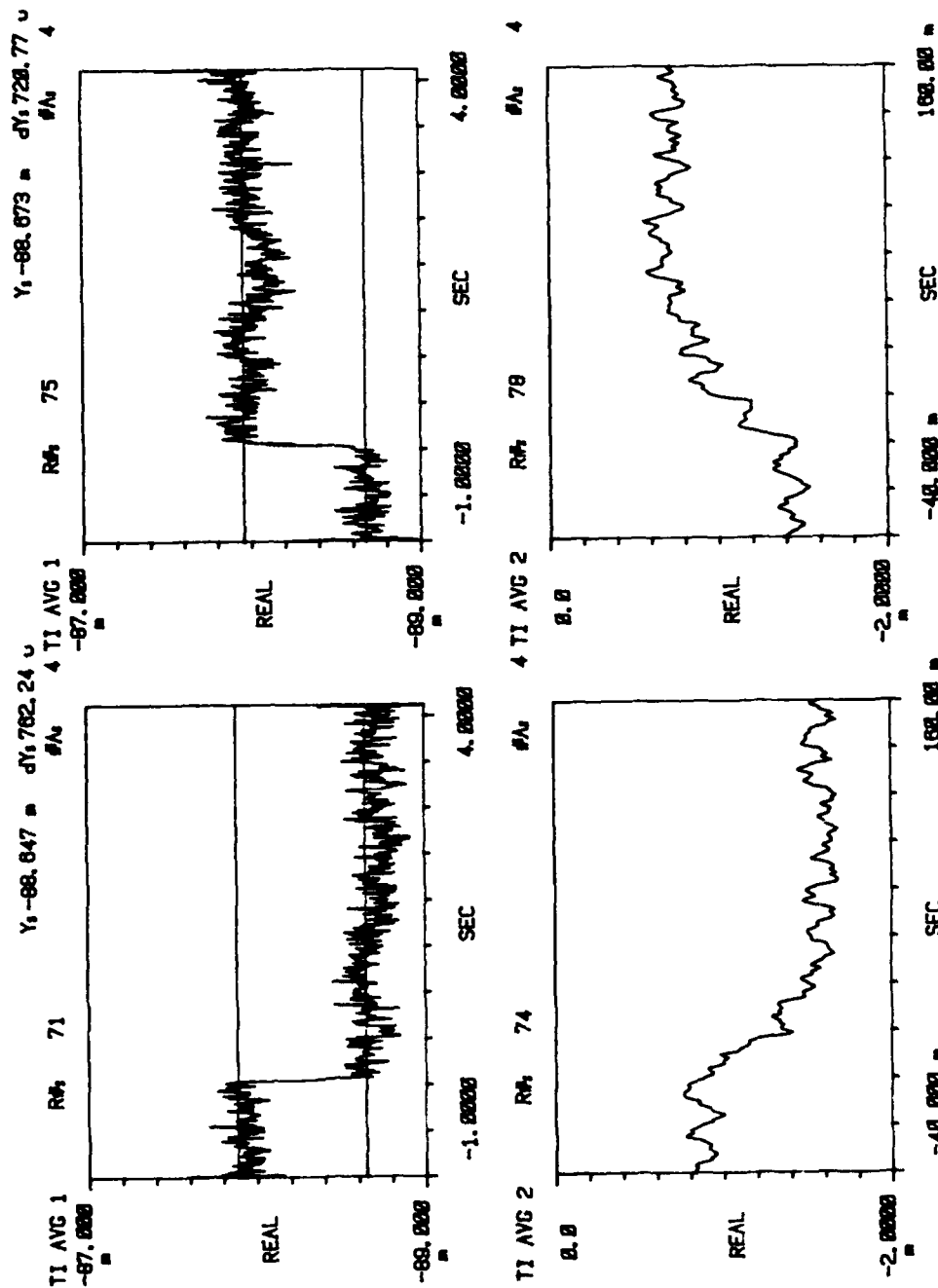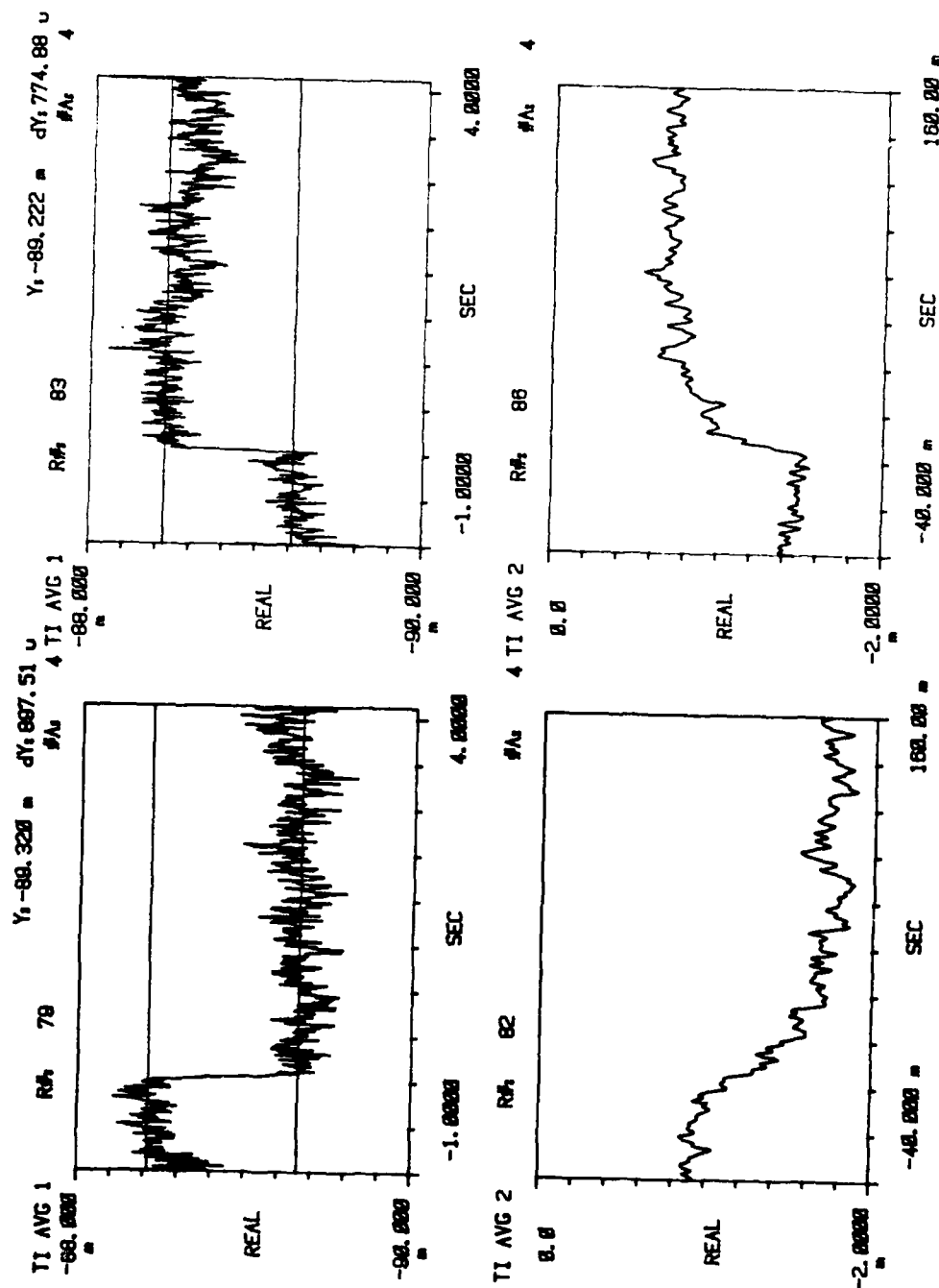
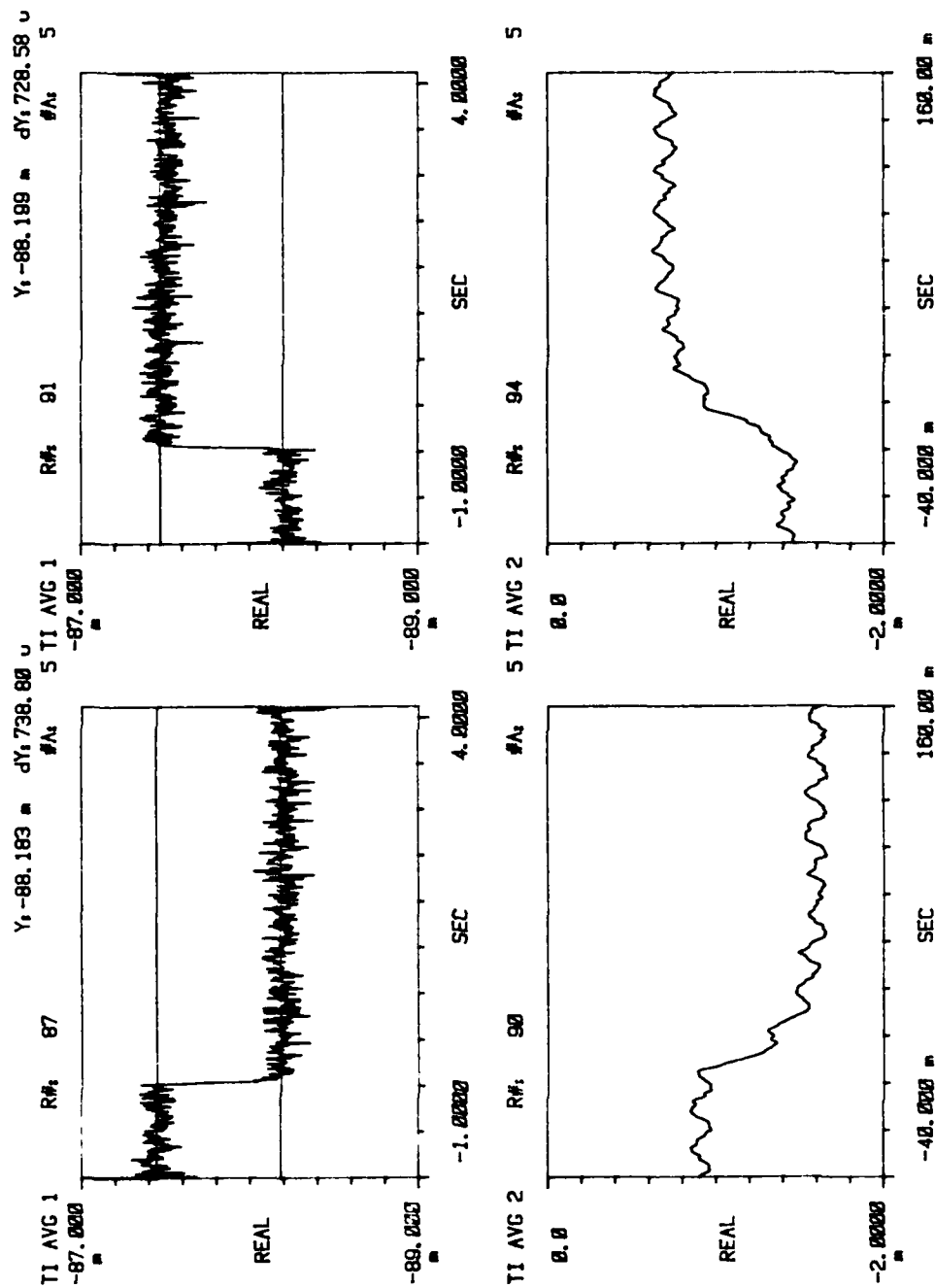Figure 8. Average of four SHAM membrane impedance measurements. Top panels: on-and off-responses, low-gain signal; bottom panels, high-gain signal. SAR = 0, R_m = 0.78 MΩ.
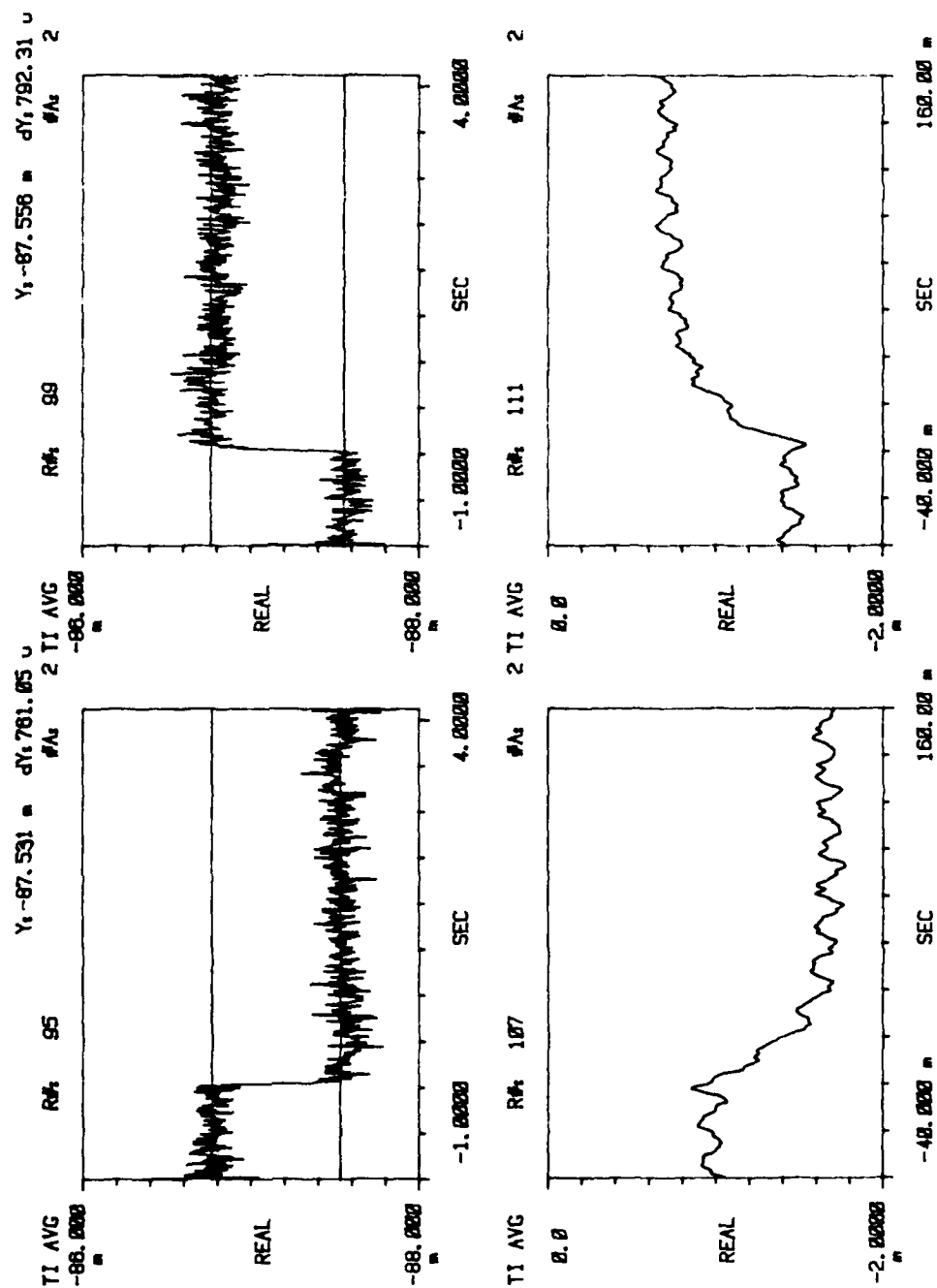
23

Figure 9. Average of four membrane impedance measurements during 2.03-mW/g CW RFR. Top panels: on-and off-responses, low-gain signal; bottom panels, high-gain signal. SAR = 0, R_m = 0.881 MΩ.

24

Figure 10. Average of five membrane impedance measurements during 20.4-mW/g CW RFR. Top panels: on-and off-responses, low-gain signal; bottom panels, high-gain signal. SAR = 0, R_m = 0.773 MΩ.

25

Figure 11. Average of five membrane impedance measurements during 141.6-mW/g CW RFR. Top panels: on-and off-responses, low-gain signal; bottom panels, high-gain signal. SAR = 0, $R_m = 0.817$ MΩ.
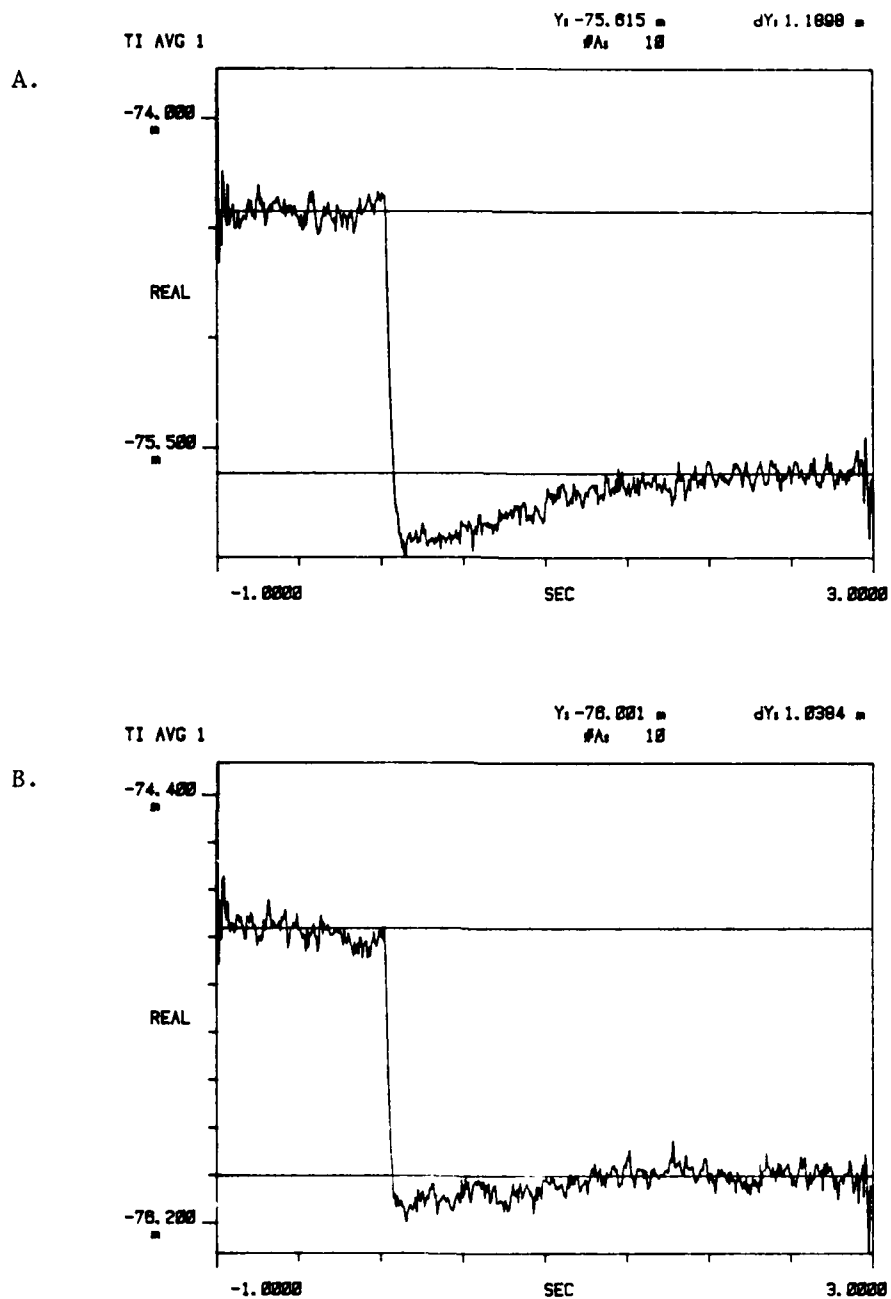
Figure 12. Membrane impedance measurements with overshoot. A (before RFR) and B (during 139-mW/g CW RFR) each show an average of 10 responses to 0.95-nA injected current pulses.

B. Membrane Voltage Noise

Fluctuations of less than roughly 1 mV in membrane potential are called membrane voltage noise and electrical activity of membrane molecular components [22]. In this program, the simultaneous microelectrode signals were used to study membrane voltage noise of cardiac-cell aggregates. Figure 13 shows two examples of recorded membrane voltage noise. Note that in each example the noise is virtually the same for both microelectrode signals because of the isopotential nature of aggregates. The high-gain recordings of these signals were played back and fed to the HP 5420A analyzer. Using its FFT (fast Fourier transform) capabilities, the analyzer performed a cross-spectrum operation on the signals in the frequency domain. With appropriate scaling of the inputs, the cross-spectrum operation gave a membrane-voltage-noise spectral density (spectrum) with units of volts^2/Hz versus frequency in Hz. After preliminary work with the analyzer defined reliable operation, a 3.125-Hz bandwidth was used for the 3-min exposures. This bandwidth gave a single run lasting 82 s and a total of 95 s for five averaged overlapping runs to match closely a BEG or END epoch of a 3-min exposure. For 2-min exposures, a 6.25-Hz bandwidth was used to obtain a 62-s total analysis duration to match the shorter BEG and END epochs. The duration of PRE and POST epochs for an exposure was matched to its BEG and END durations.

Figures 14 through 21 show examples of the spectra derived from different aggregates for different sham and RFR conditions. Each figure shows the results for PRE, BEG, END, and POST analysis epochs associated with an RFR exposure. From these spectra, it is seen that low frequency energy (from 0.1 to 0.5 Hz) dominated the spectra and was somewhat variable. Systematic changes in the spectra did not always occur with an RFR exposure level or modulation. In view of these variations in spectra, statistical tests were made on the spectra power for different RFR-induced changes. For these tests, the power (in volts^2) from 0.1 to 1.0 Hz under each spectrum was found by using an analyzer calculating function. Powers for similar exposures were grouped and tested statistically for differences between each RFR condition and non-RFR conditions.

Initial experiments done in E818A medium yielded data on membrane voltage data. For analysis, data were taken from 16 sham exposures and 21 exposures to 2450-MHz CW RFR: 7 exposures to 1.4-2.8 mW/g (low dose), 7 to 13.9-23.5 mW/g (medium dose), and 7 to 102.4-143.4 mW/g (high dose) in five experiments. Scatter plots of these data suggested a difference between noise power in nonexposure analysis epochs and noise power in the analysis epochs during medium and high doses, or SARs of 4.1-143.4 mW/g. The results of a statistical analysis applied to these data are shown in Figure 22. Data were pooled by combining noise powers from (1) all 106 available nonexposure analysis epochs: PRE, BEG, END, and POST of sham exposures and PRE and POST of RFR exposures; (2) 85 of these nonexposure epochs: 21 RFR-exposure POSTs excluded; and (3) 28 RFR-exposure epochs: BEG and END of medium- and high-dose exposures. Figure 22 shows combinations 1 and 3 of these data an.. the regression lines derived for each condition. A z-test showed that the slope of 0.80 for the exposure regression lines was significantly different from the slope of 0.38 for the illustrated nonexposure regression line at the 0.05 level, also that slopes for combinations 2 and 3 were significantly different.
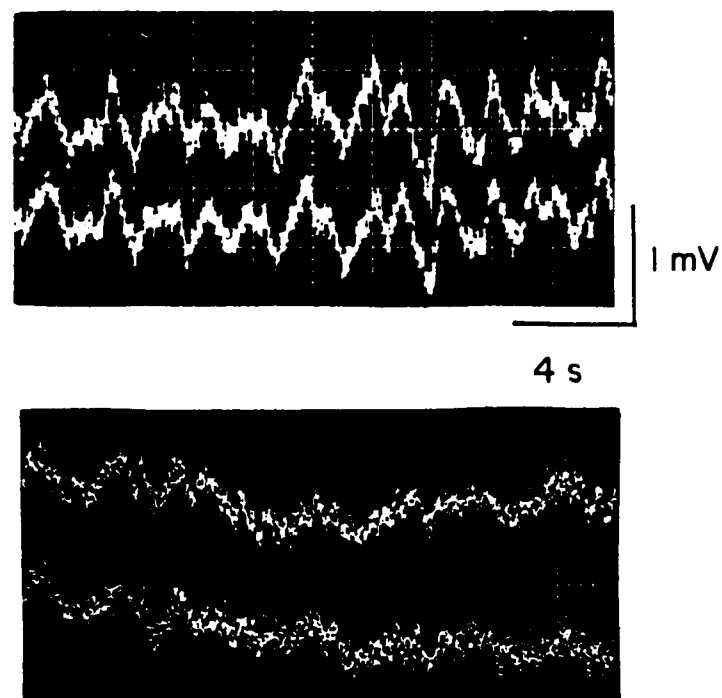
Figure 13. Membrane voltage noise from cardiac-cell aggregates. Data from two different aggregates, each with two microelectrodes recording noise. Calibrations are for both examples.
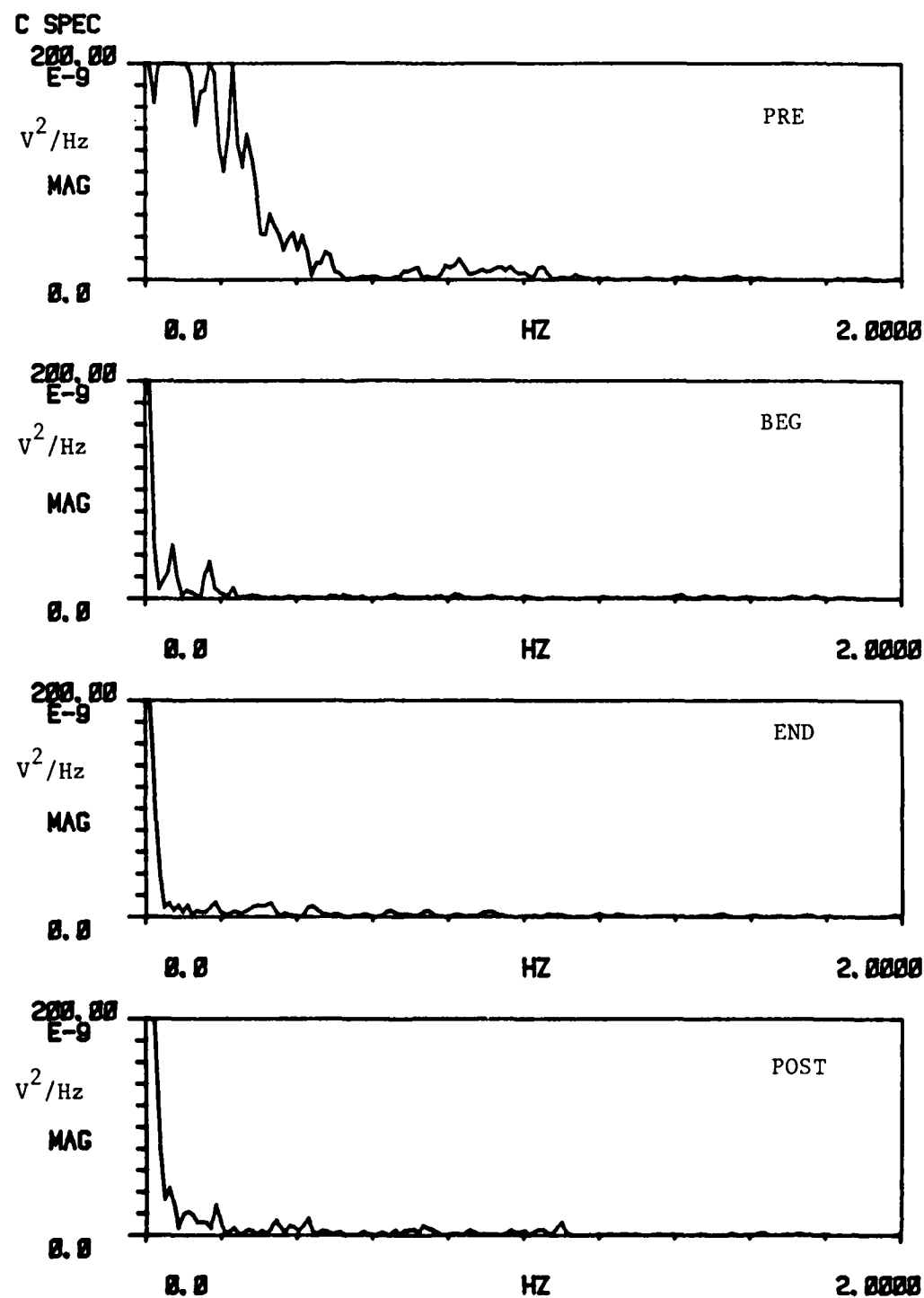
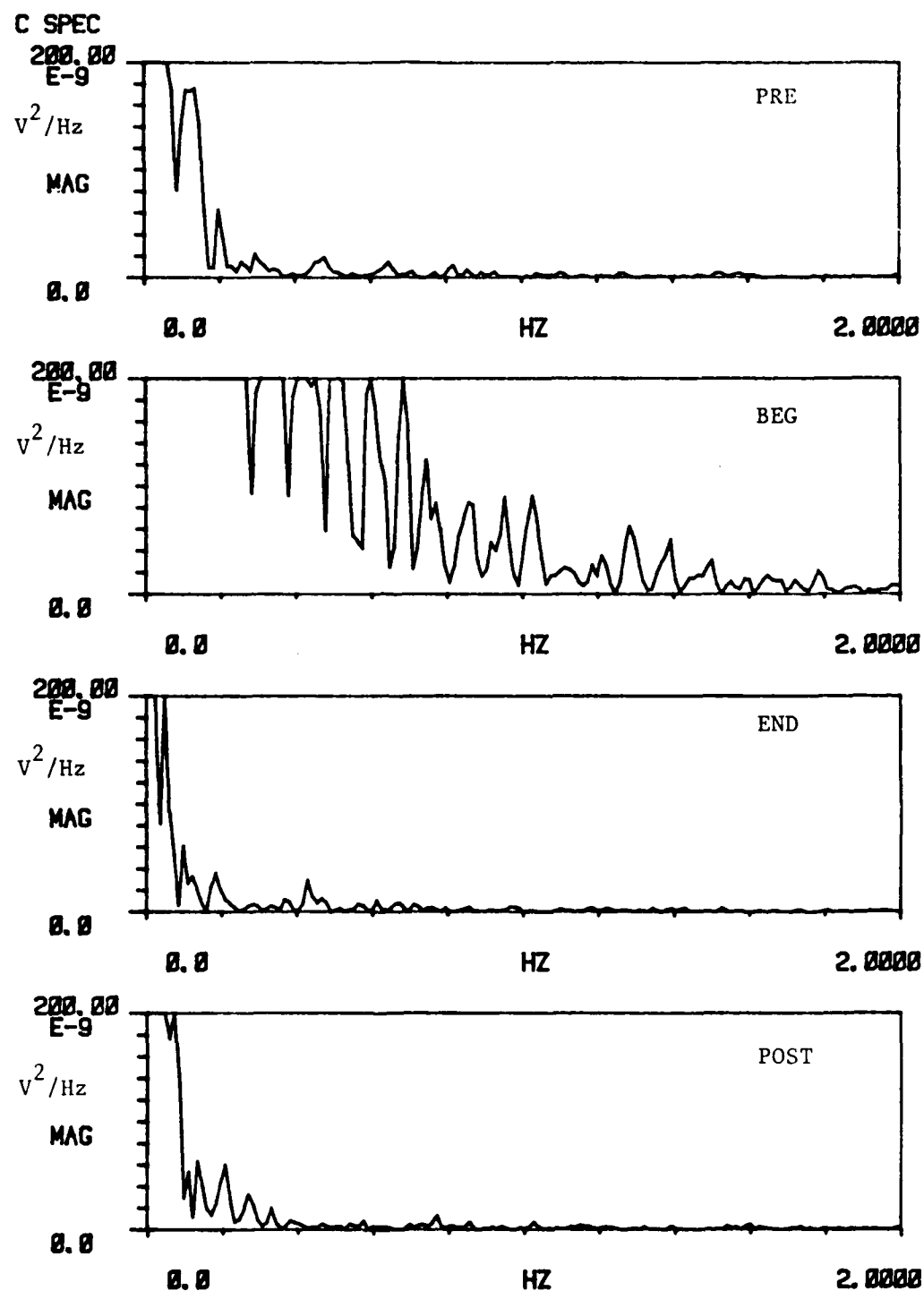Figure 14. Membrane-voltage-noise spectral densities for a 3-min SHAM exposure.

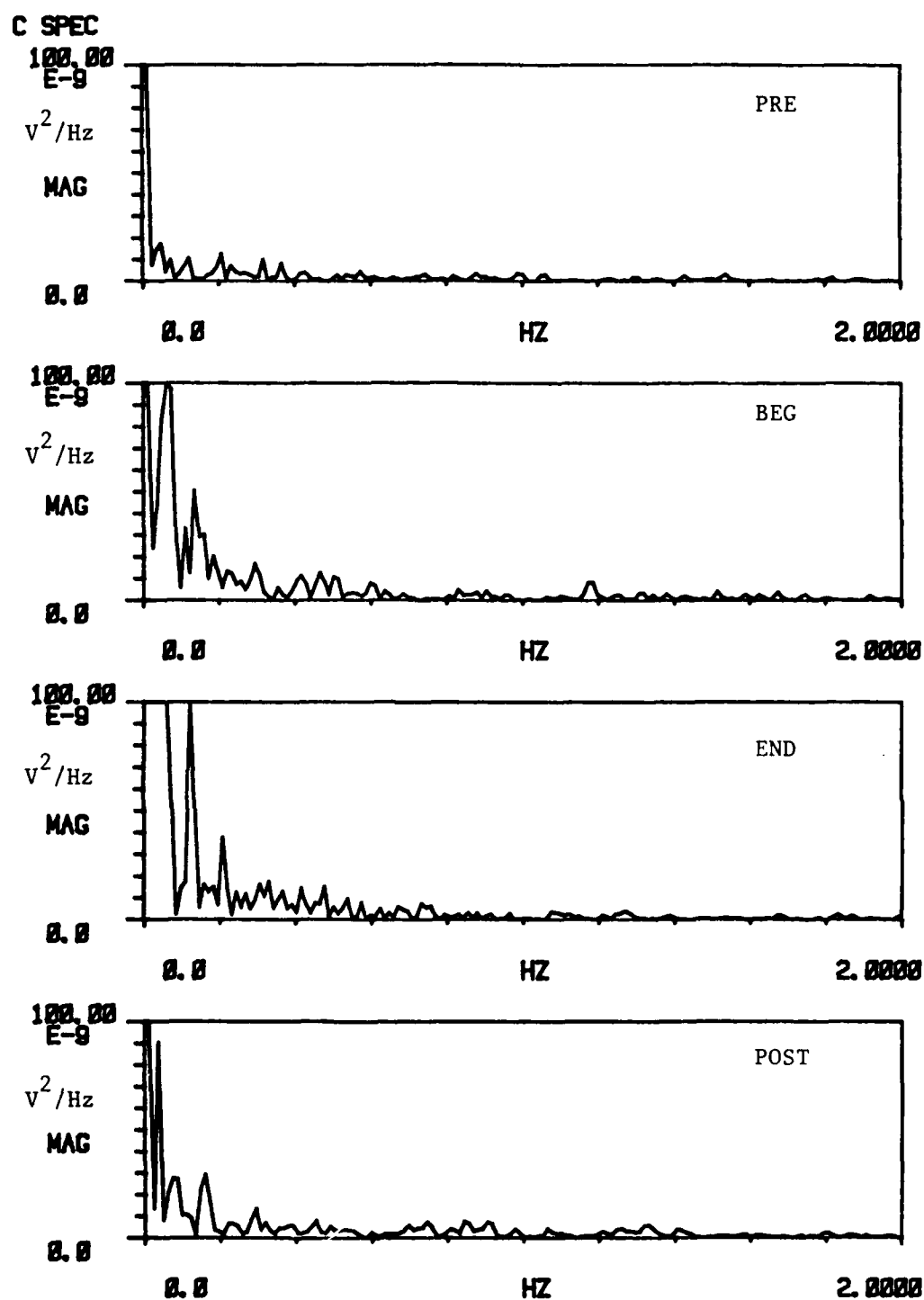Figure 15. Membrane-voltage-noise spectral densities for second 3-min SHAM exposure.

31

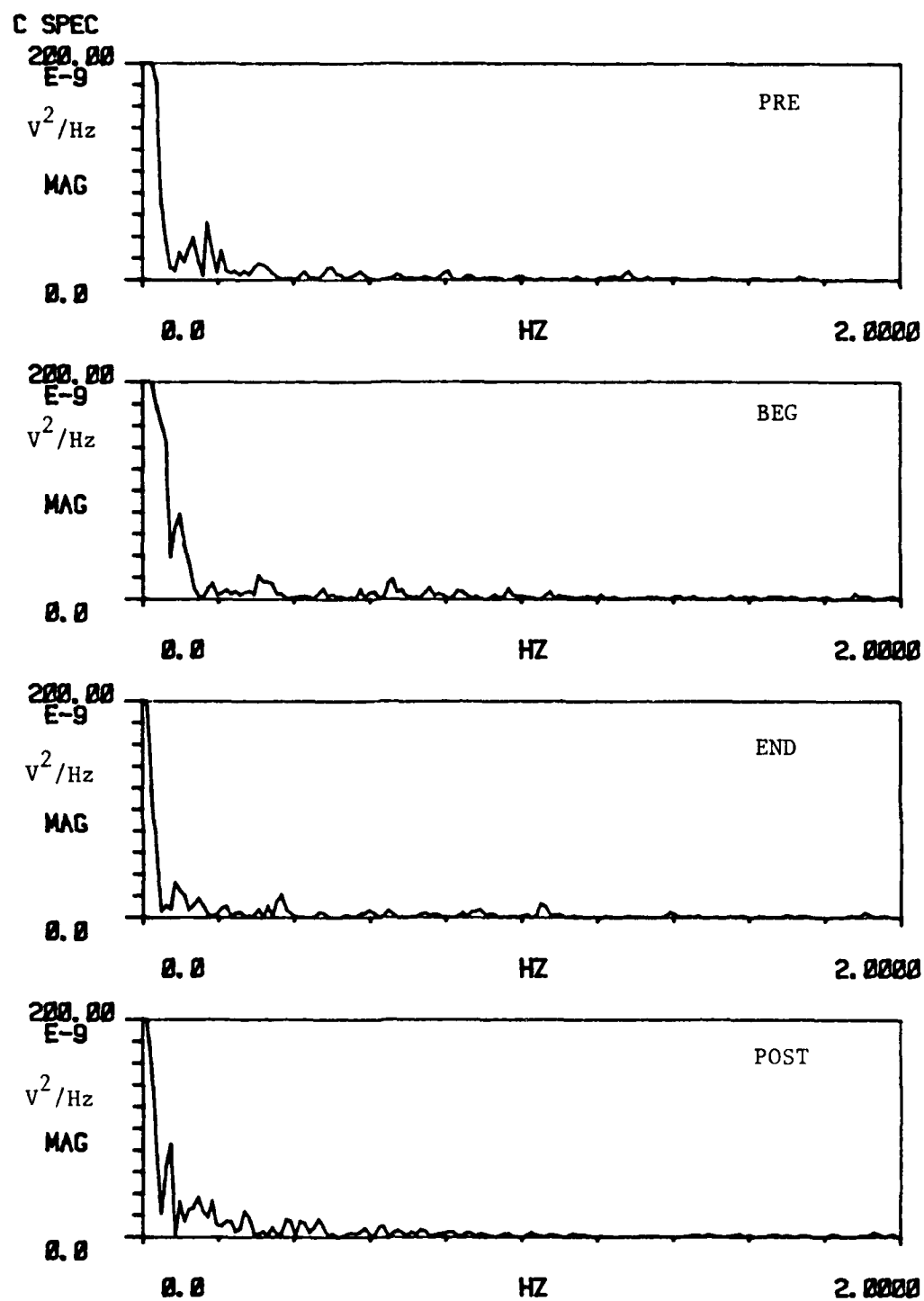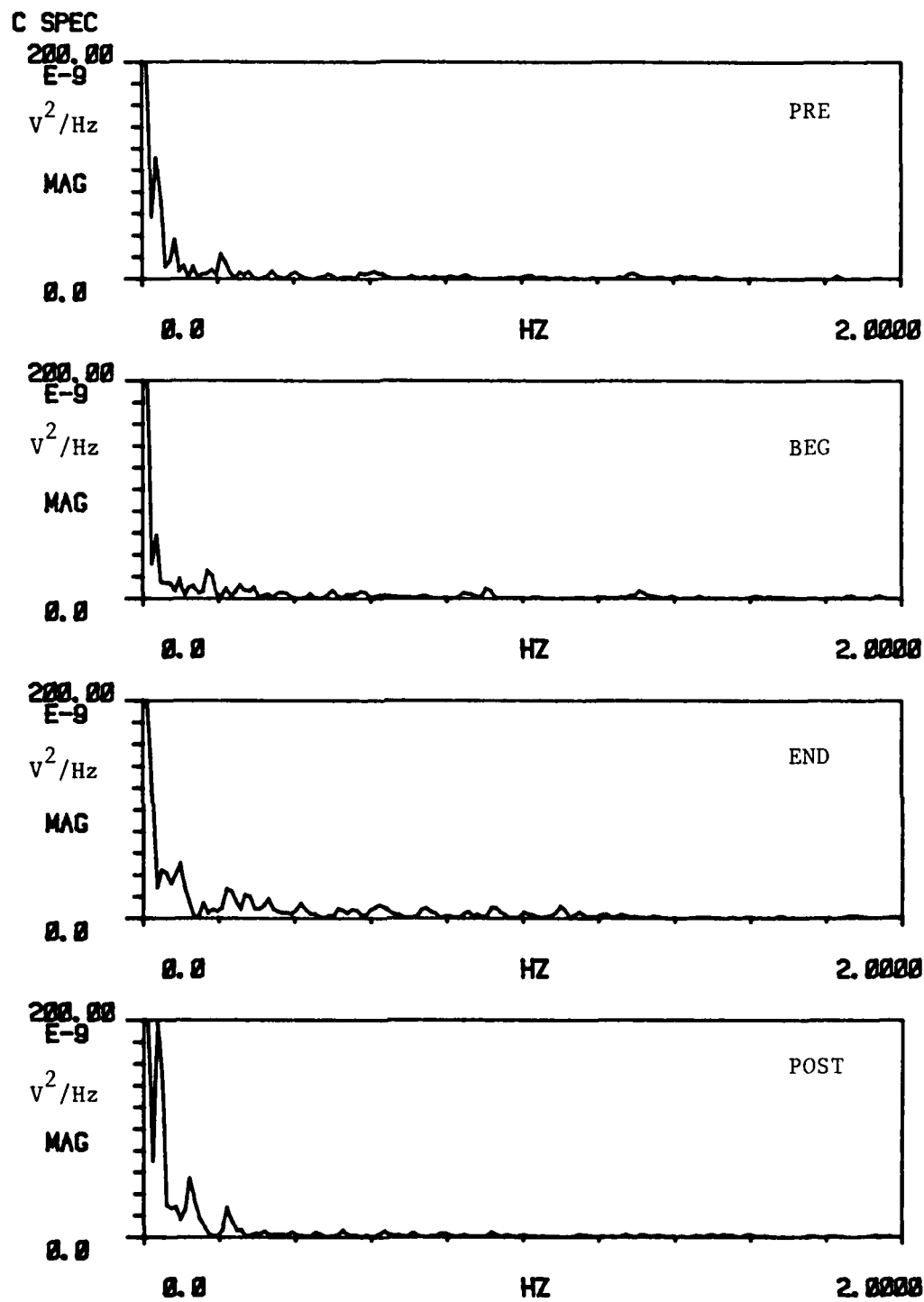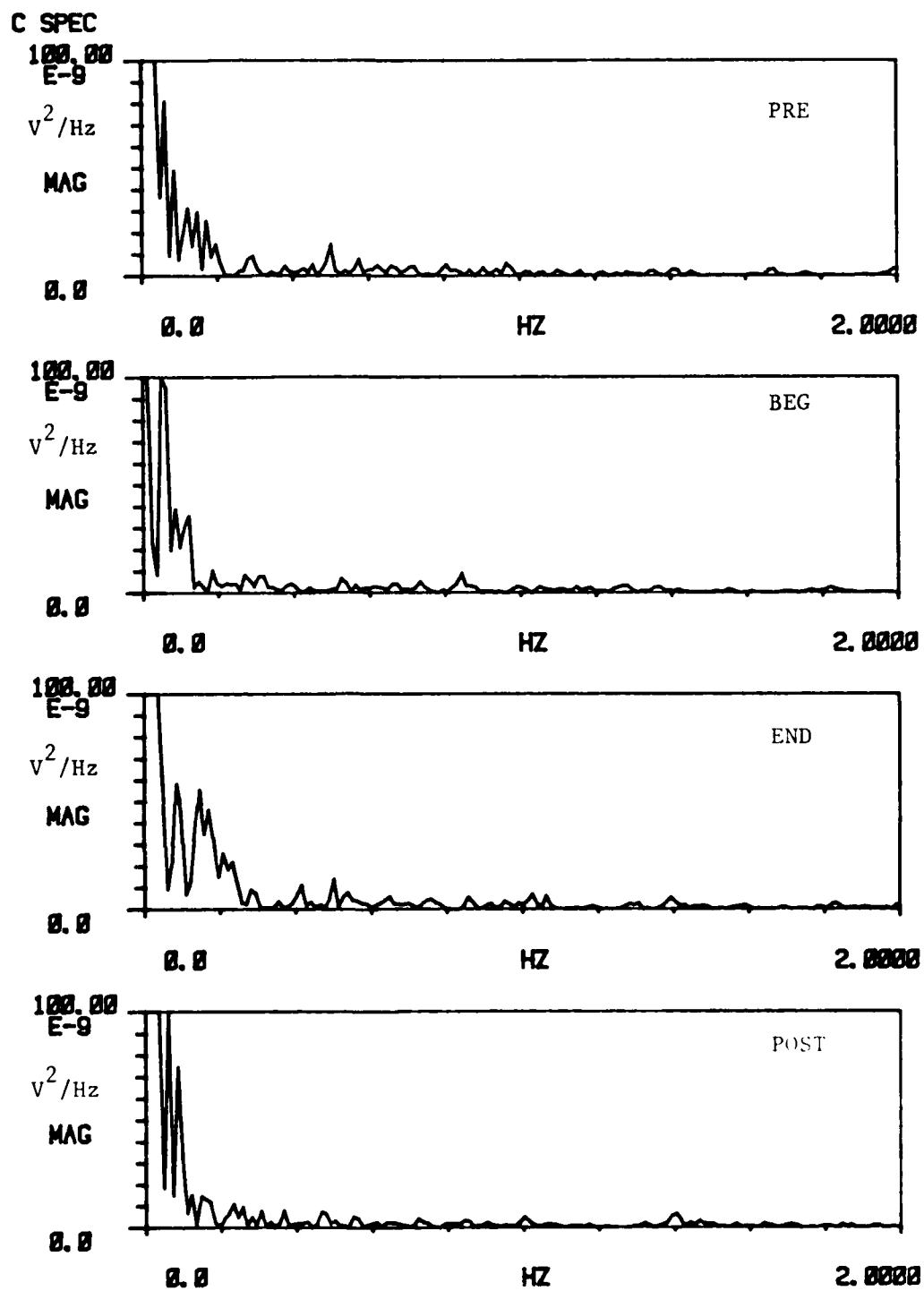Figure 16. Membrane-voltage-noise spectral densities for a third 3-min SHAM exposure.

Figure 17. Membrane-voltage-noise spectral densities for a 3-min exposure to 9.53-mW/g CW RFR.

33

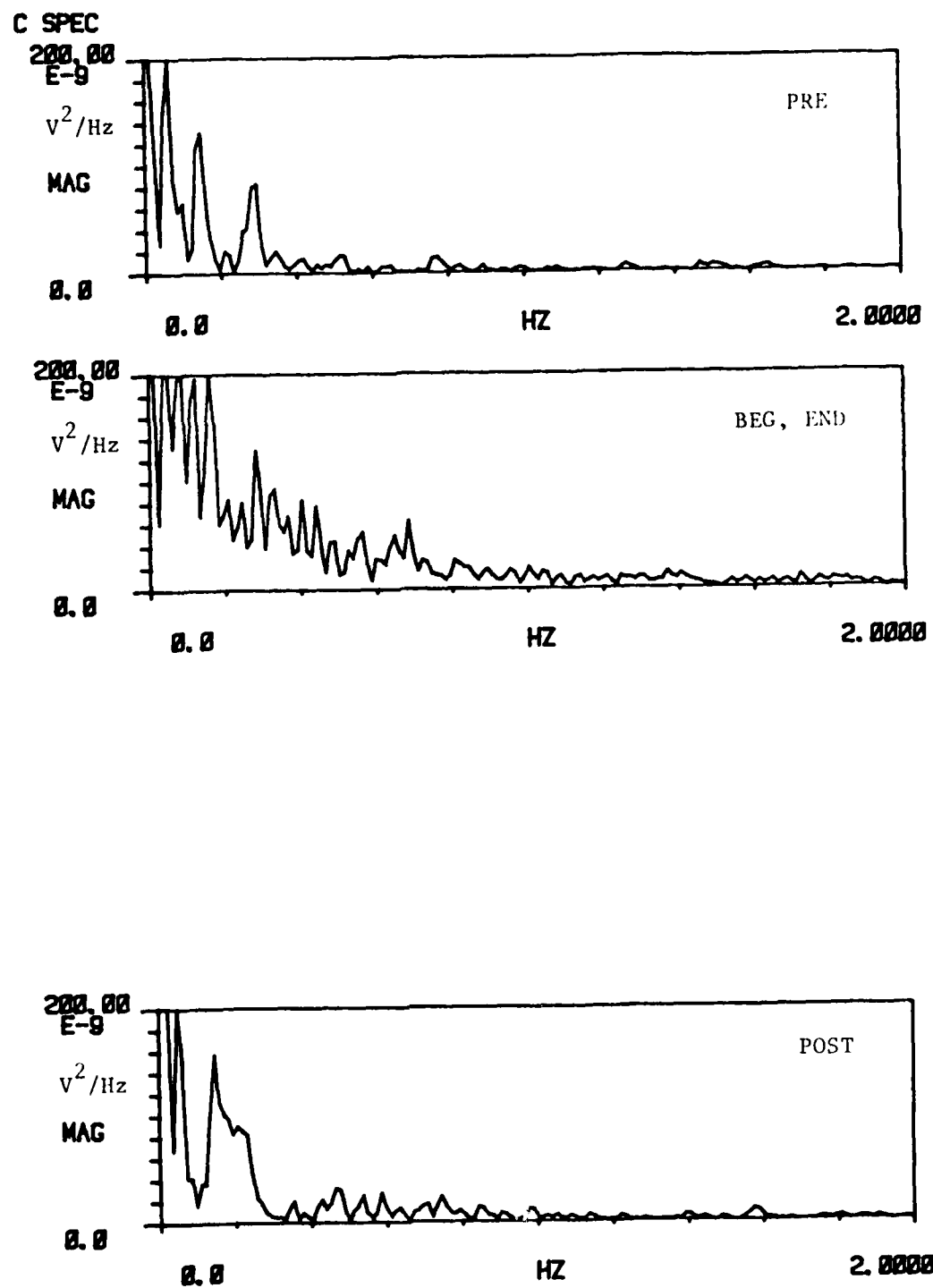Figure 18. Membrane-voltage-noise spectral densities for a 3-min exposure to 9.33-mW/g CW RFR.

Figure 19. Membrane-voltage-noise spectral densities for a 3-min exposure to 7.39-mW/g PW RFR.

Figure 20. Membrane-voltage-noise spectral densities for a 2-min exposure to 7.39-mW/g PW RFR.
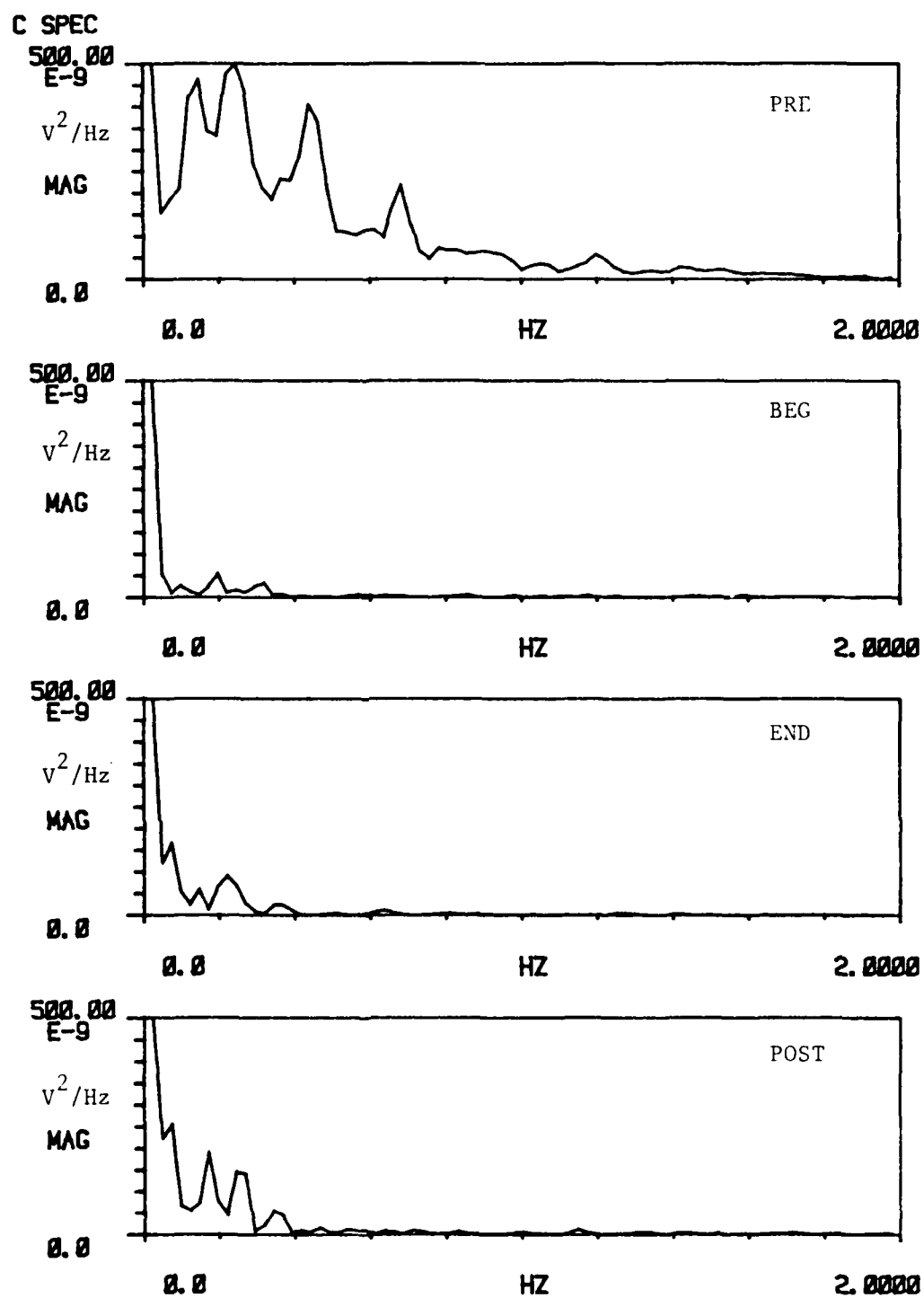
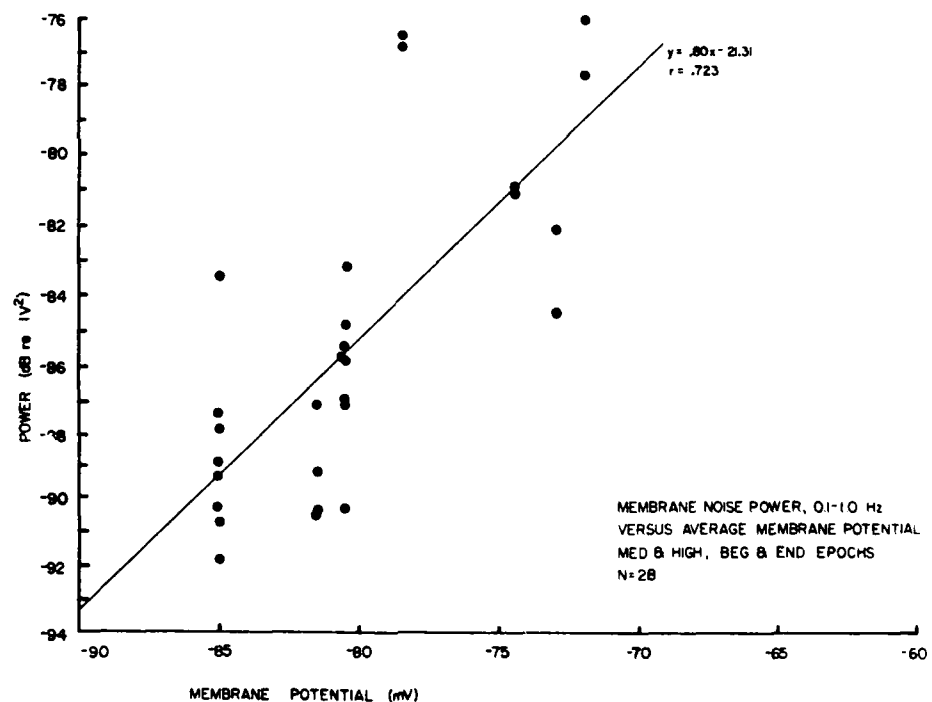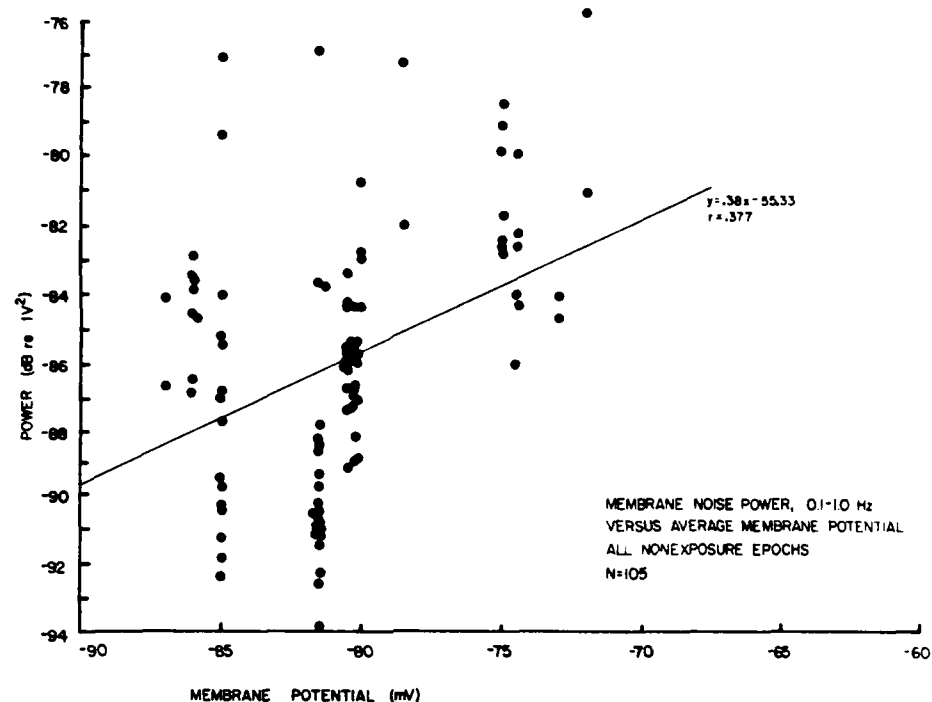Figure 21. Membrane-voltage-noise spectral densities for a 2-min SHAM exposure.

Figure 22. Plots of membrane voltage noise power (0.1-1.0 Hz) for 105 non-
exposure analysis epochs (top) and for 28 medium- and high-dose
analysis epochs (bottom) of aggregates in E818A medium. Regression
analysis of each set of data gave a line with the equation and
correlation coefficient shown.

The two regression lines for combinations 1 and 3 intersected very near a membrane potential of -81 mV. This meant that, on the average in these five experiments, CW RFR caused a decrease in noise power when membrane potential was more negative than -81 mV and an increase in noise power when membrane potential was more positive than -81 mV. Further experiments were then done, using 818A medium which gave resting membrane potentials in the -55 to -45 mV range, to explore increases in power and to increase the overall data base.

Two major statistical analyses were used on the combined data from E818A and 818A experiments. Based upon power differences (designated DIFF), the average power of SHAM-exposure (0 SAR) analysis epochs for an aggregate was subtracted from all other powers for that aggregate. This procedure eliminated much of the interaggregate variability. In another analysis, PRE power for each RFR exposure was subtracted from the subsequent BEG, END, and POST epochs for that exposure, emphasizing changes (designated CHANGE) in power. In each type of analysis, the powers were plotted against membrane potential and a least-squares regression analysis [31] was carried out to fit a straight line to the data for each RFR condition. Slopes of these regression lines were tested with two-tailed t-tests [22]. Slopes were considered significantly different if the t-test revealed a significance level of 0.05 or less. In some cases, two-tailed t-tests of means were performed with the same criteria.

Figures 23 through 28 show the DIFF analysis for 3-min RFR exposures. Slopes for BEG, END, and POST epochs were not significantly different from the respective PRE slope for 1-5 and 5-15 mW/g CW (Figs. 23 and 24). The BEG (and only BEG) slope significantly differed from the PRE slope for 15-30 mW/g CW (t=2.623, df=36; Fig. 25). For the highest CW levels (100-200 mW/g), the BEG, END, and POST slopes again did not significantly differ from the PRE slope (Fig. 26). In this last case of high SAR, the BEG t=1.423 (with df=22) is significant only at the 0.20 level. For 5-15 and 15-30 mW/g PW (Figs. 27 and 28), the BEG, END, and POST slopes did not differ significantly from the respective PRE slope at the 0.05 level. In Figure 28, one data point for 43.8-mW/g PW is shown but was not used in the statistical analysis. For 3-min SHAM exposures (Fig. 29), the BEG (and only BEG) slope was significantly different from the PRE slope; t=2.258, df=80.

Figures 30 through 36 show the CHANGE analysis for 3-min exposures at 1-5, 5-15, 15-30, and 100-200 mW/g CW; 5-15 and 15-30 mW/g PW; and SHAM respectively. In Figure 33, data points shown for 231-mW/g CW were not used in statistical analyses. In Figure 35, a data point shown for 43.8-mW/g PW was not used in statistical analysis. For CHANGE, BEG, and END, slopes were tested against the slope for that SAR's POST epoch, taken as a chronologically close non-RFR epoch. In addition, BEG, END, and POST slopes were tested for each SAR against the same analysis epoch for SHAM exposures (Fig. 36). No significant differences were found in slopes in tests using an SAR's own POST epoch. In tests against SHAM analysis epochs, the 1-5 mW/g CW BEG slope was significantly different from the SHAM BEG slope; t=-2.122, df=59. The END and POST slopes of 5-15 mW/g PW were different from SHAM epochs at the 0.10 level with t=1.936 and 1.886 and df=45 and 42; the critical t to be exceeded was about 2.016. The POST slope of 15-30 mW/g PW also was different from the SHAM POST slope at the 0.10 level; t=1.7735, df=39.
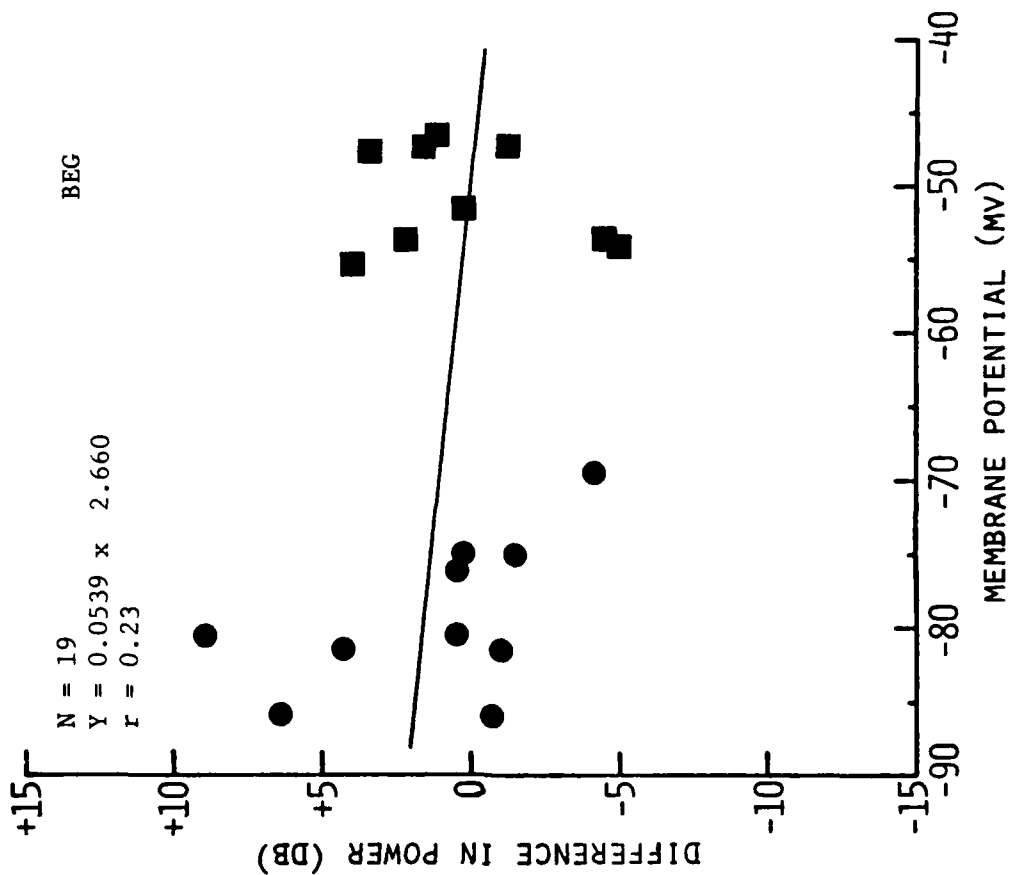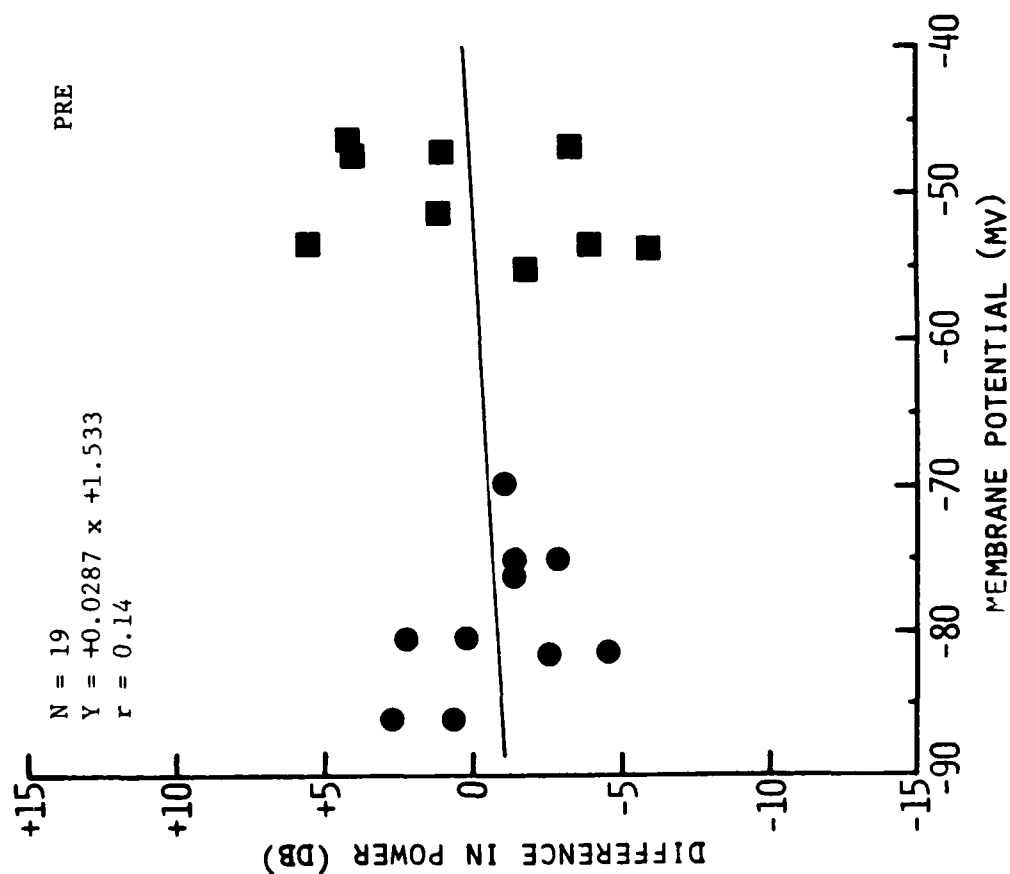
Figure 23A. DIFF analysis of membrane voltage noise power for 3-min 1-5 mW/g CW RFR exposures.
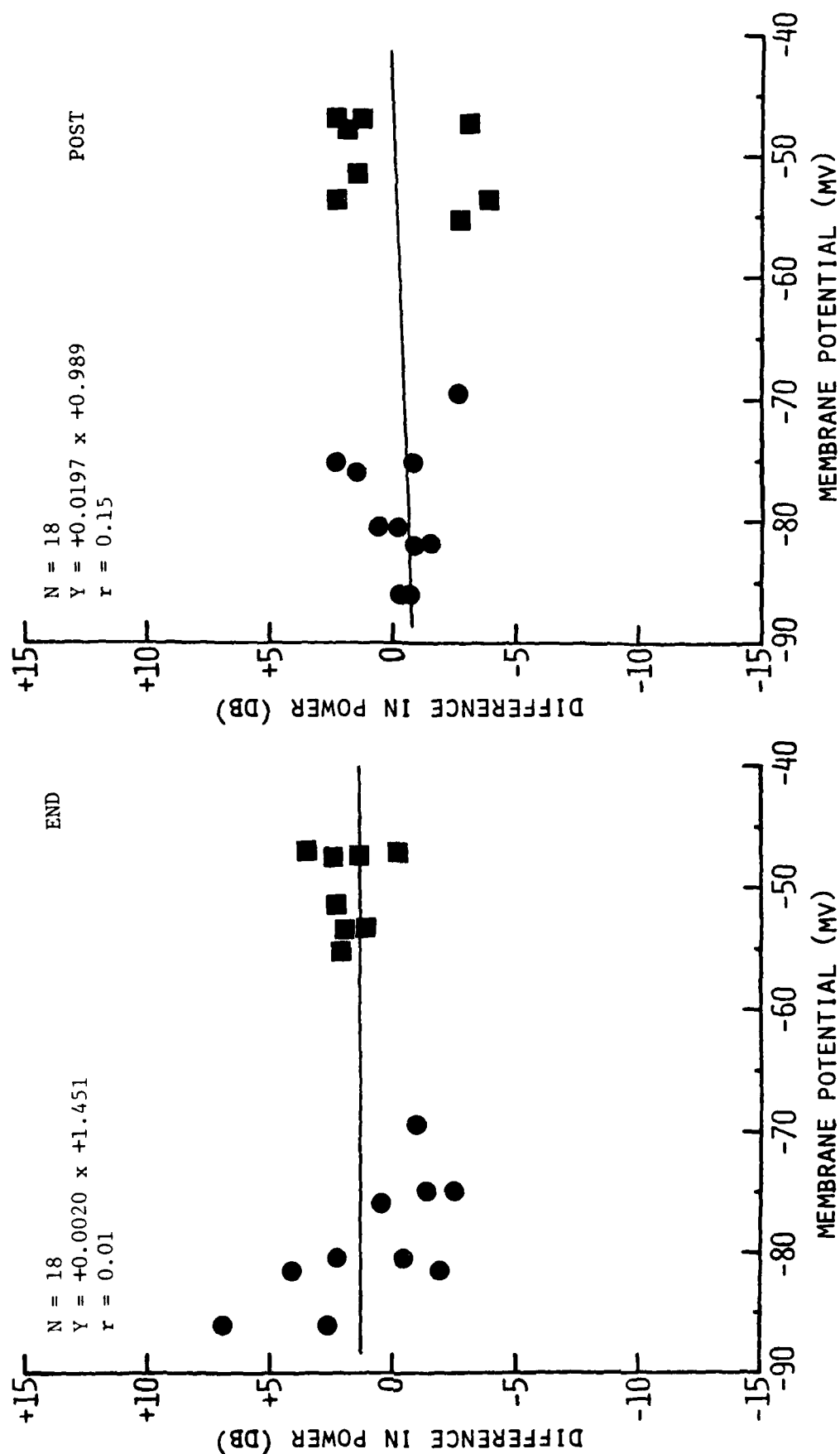
40

Figure 23B. DIFF analysis of membrane voltage noise power for 3-min 1-5 mW/g CW RFR exposures.
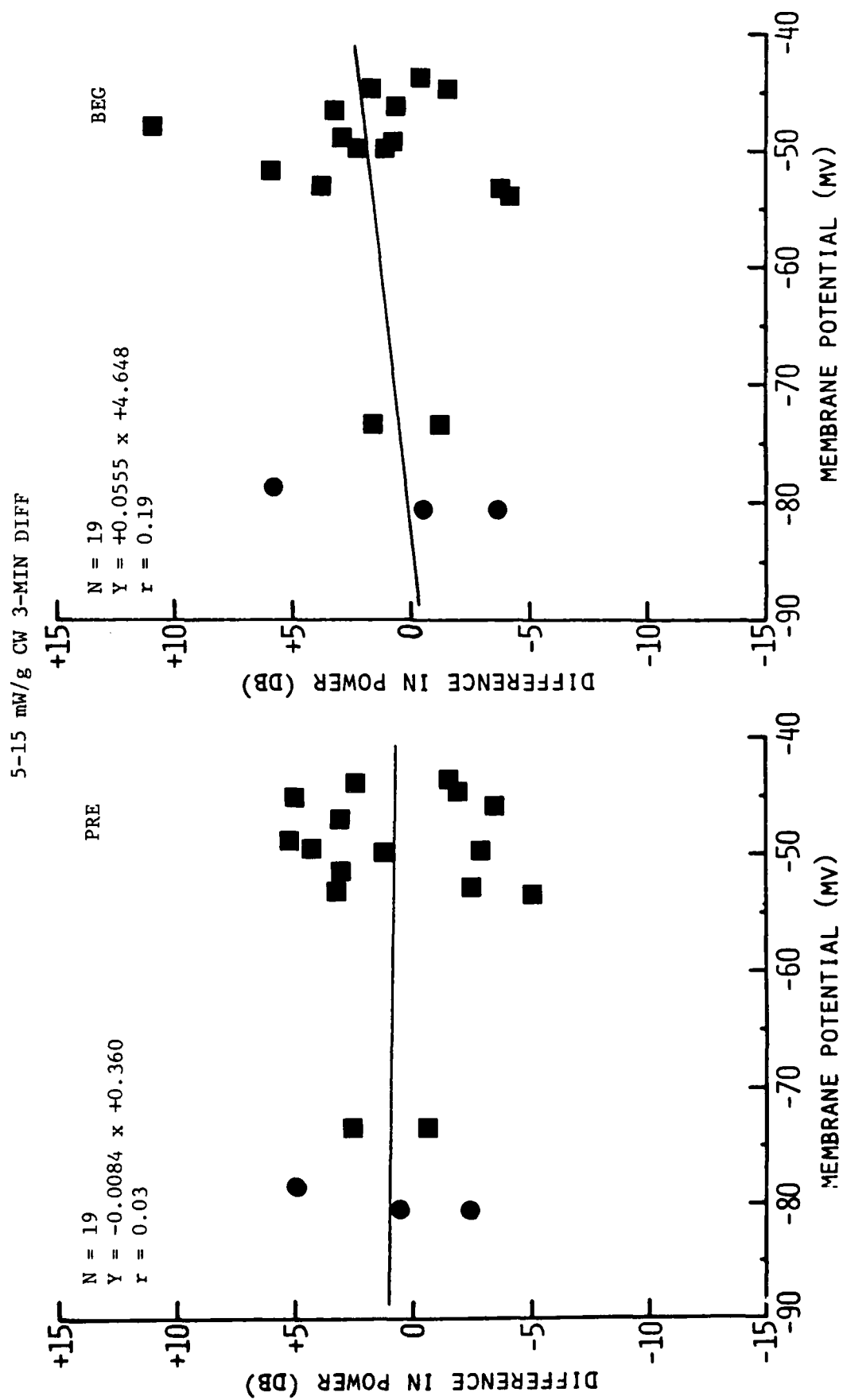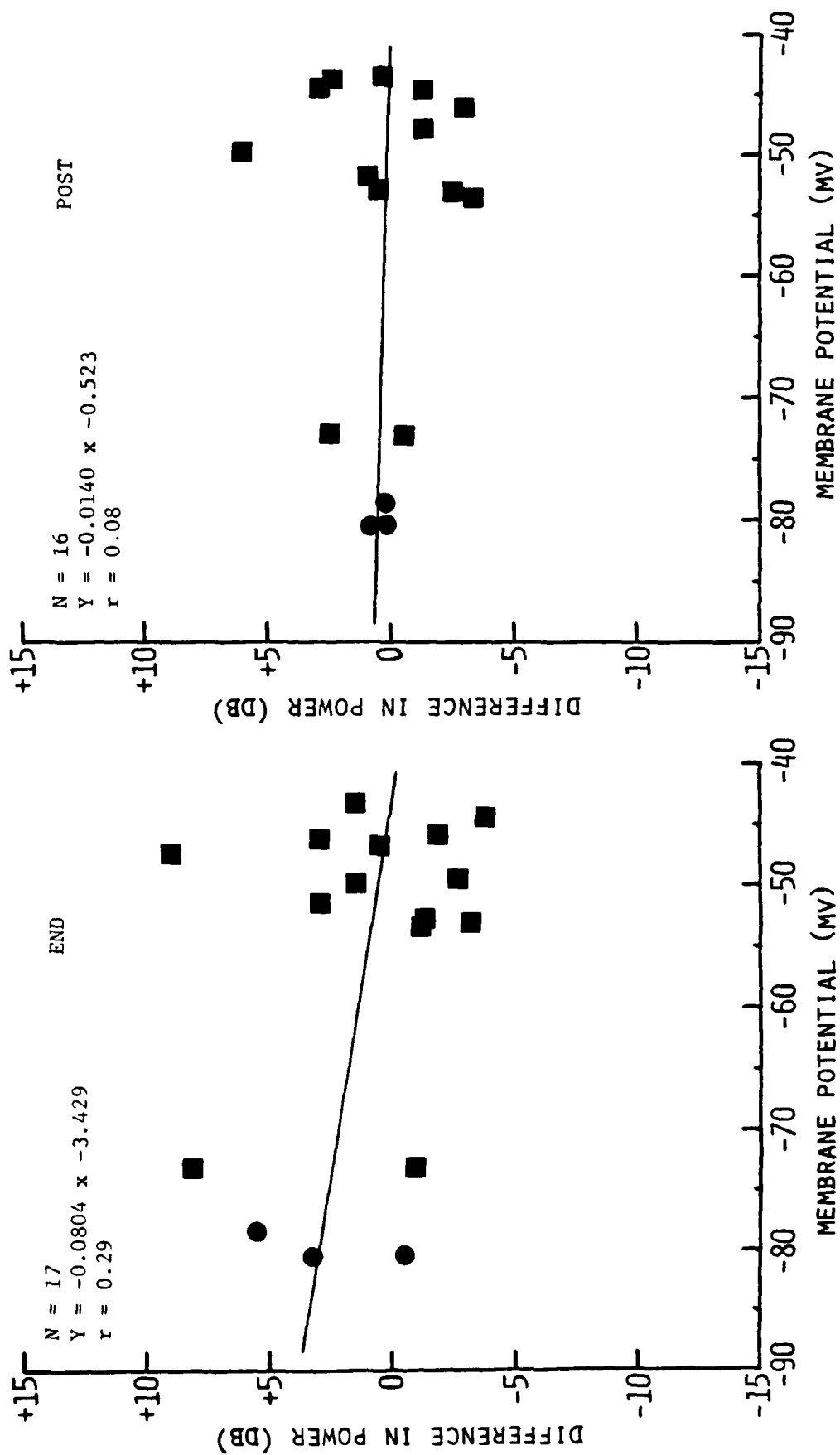
41

Figure 24A. DIFF analysis of membrane voltage noise power for 3-min 5-15 mW/g CW RFR exposures.

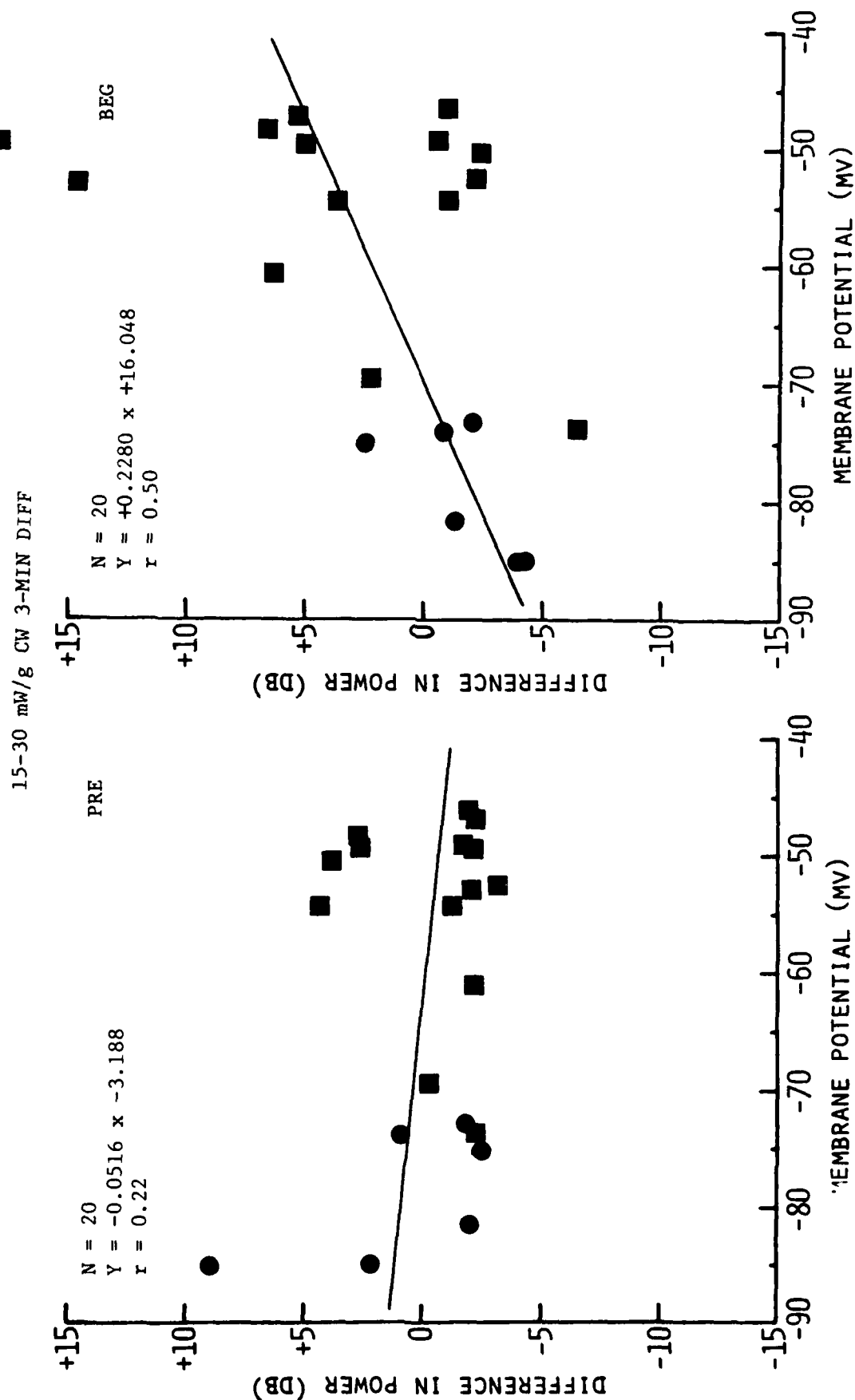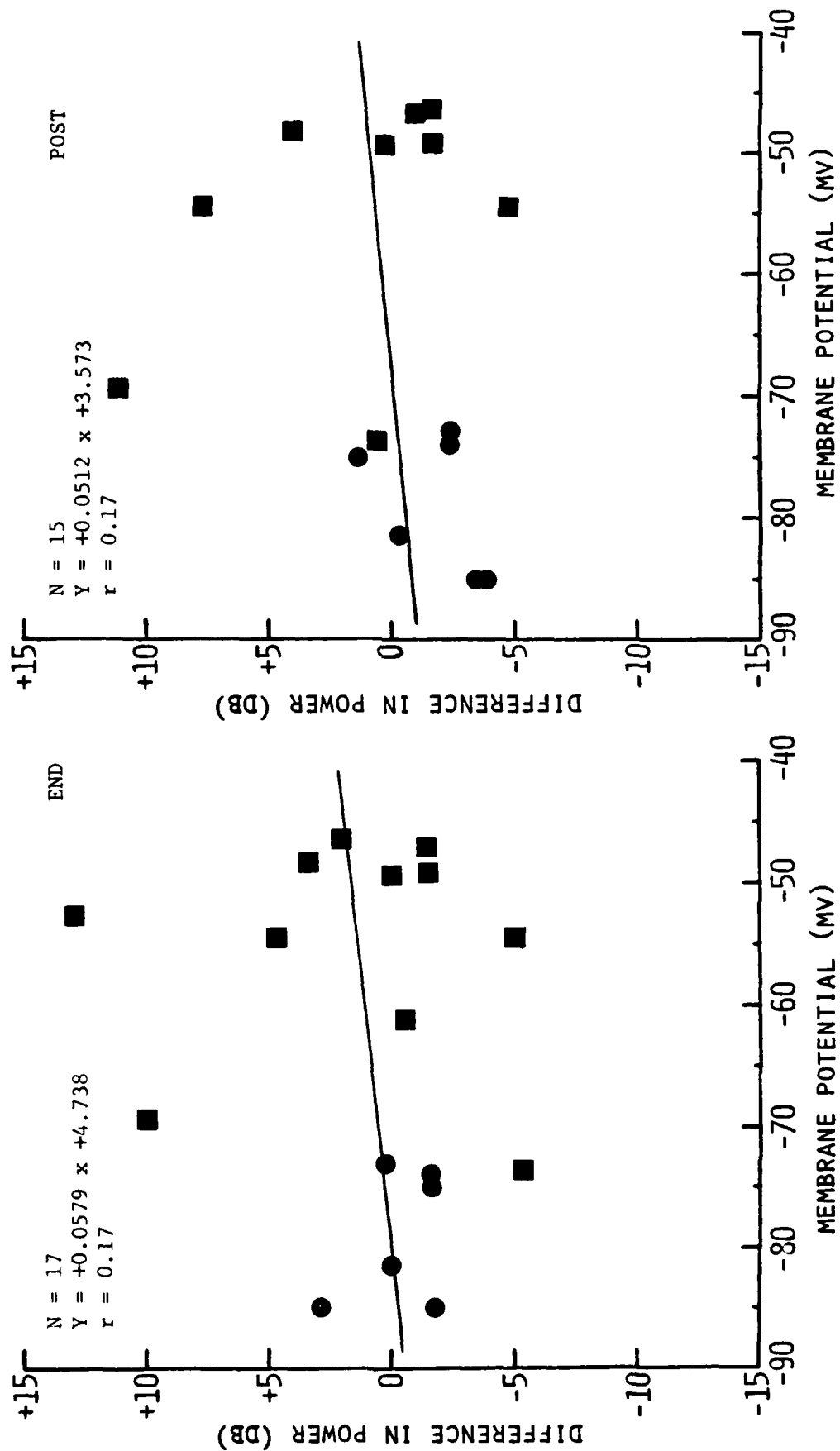Figure 24B. DIFF analysis of membrane voltage noise power for 3-min 5-15 mW/g CW RFR exposures.

43

15-30 mW/g CW 3-MIN DIFF

BEG

N = 20
Y = +0.2280 x +16.048
r = 0.50

DIFFERENCE IN POWER (DB)

MEMBRANE POTENTIAL (MV)

PRE

N = 20
Y = -0.0516 x -3.188
r = 0.22

DIFFERENCE IN POWER (DB)

MEMBRANE POTENTIAL (MV)

Figure 25A. DIFF analysis of membrane voltage noise power for 3-min 15-30 mW/g CW RFR exposures.

44

Figure 25B. DIFF analysis of membrane voltage noise power for 3-min 15-30 mW/g CW RFR exposures.
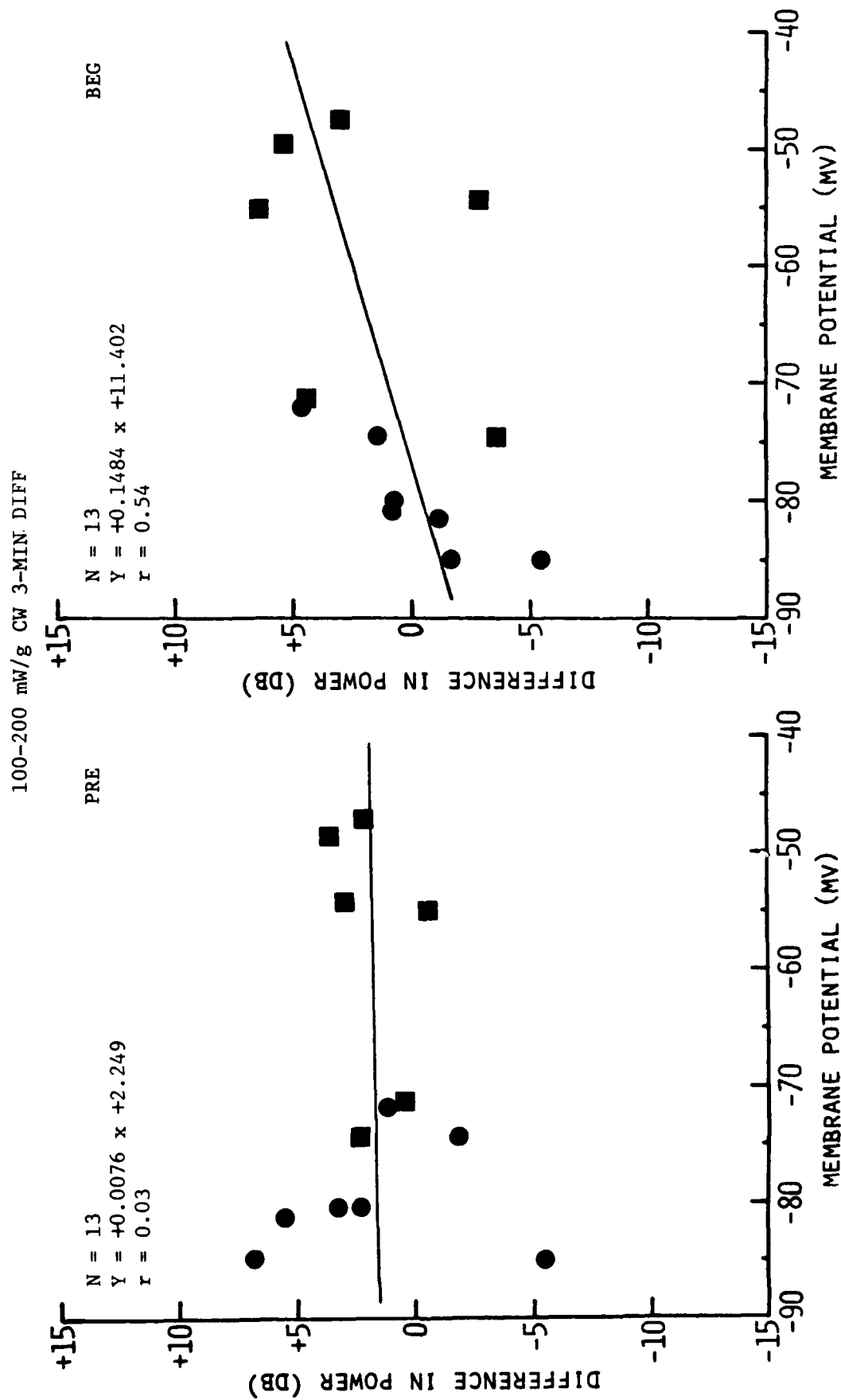
Figure 26A. DIFF analysis of membrane voltage noise power for 3-min 100-200 mW/g CW RFR exposures.
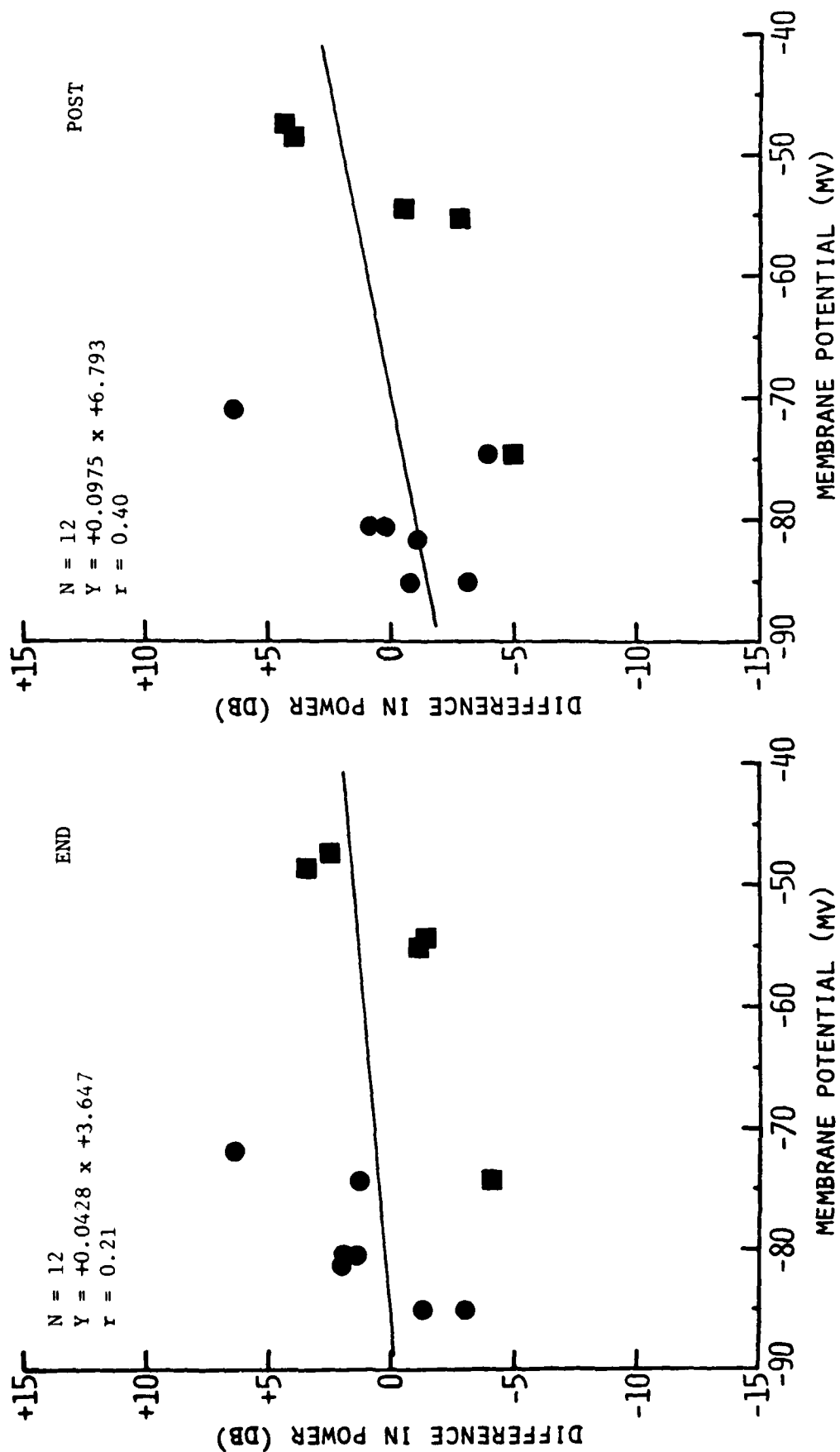
Figure 26B. DIFF analysis of membrane voltage noise power for 3-min 100-200 mW/g CW RFR exposures.
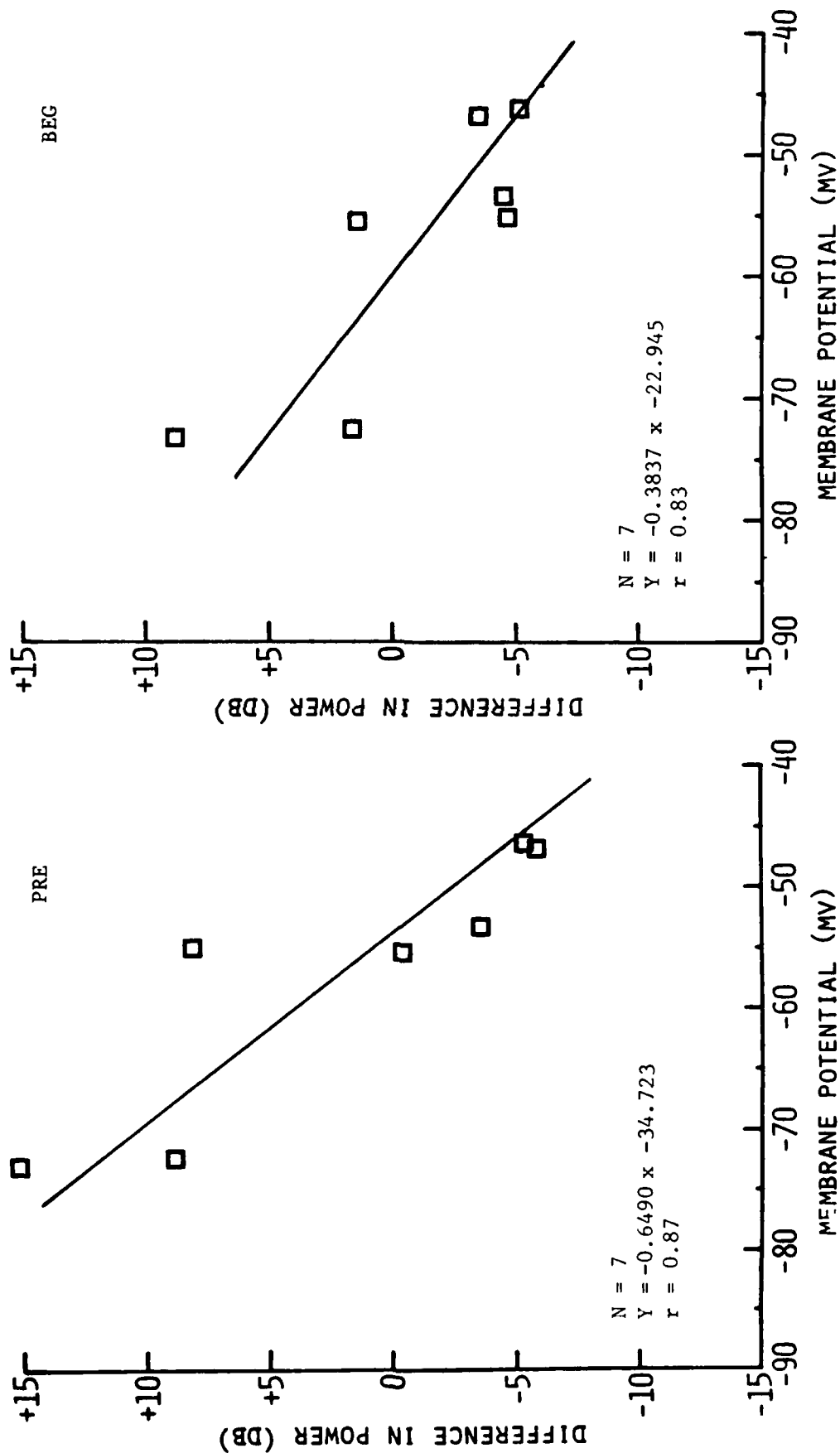
47

Figure 27A. DIFF analysis of membrane voltage noise power for 3-min 5-15 mW/g PW RFR exposures.

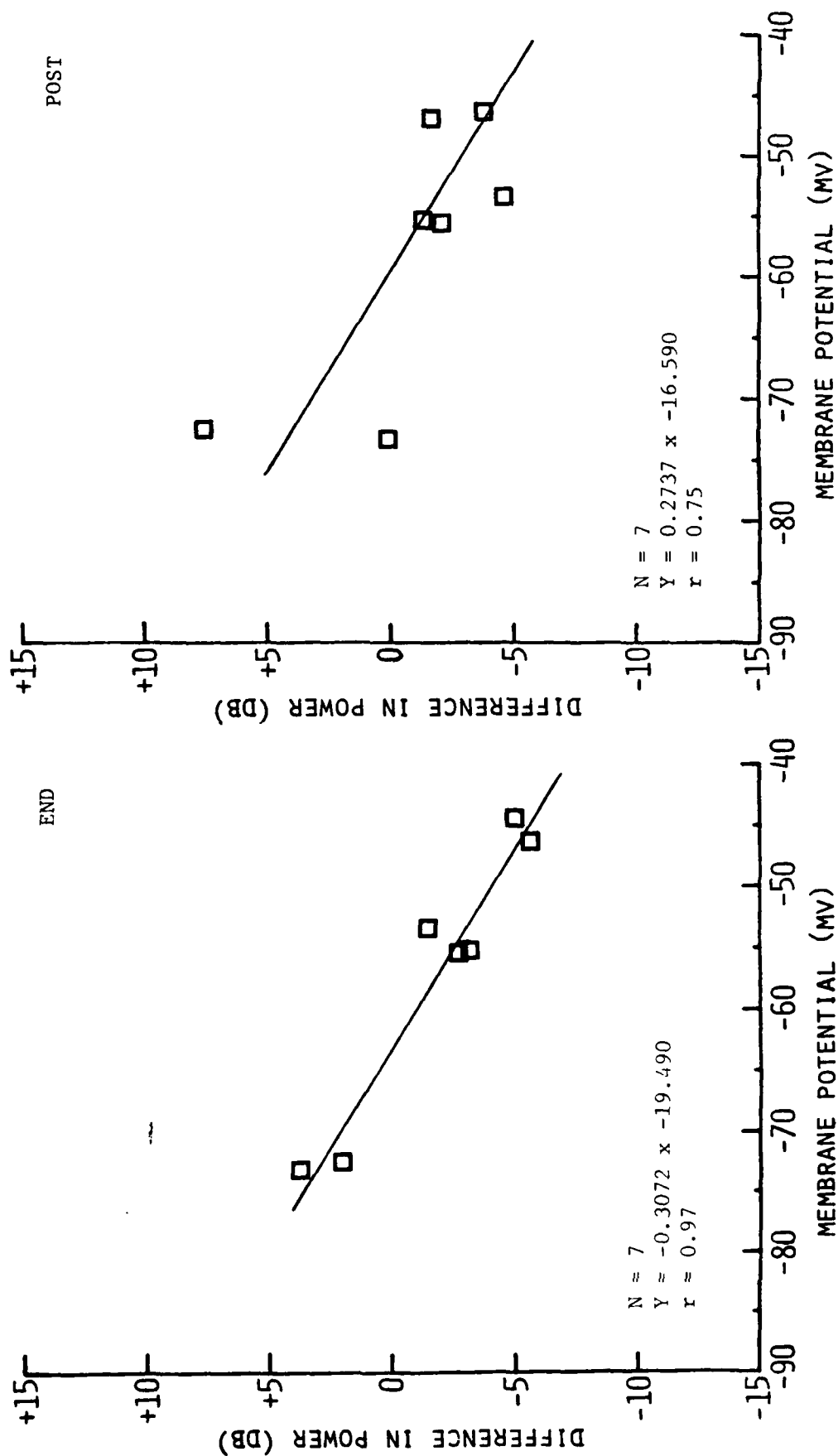Figure 27B. DIFF analysis of membrane voltage noise power for 3-min 5-15 mW/g PW RFR exposures.
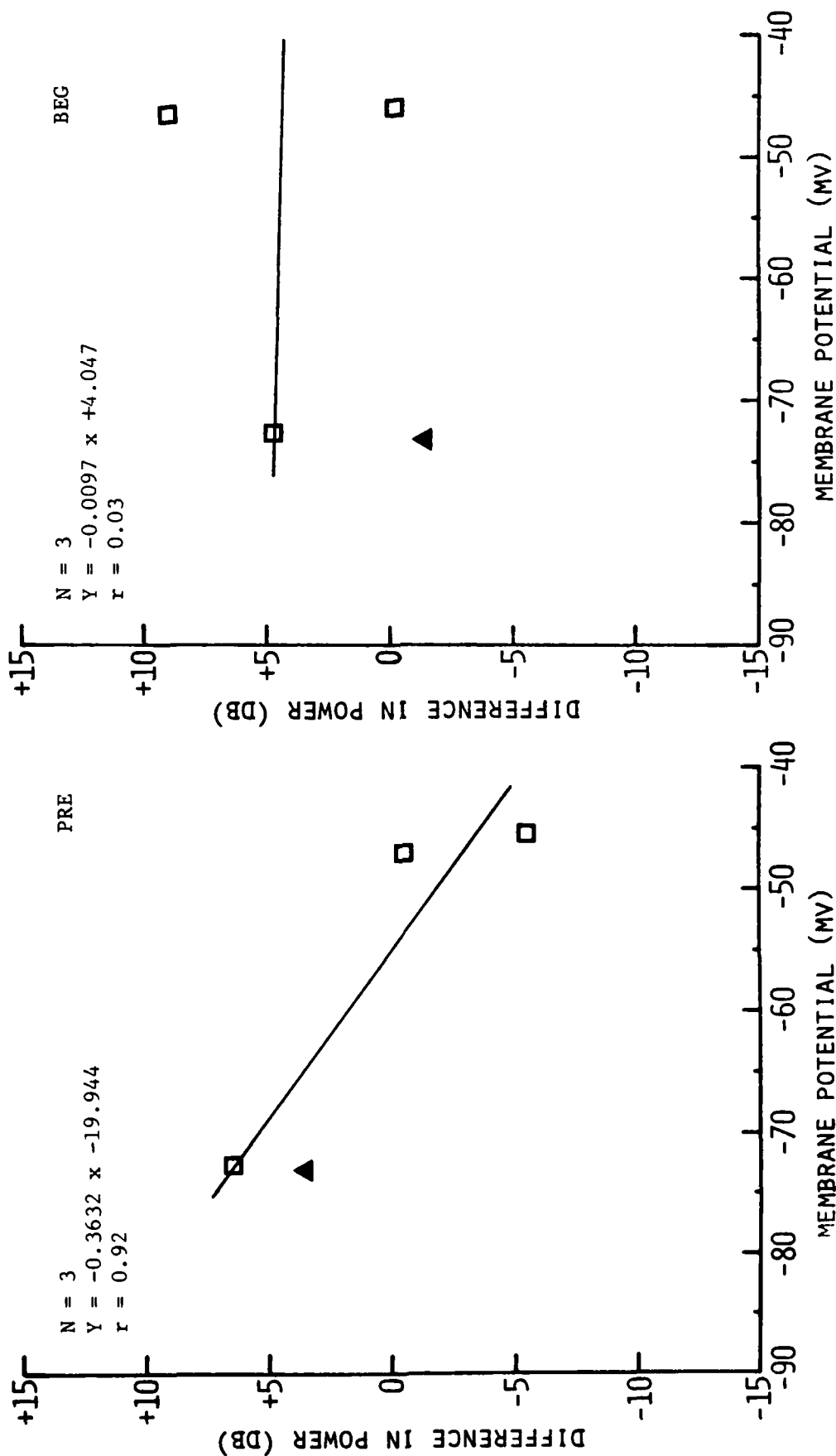
49

Figure 28A. DIFF analysis of membrane voltage noise power for 3-min 15-30 mW/g PW RFR exposures. Triangles represent data from one exposure of 43.8-mW/g PW RFR.
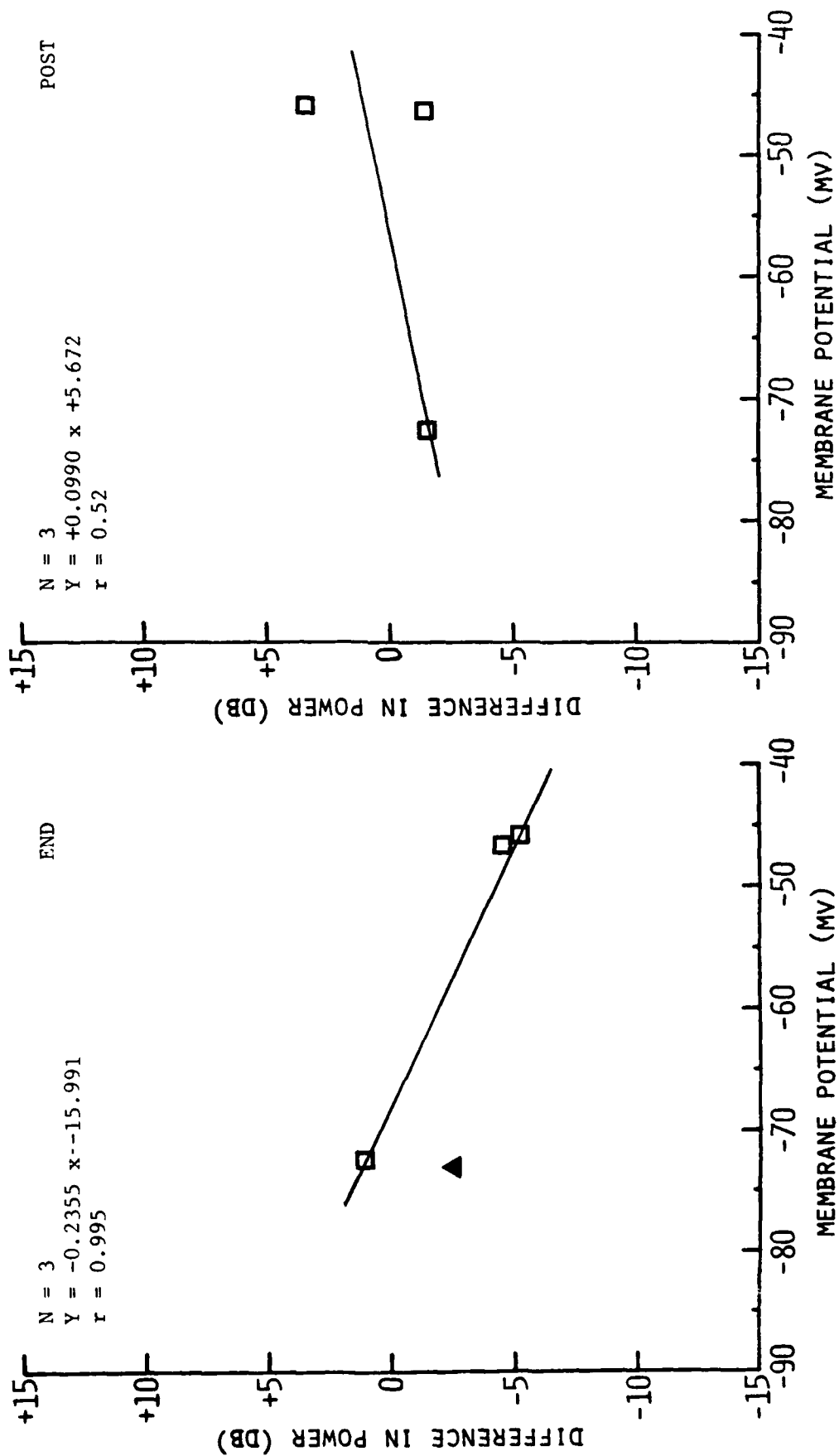
Figure 28B. DIFF analysis of membrane voltage noise power for 3-min 15-30 mW/g PW RFR exposures. Triangles represent data from one exposure of 43.8-mW/g PW RFR.
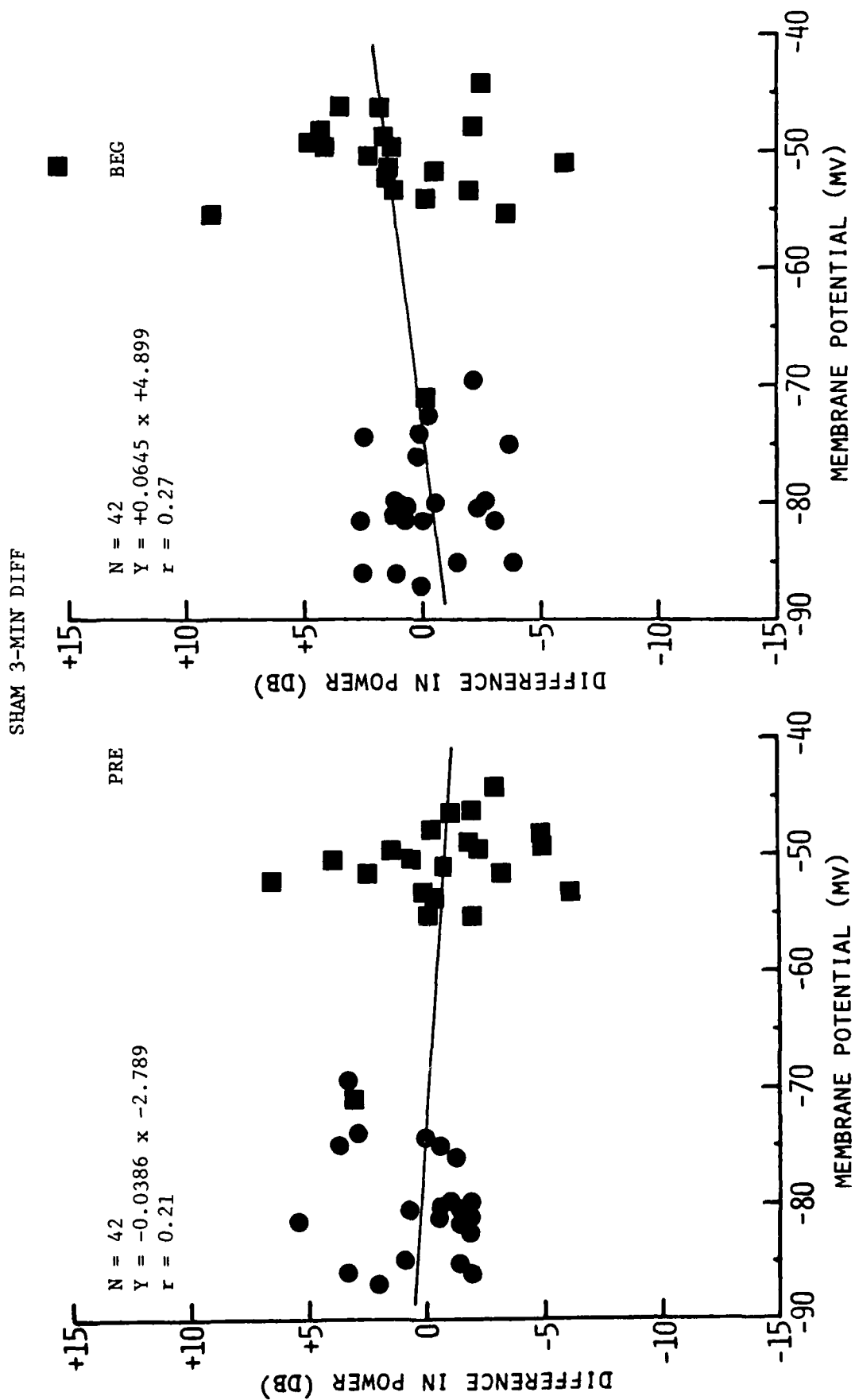
51

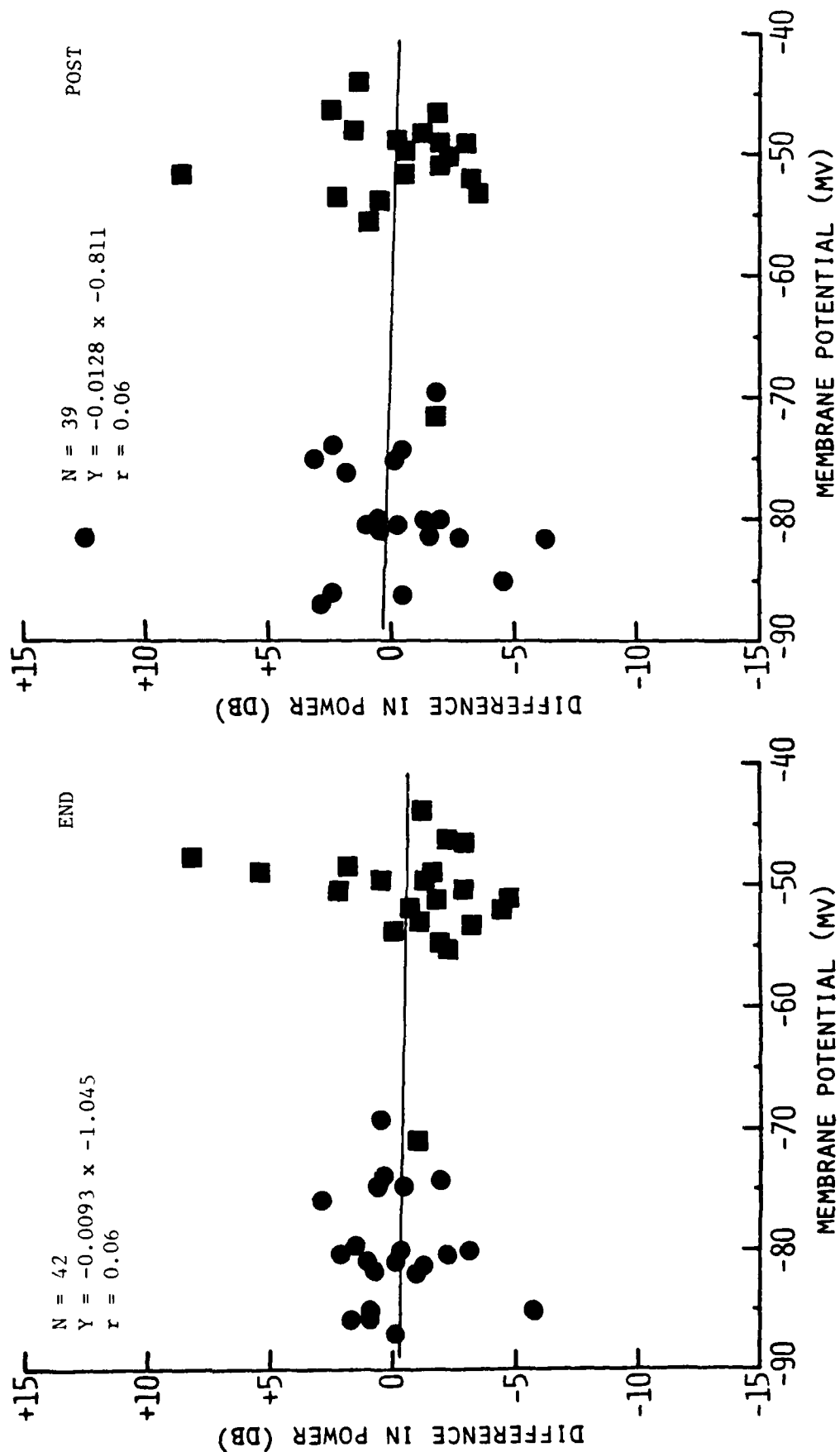Figure 29A. DIFF analysis of membrane voltage noise power for 3-min SHAM exposures.

52

Figure 29B. DIFF analysis of membrane voltage noise power for 3-min SHAM exposures.

53

Figure 30A. CHANGE analysis of membrane voltage noise power for 3-min 1-5 mW/g CW RFR exposures.

Figure 30B. CHANGE analysis of membrane voltage noise power for 3-min 1-5 mW/g CW RFR exposures.

55

5-15 mW/g CW 3-MIN CHANGE

N = 20
Y = +0.0653 x +4.403
r = 0.26

BEG

CHANGE IN POWER (DB)

MEMBRANE POTENTIAL (MV)

MEMBRANE POTENTIAL (MV)

CHANGE IN POWER (DB)

Figure 31A. CHANGE analysis of membrane voltage noise power for 3-min 5-15 mW/g CW RFR exposures.

56

Figure 31B. CHANGE analysis of membrane voltage noise power for 3-min 5-15 mW/g CW RFR exposures.

POST

N = 16
Y = +0.0073 x +0.1293
r = 0.03

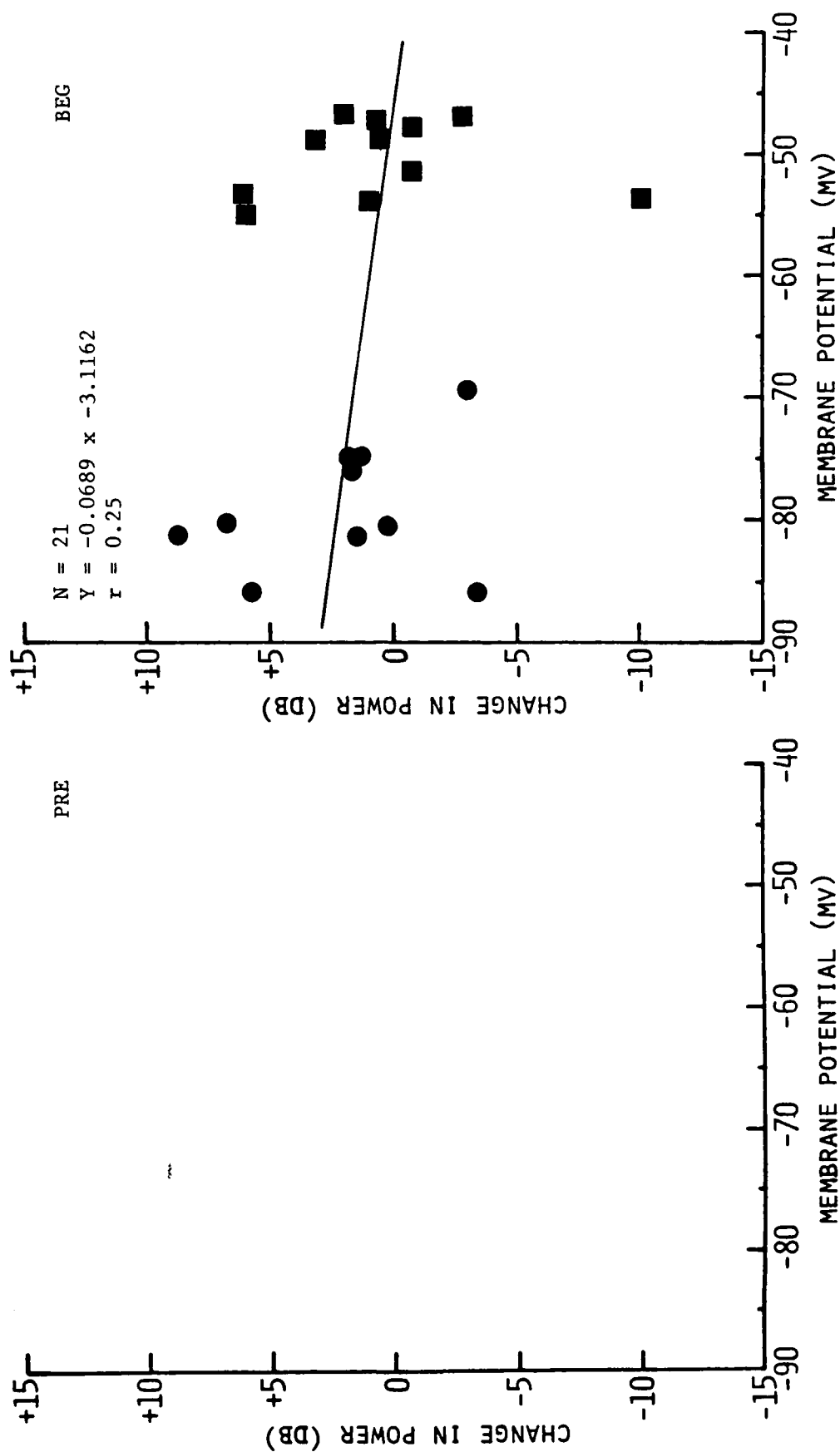END

N = 18
Y = -0.0347 x -0.808
r = 0.13

57

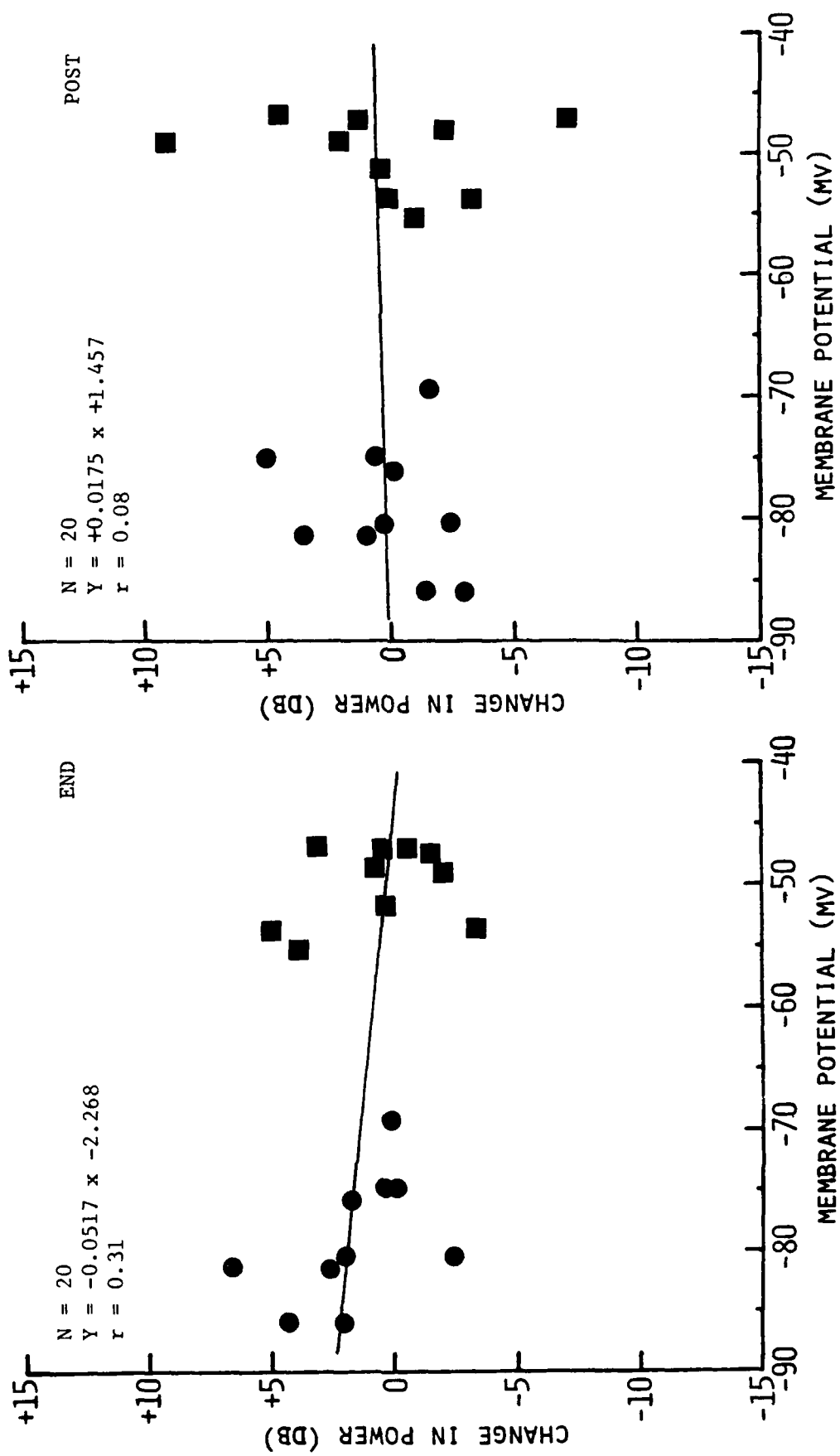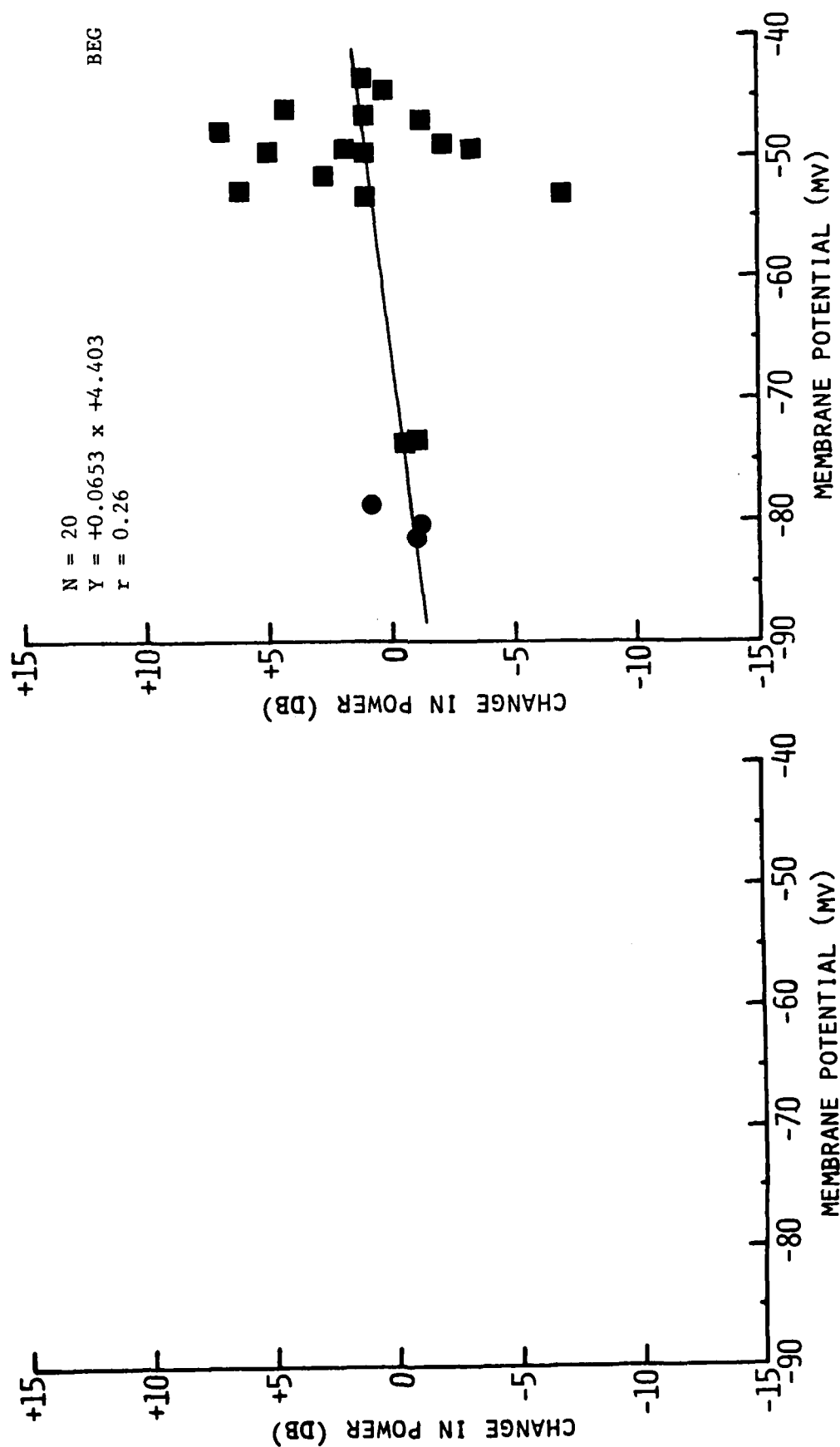Figure 32A. CHANGE analysis of membrane voltage noise power for 3-min 15-30 mW/g CW RFR exposures.

Figure 32B. CHANGE analysis of membrane voltage noise power for 3-min 15-30 mW/g CW RFR exposures.

Figure 33A. CHANGE analysis of membrane voltage noise power for 3-min 100-200 mW/g CW RFR exposures.

60

Figure 33B. CHANGE analysis of membrane voltage noise power for 3-min 100-200 mW/g CW RFR exposures. Triangles represent data from two exposures of 231 mW/g CW RFR.
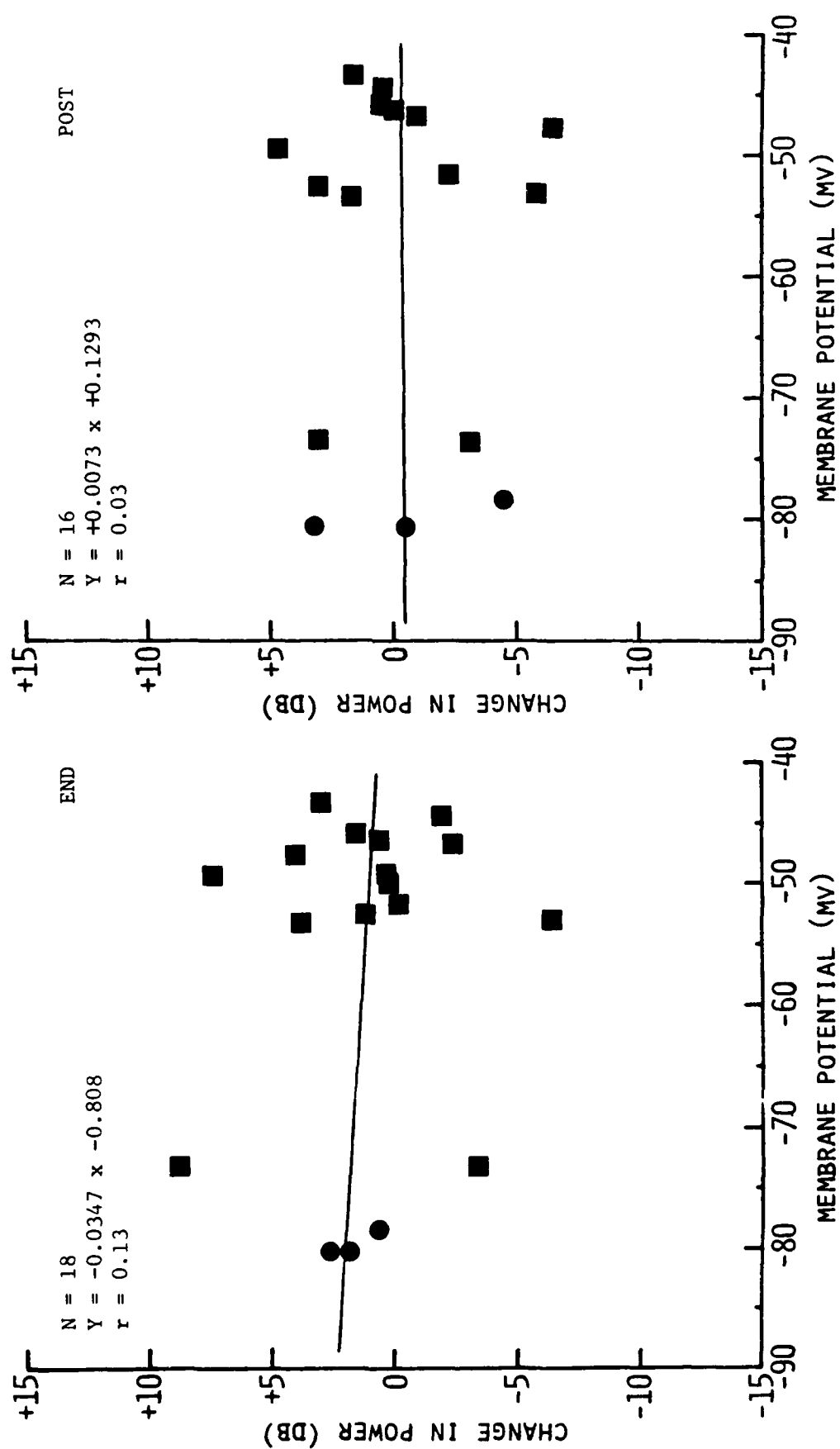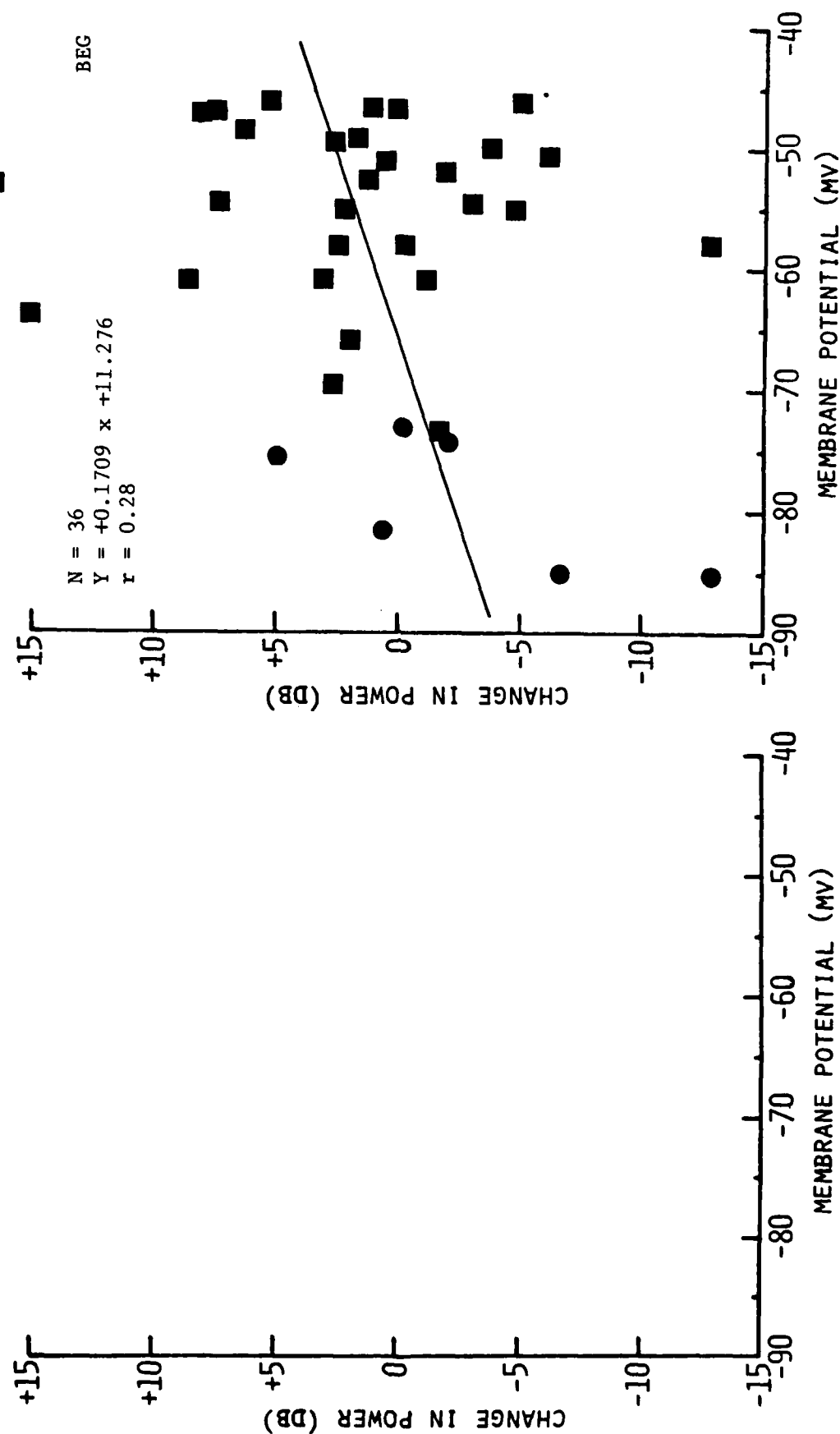
Figure 34A. CHANGE analysis of membrane voltage noise power for 3-min 5-15 mW/g PW RFR exposures.
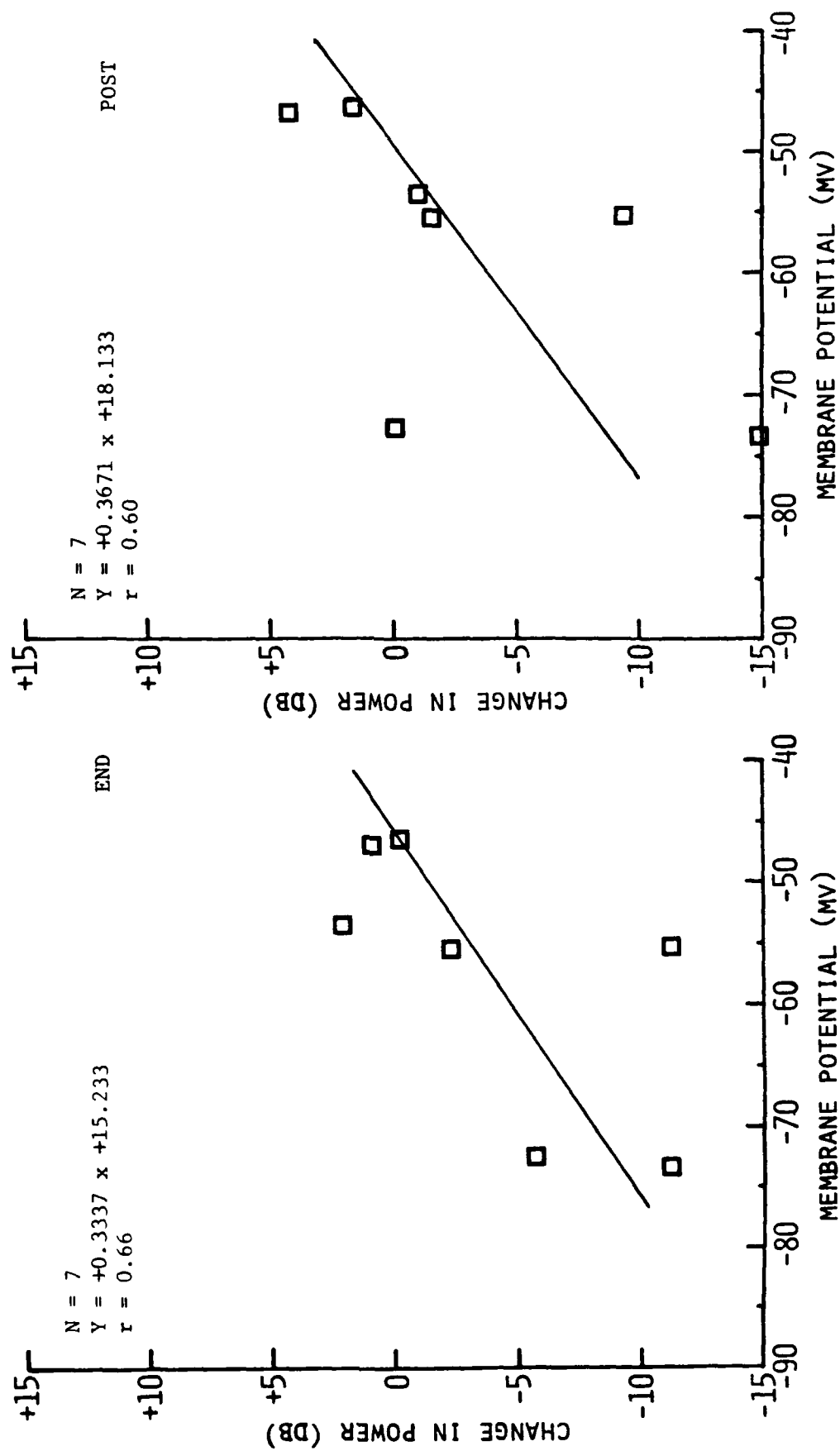
5-15 mW/g PW 3-MIN CHANGE

BEG

N = 7
Y = +0.2572 x +11.778
r = 0.51

CHANGE IN POWER (DB)

MEMBRANE POTENTIAL (MV)
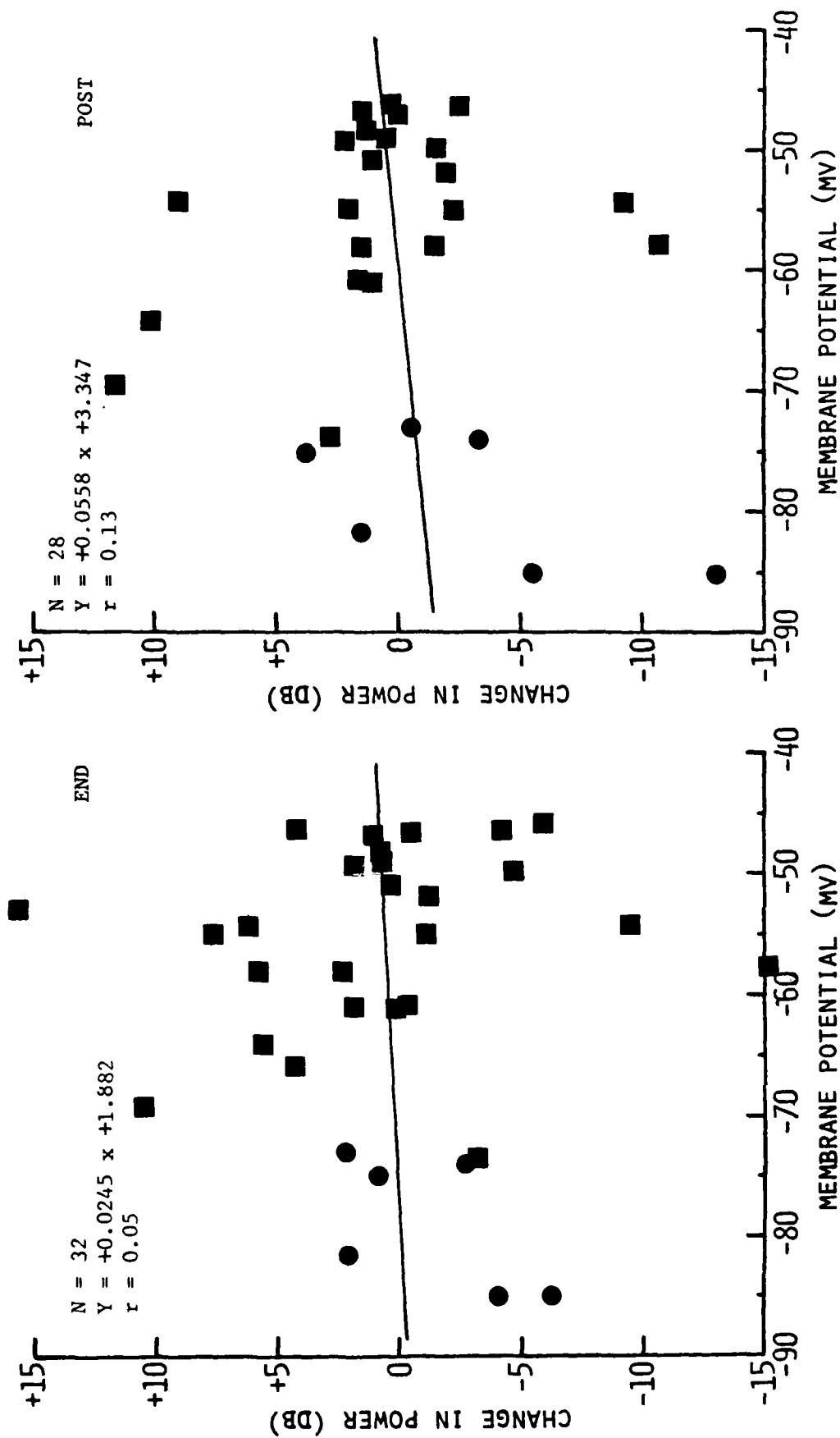
Figure 34B. CHANGE analysis of membrane voltage noise power for 3-min 5-15 mW/g PW RFR exposures.

63

15-30 mW/g PW 3-MIN CHANGE

N = 4
Y = +0.2332 x +15.806
r = 0.63

BEG

CHANGE IN POWER (DB)

MEMBRANE POTENTIAL (MV)

MEMBRANE POTENTIAL (MV)

CHANGE IN POWER (DB)

Figure 35A. CHANGE analysis of membrane voltage noise power for 3-min 15-30 mW/g PW RFR exposures. Triangles represent data from one exposure of 43.8-mW/g RFR.

64

Figure 35B. CHANGE analysis of membrane voltage noise power for 3-min 15-30 mW/g PW RFR exposures. Triangles represent data from one exposure of 43.8-mW/g RFR.

SHAM 3-MIN CHANGE

N = 42
Y = +0.1031 x +7.688
r = 0.32

BEG
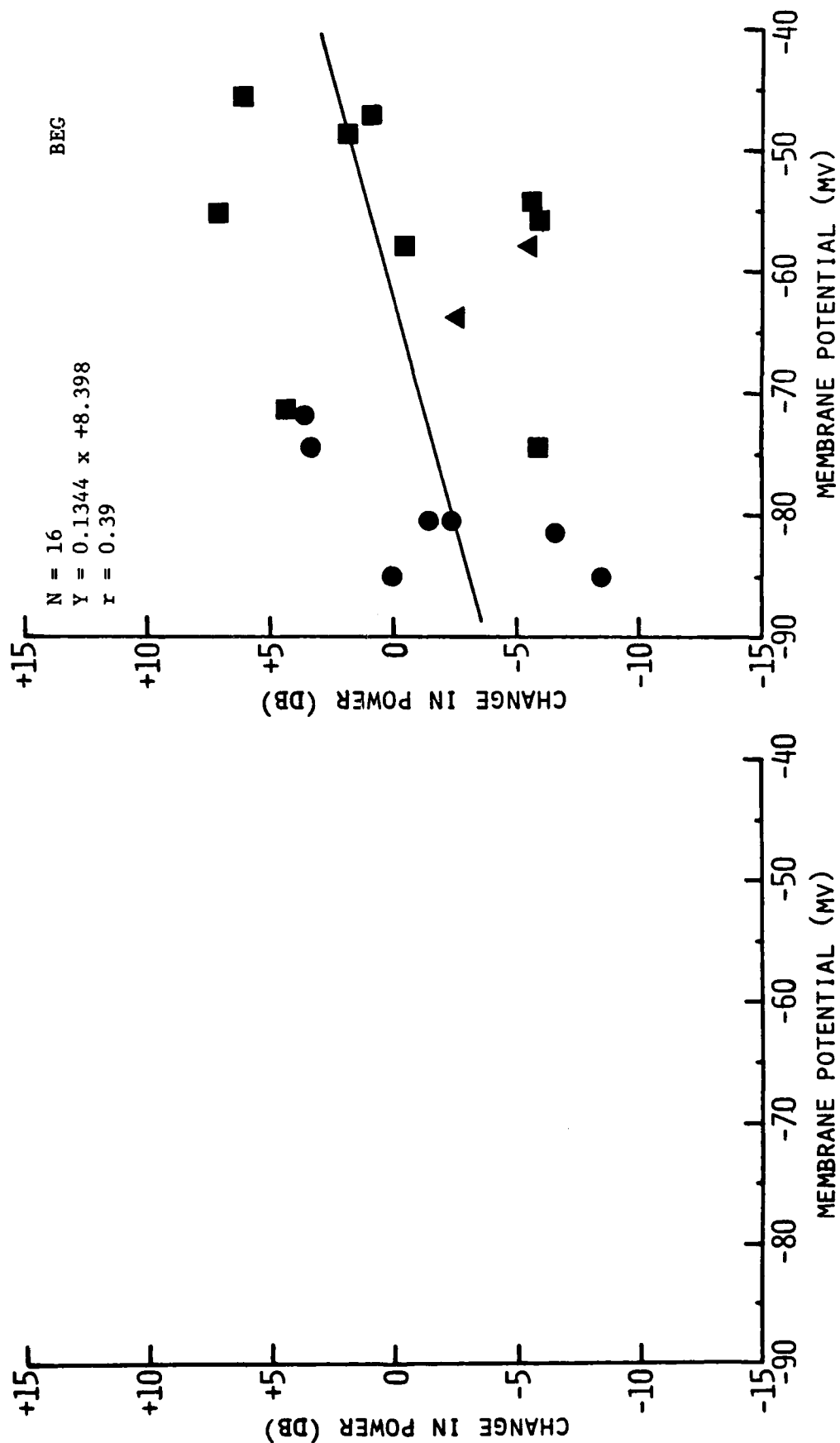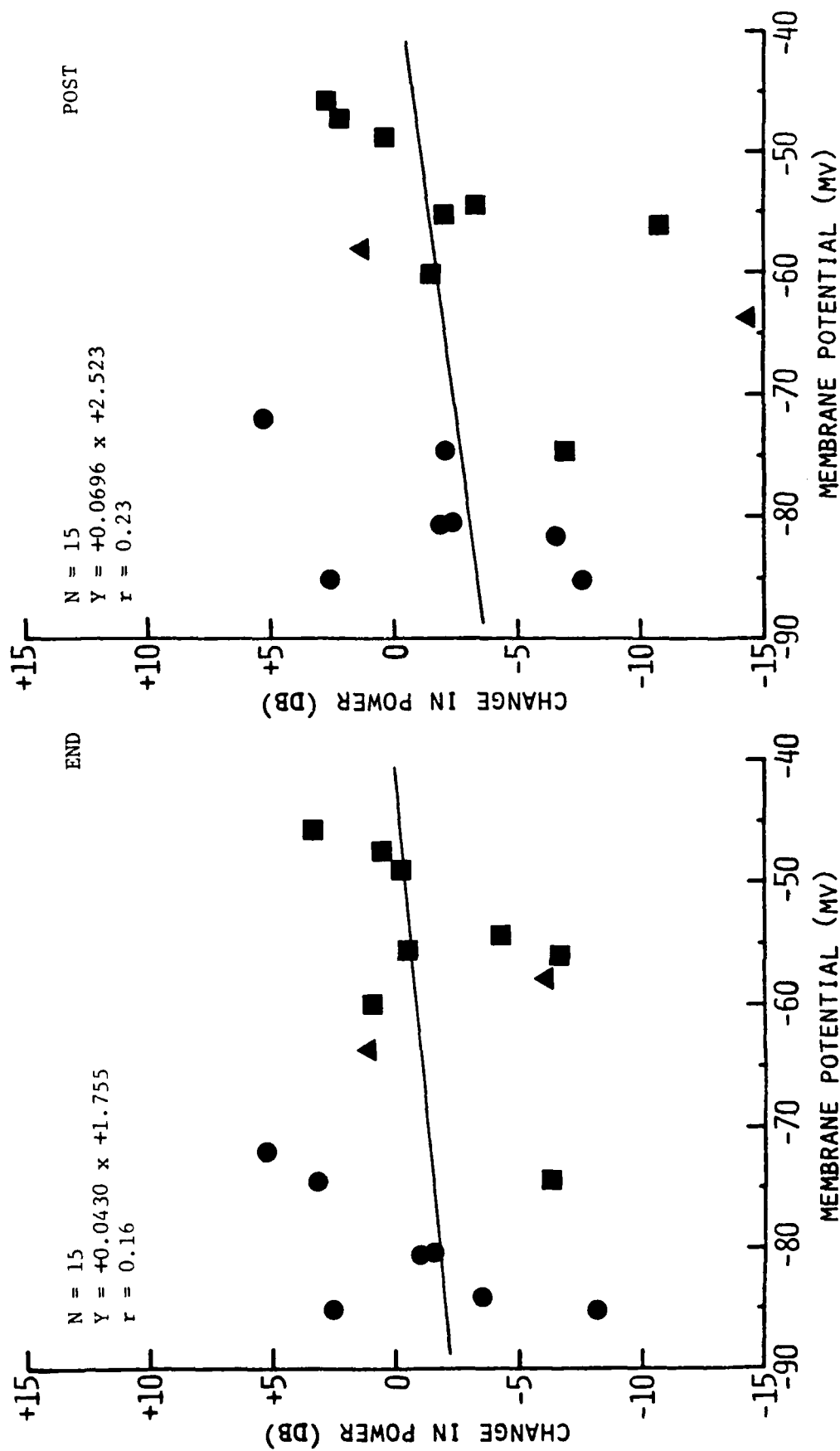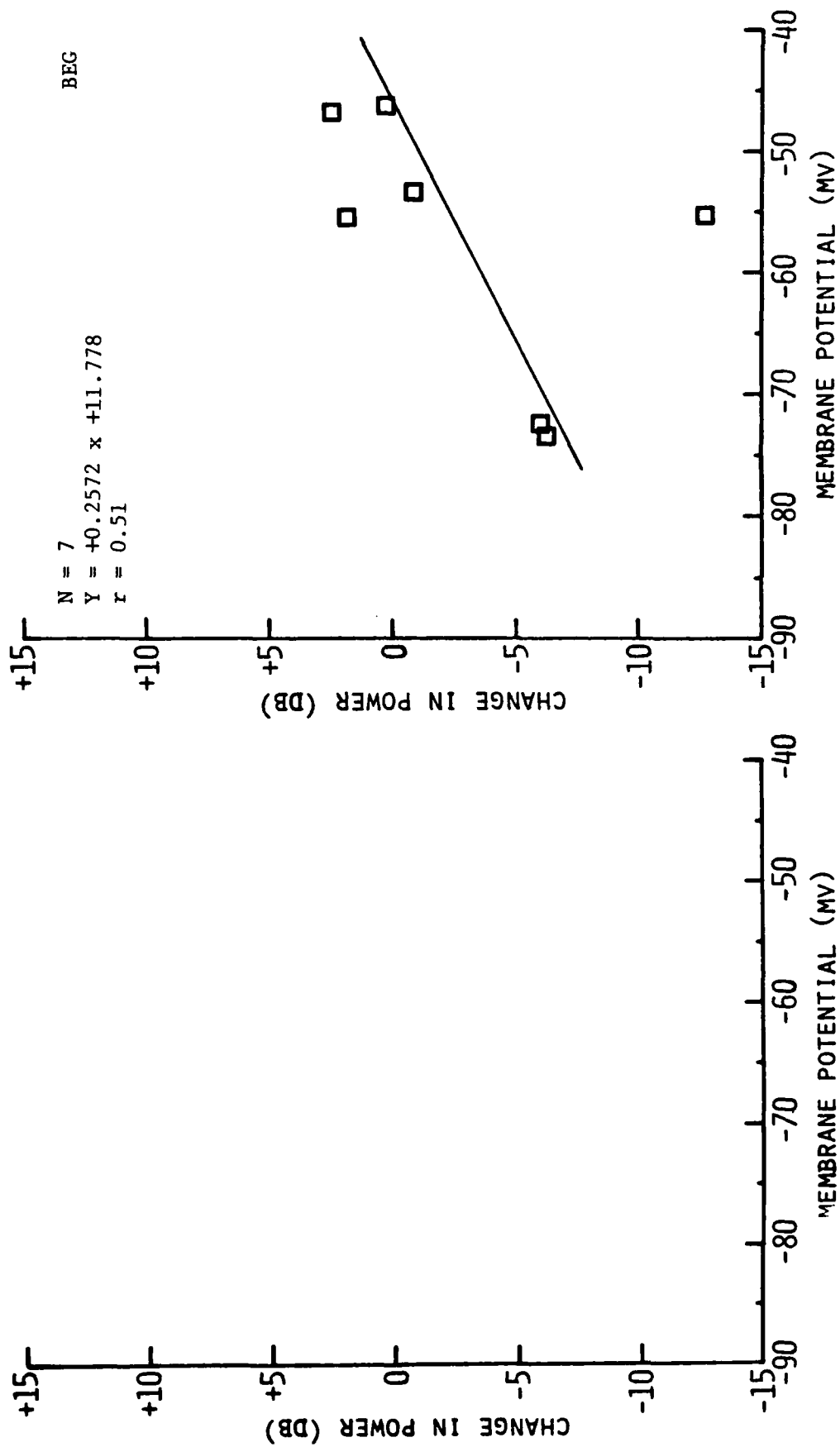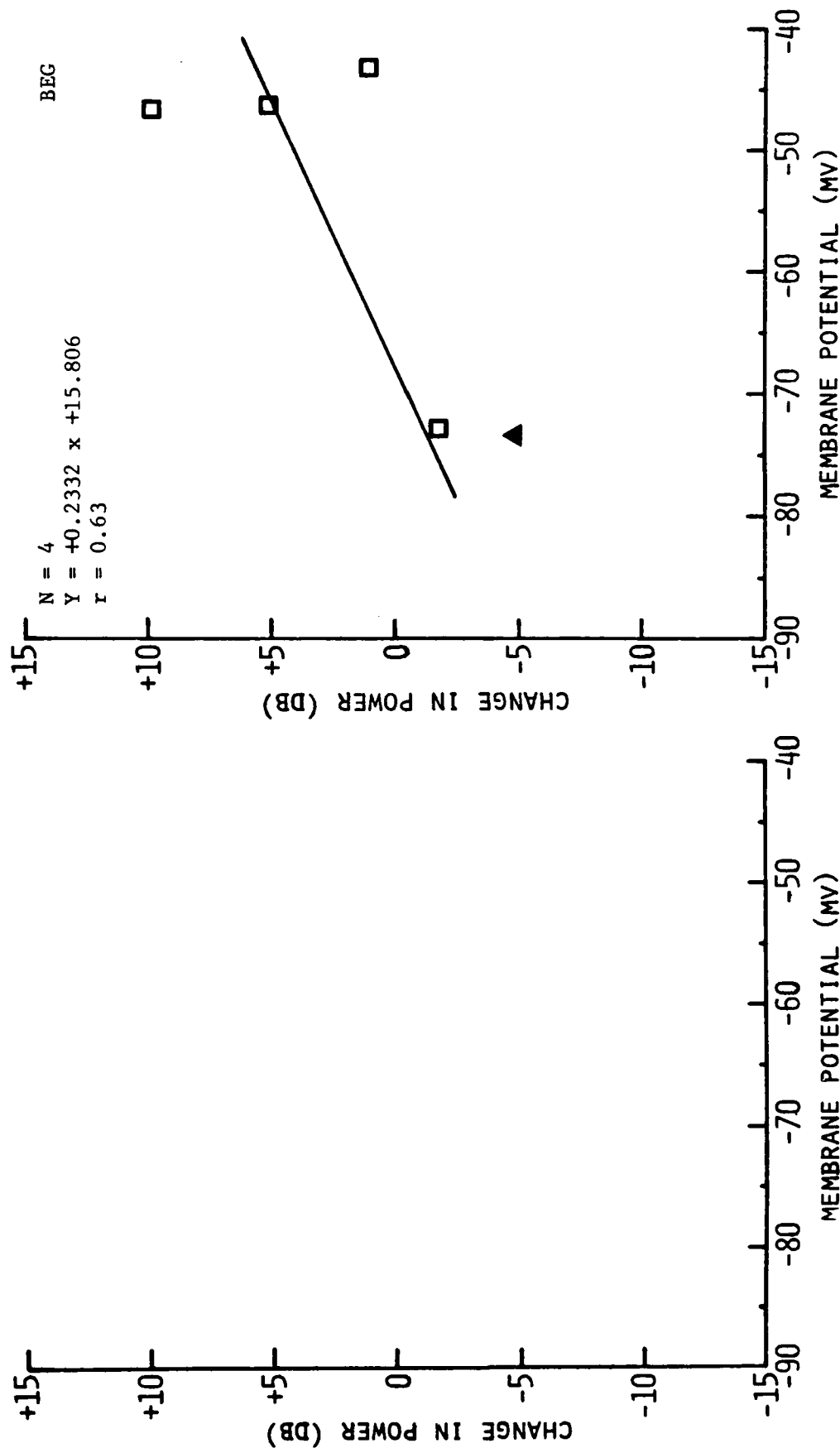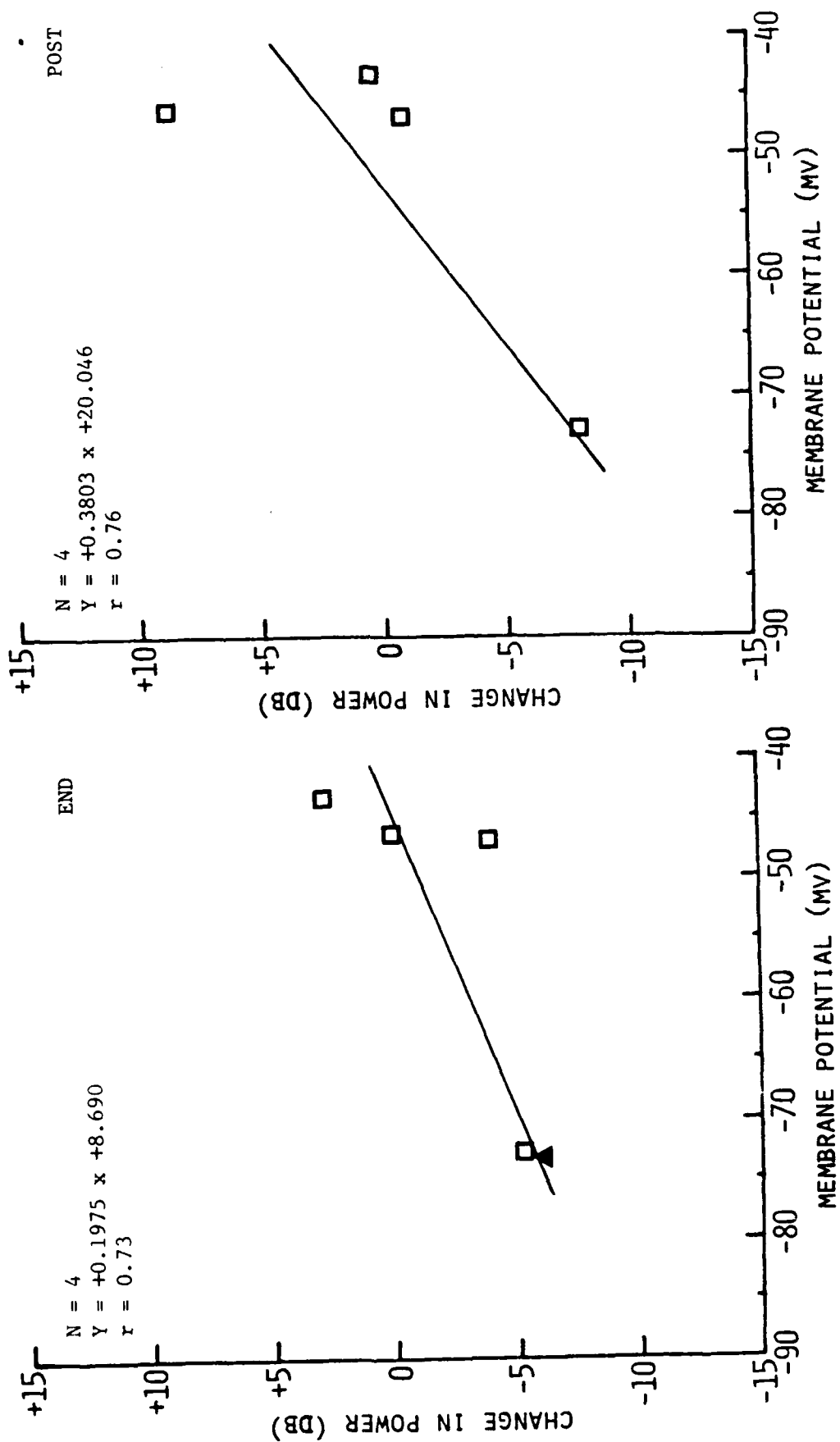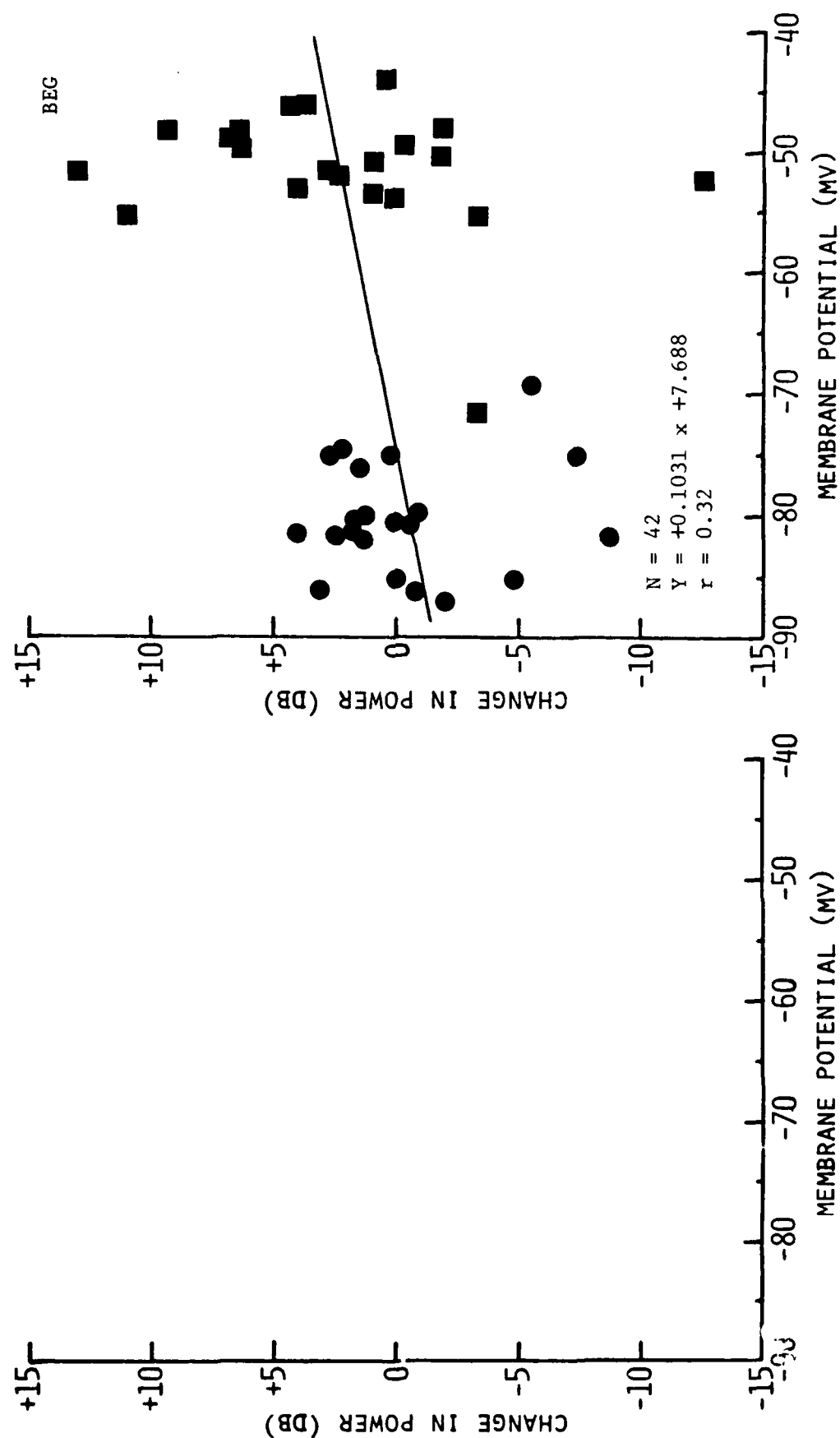
Figure 36A. CHANGE analysis of membrane voltage noise power for 3-min SHAM exposures.
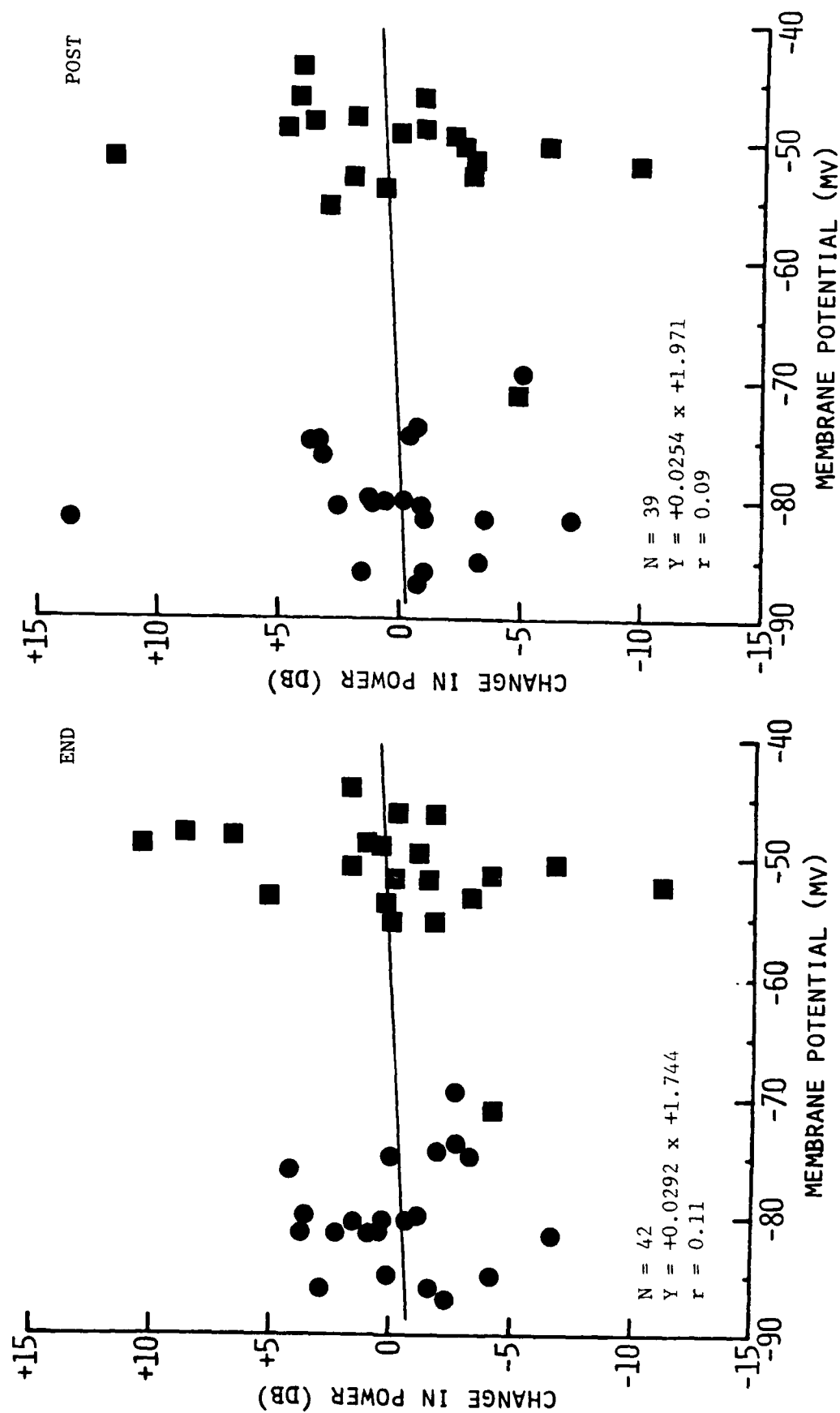
66

Figure 36B. CHANGE analysis of membrane voltage noise power for 3-min SHAM exposures.

67

To provide larger data bases for testing, data from CW and PW exposures were pooled for 5-15 and 15-30 mW/g, for which both CW and PW data were available. The same tests of DIFF and CHANGE data described above were applied to these combined data groupings. For the combined CHANGE, no significant differences were found. For DIFF, the slope of BEG 15-30 mW/g was significantly different from the PRE slope at the 0.01 level; t=2.9236, df=42. This was the only significant difference found for the combined DIFF. The combined DIFF analyses for 5-15 and 15-30 mW/g are shown in Figures 37 and 38.

Figures 39 through 42 show the DIFF analysis for 2-min exposures at 5-15 mW/g CW, 5-15 mW/g PW, 15-30 mW/g PW, and SHAM respectively. Slopes in the first two groups were not significantly different from PRE slopes. Because of the small range of membrane potentials, regression analyses were not done on the latter two groups. Instead, conventional two-tailed t-tests on the means of DIFF powers were performed; and for completeness, they were done for all 2-min groups. The 15- to 30-mW/g PW BEG mean was significantly different from its respective PRE mean at the 0.01 level with t=-3.373 and df=8; this was the only significantly different 2-min DIFF.

Figures 43 through 46 show the CHANGE analysis for 2-min exposures at 5-15 mW/g CW, 5-15 mW/g PW, 15-30 mW/g PW, and SHAM respectively. For the reasons cited above for DIFF analysis, straight-line fits were done only for the 5- to 15-mW/g PW CHANGE; no significant difference in slopes was found. The 2-min CHANGE means were tested using two-tailed t-tests as for DIFF; no significant difference in means was found.

As done for 3-min data to obtain a larger data base, 2-min data from CW and PW exposures were pooled for 5-15 mW/g. The combined DIFF analysis is shown in Figure 47. Although DIFF END slope had a t value of -1.763, this was significant at only the 0.10 level with df=22. Thus, no significant differences were seen in slopes and means of DIFF and CHANGE analyses.

The temperature dependence of membrane voltage noise was investigated in aggregates in E818A medium. Figure 48 shows these results obtained for a range of membrane potentials. In five of six cases, the membrane voltage noise decreased as temperature rose from $36^{\circ}C$ to $38^{\circ}C$; from $37^{\circ}C$ to $38^{\circ}C$, the noise decreased in all six cases. This latter range was the temperature range in aggregate experiments since the maximum temperature elevation with the highest SAR was $0.9^{\circ}C$ as measured with the Vitek model 101 Electrothermia Monitor.

The significant differences found for membrane voltage noise are summarized as follows. In 3-min exposures, significant differences were seen for the 15- to 30-mW/g CW BEG DIFF slope (0.05 level), SHAM BEG DIFF slope (0.05 level), 15- to 30-mW/g combined CW/PW BEG DIFF slope (0.01 level), and 1- to 5-mW/g CW BEG CHANGE slope (0.05 level). For 2-min exposures, a significant difference was seen for the 15- to 30-mW/g PW BEG DIFF mean (0.01 level). The most significant differences are associated with SAR levels of 15-30 mW/g. For 3-min CW exposures, the change was an increase in slope--indicating an increase in DIFF power at membrane potentials more positive than -60 mV. This was consistent with the results for initial experiments in E818A medium for 3-min CW RFR exposures with SARs of 14 to 143.4 mW/g. For 2-min PW exposures, however, the power decreased for membrane potentials more positive than -60 mV. This may indicate a difference between CW and PW effects on the cardiac-cell excitable membrane.

Figure 37A. DIFF analysis of membrane voltage noise power for 3-min 5-15 mW/g CW (solid symbols) and PW (open symbols) RFR exposures.

Figure 37B. DIFF analysis of membrane voltage noise power for 3-min 5-15 mW/g CW (solid symbols) and PW (open symbols) RFR exposures.

15-30 mW/g CW & PW 3-MIN DIFF

BEG

PRE

N = 23
Y = +0.2069 x +14.914
r = 0.47

N = 23
Y = -0.0833 x -5.050
r = 0.33

Figure 38A. DIFF analysis of membrane voltage noise power for 3-min 15-30 mW/g CW (solid) symbols) and PW (open symbols) RFR exposures.
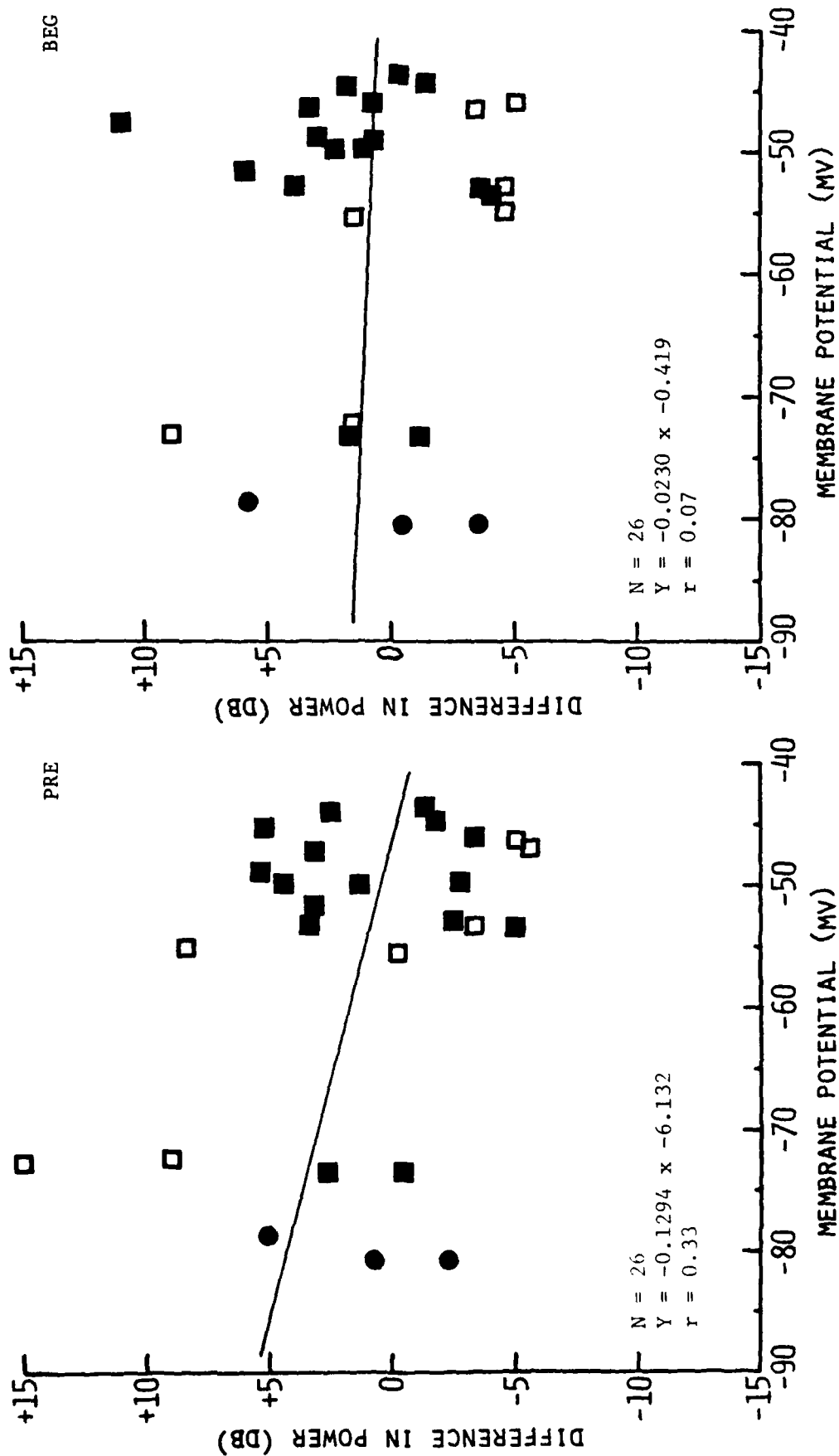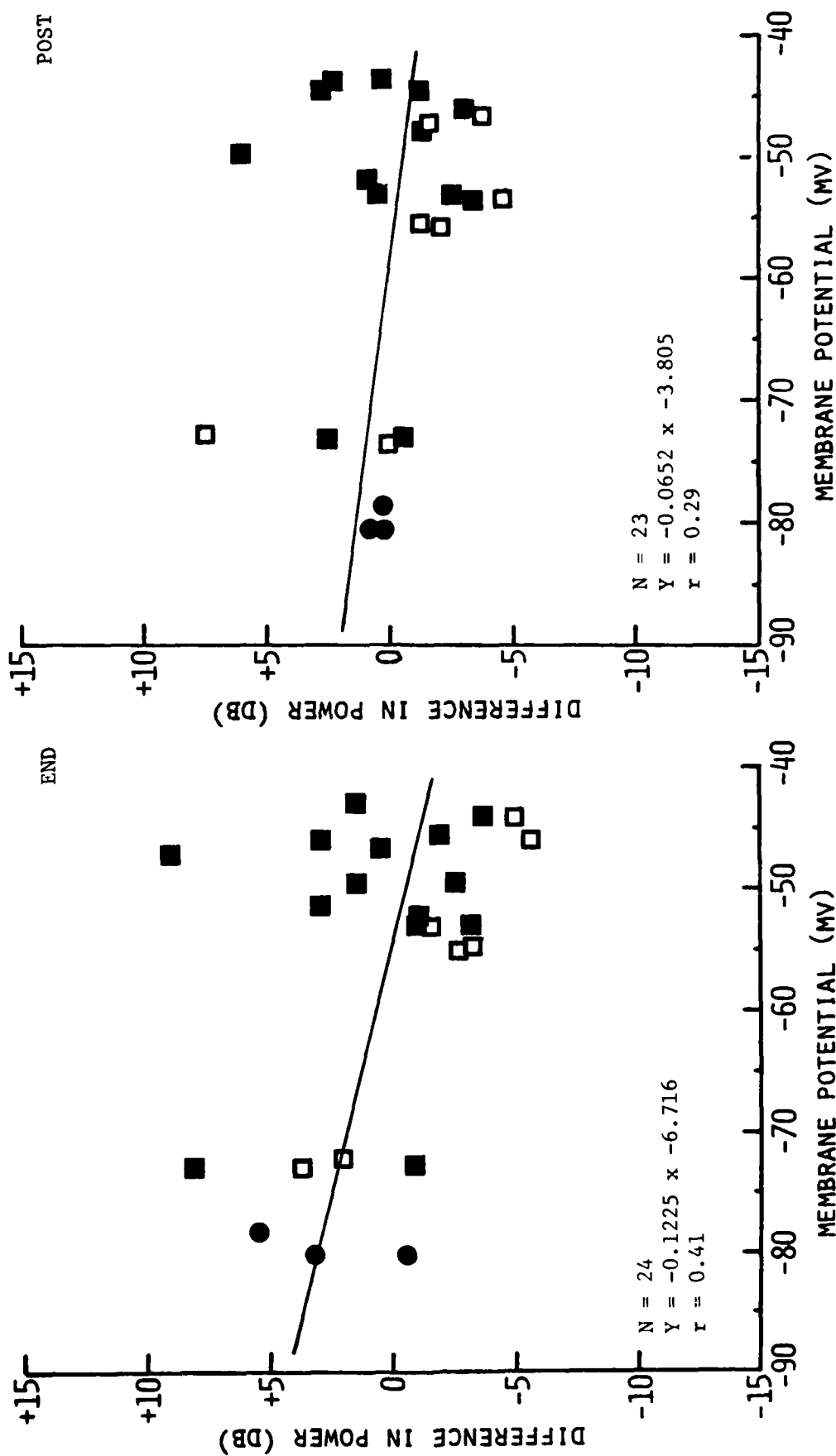
71
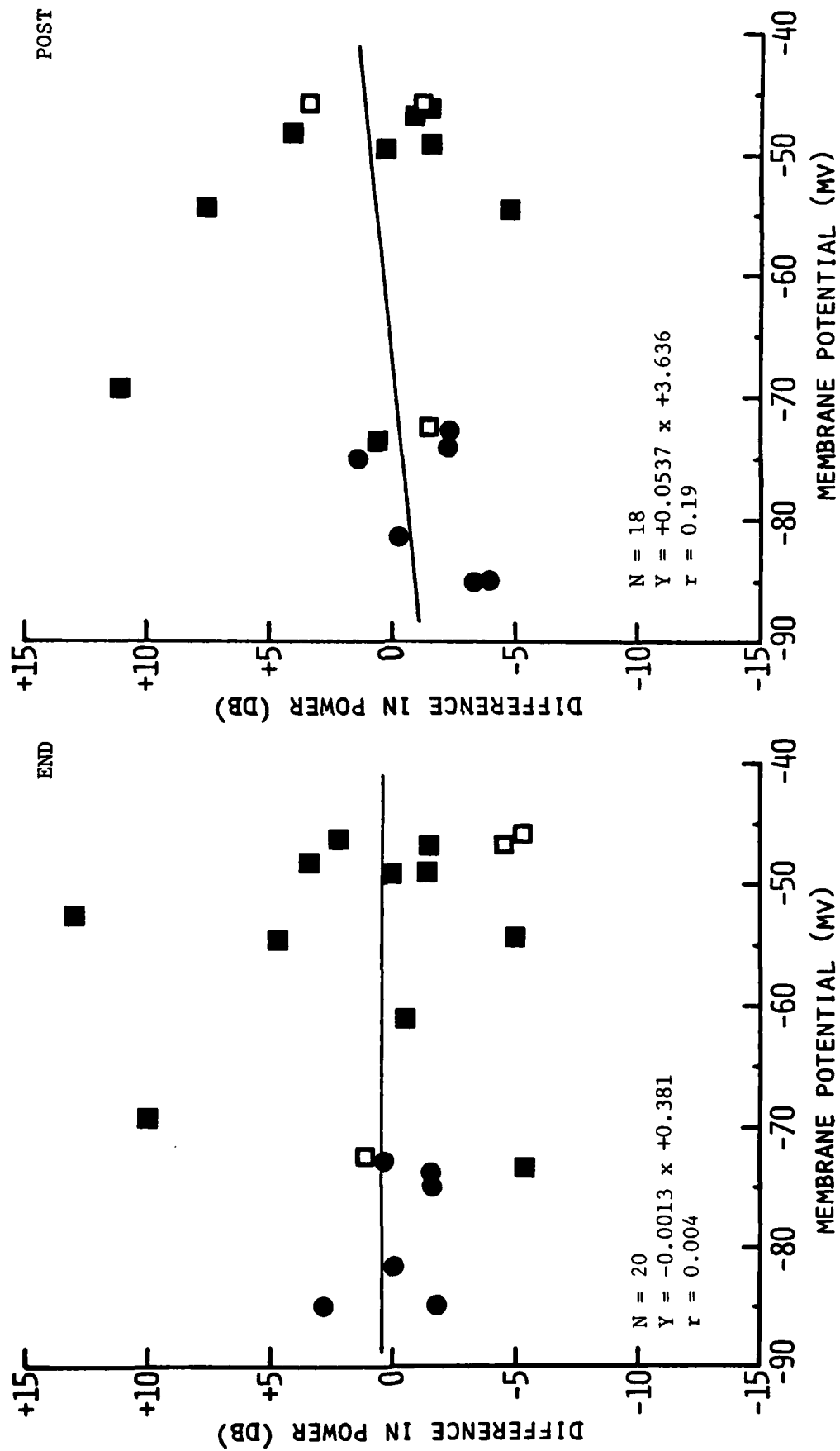
Figure 38B. DIFF analysis of membrane voltage noise power for 3-min 15-30 mW/g CW (solid symbols) and PW (open symbols) RFR exposures.

Figure 39A. DIFF analysis of membrane voltage noise power for 2-min 5-15 mW/g CW RFR exposures.

5-15 mW/g CW 2-MIN DIFF

BEG

$N = 5$
$Y = -0.6304 \; X \; -32.161$
$r = 0.45$

PRE

$N = 5$
$Y = -0.4760 \; x \; -27.910$
$r = 0.54$
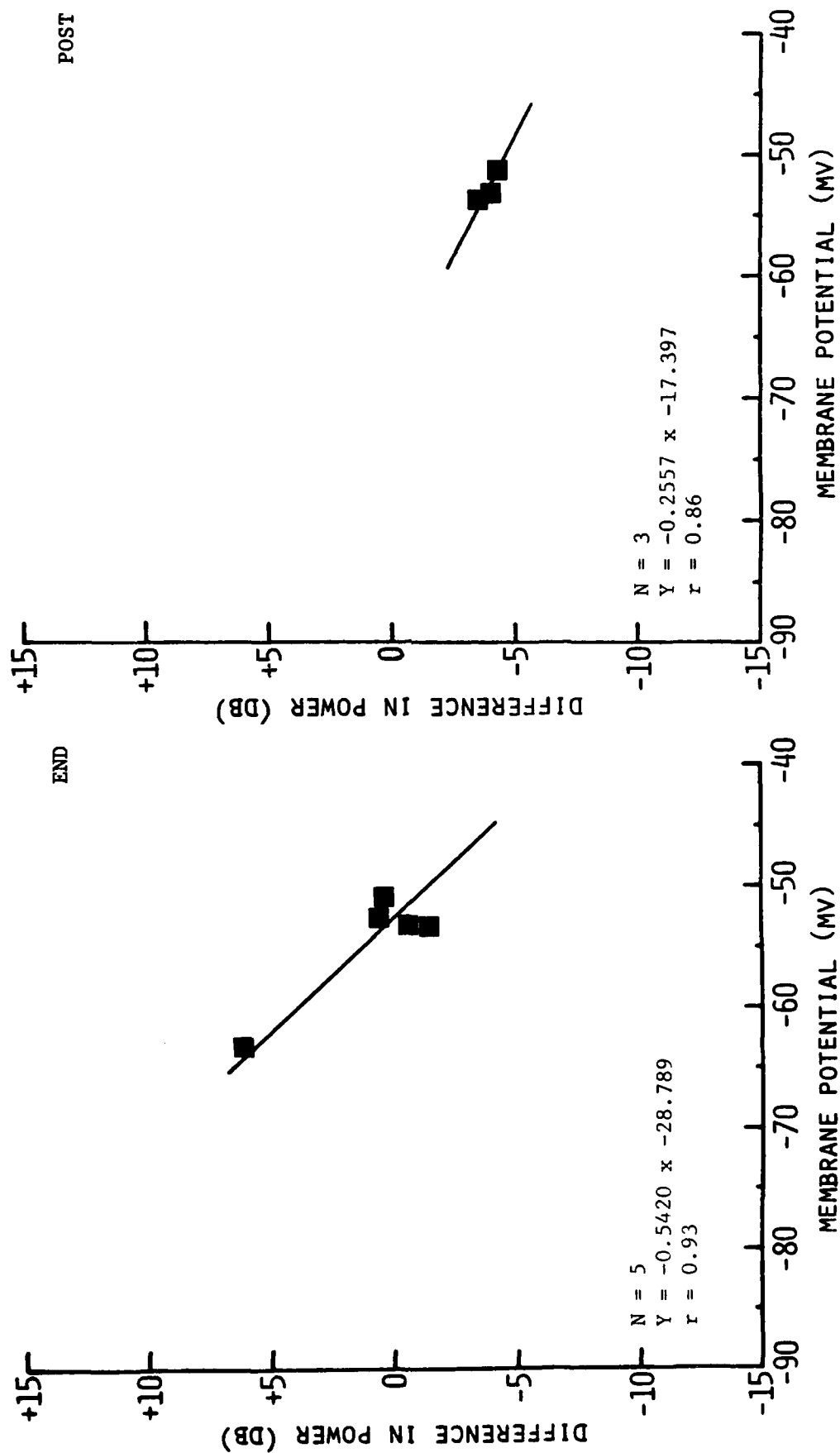
Figure 39B. DIFF analysis of membrane voltage noise power for 2-min 5-15 mW/g CW RFR exposures.

74

Figure 40A. DIFF analysis of membrane voltage noise power for 2-min 5-15 mW/g PW RFR exposures.

5-15 mW/g PW 2-MIN DIFF

BEG

N = 8
Y = 0.0967 x -5.857
r = 0.14

MEMBRANE POTENTIAL (MV)

DIFFERENCE IN POWER (DB)

PRE

N = 8
Y = +0.0144 x +2.210
r = 0.02

MEMBRANE POTENTIAL (MV)

DIFFERENCE IN POWER (DB)

75
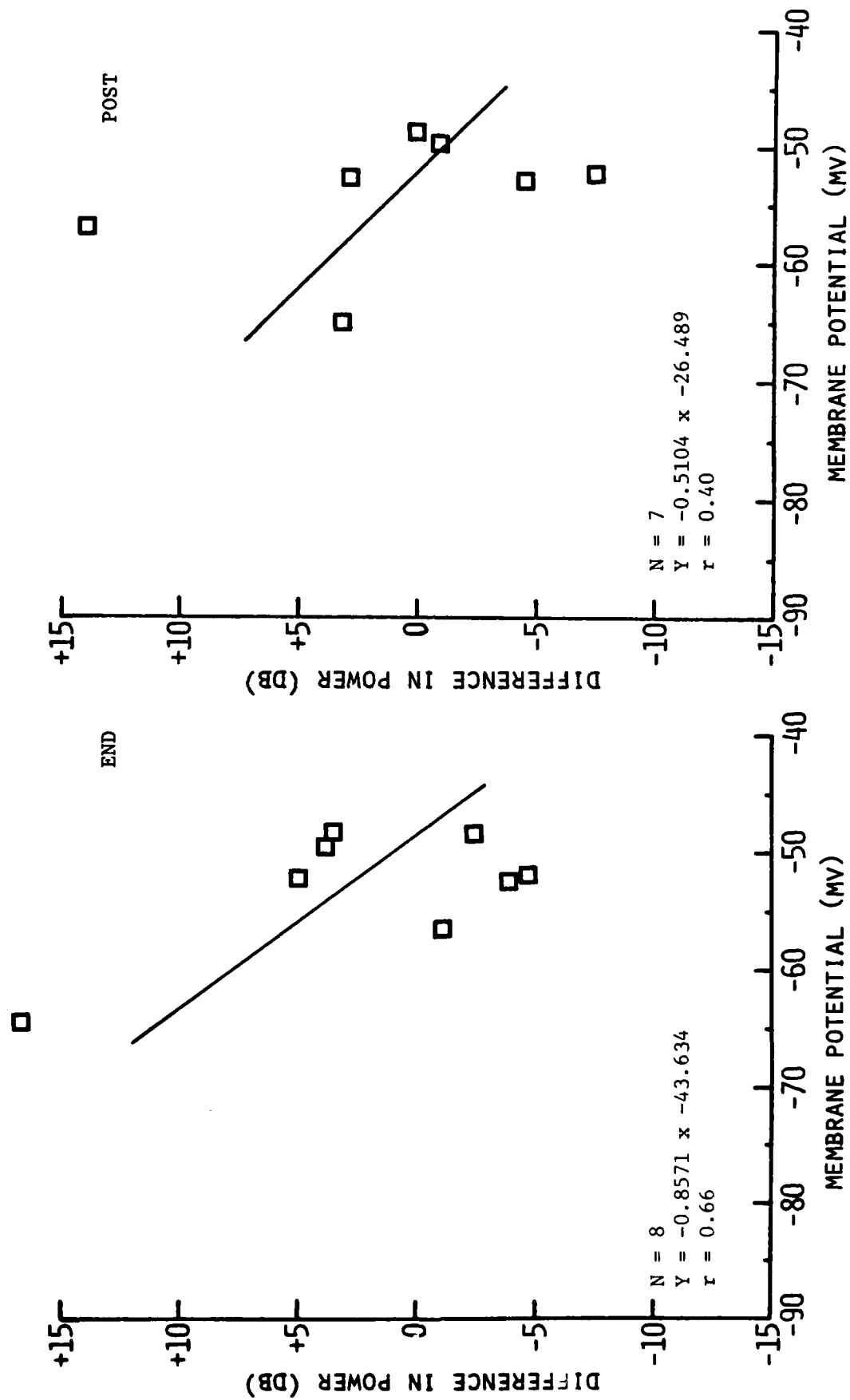
Figure 40B. DIFF analysis of membrane voltage noise power for 2-min 5-15 mW/g PW RFR exposures.

Figure 41A. DIFF analysis of membrane voltage noise power for 2-min 15-30 mW/g PW RFR exposures.
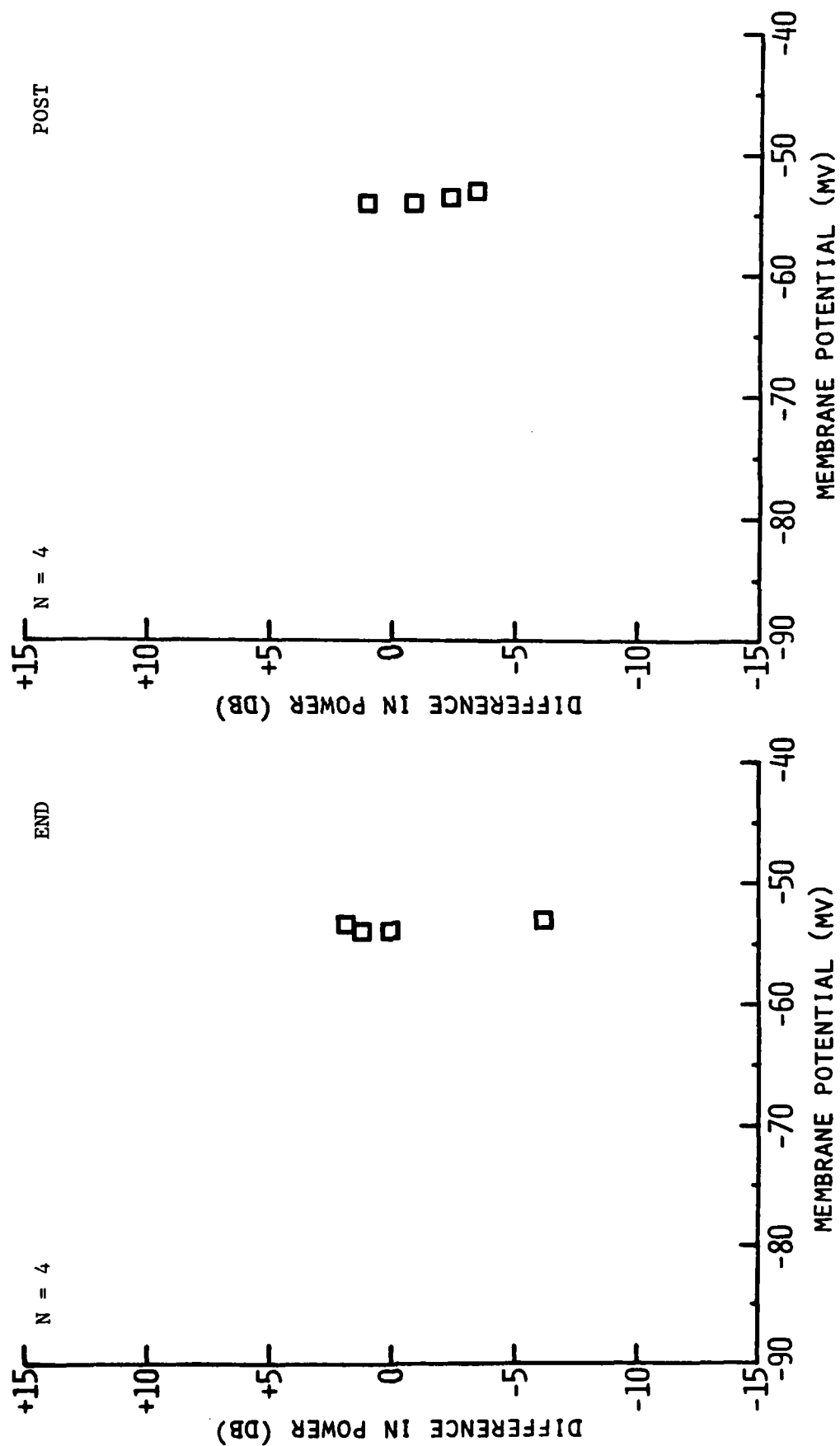
Figure 41B. DIFF analysis of membrane voltage noise power for 2-min 15-30 mW/g PW RFR exposures.
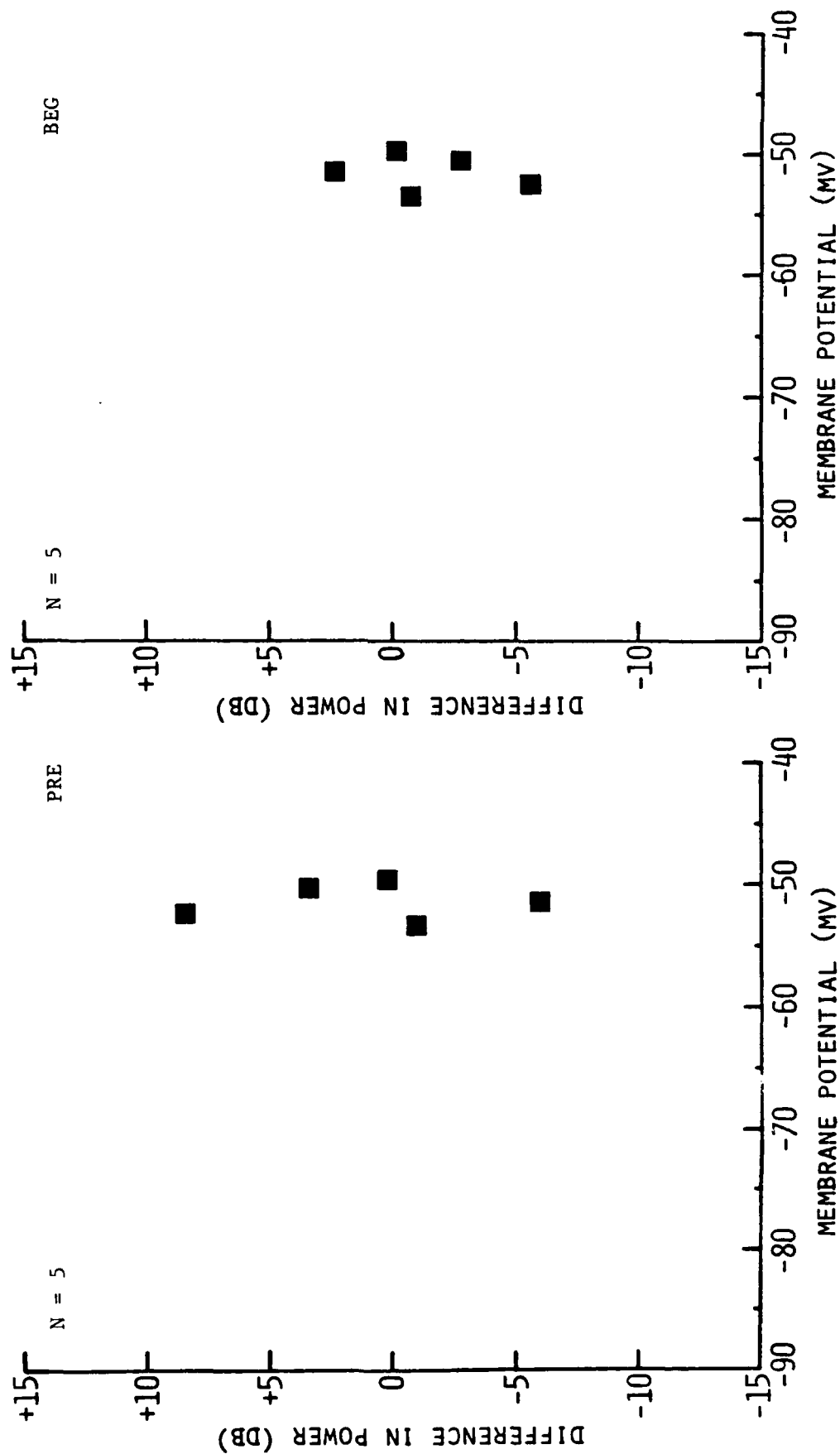
Figure 42A. DIFF analysis of membrane voltage noise power for 2-min SHAM exposures.

79
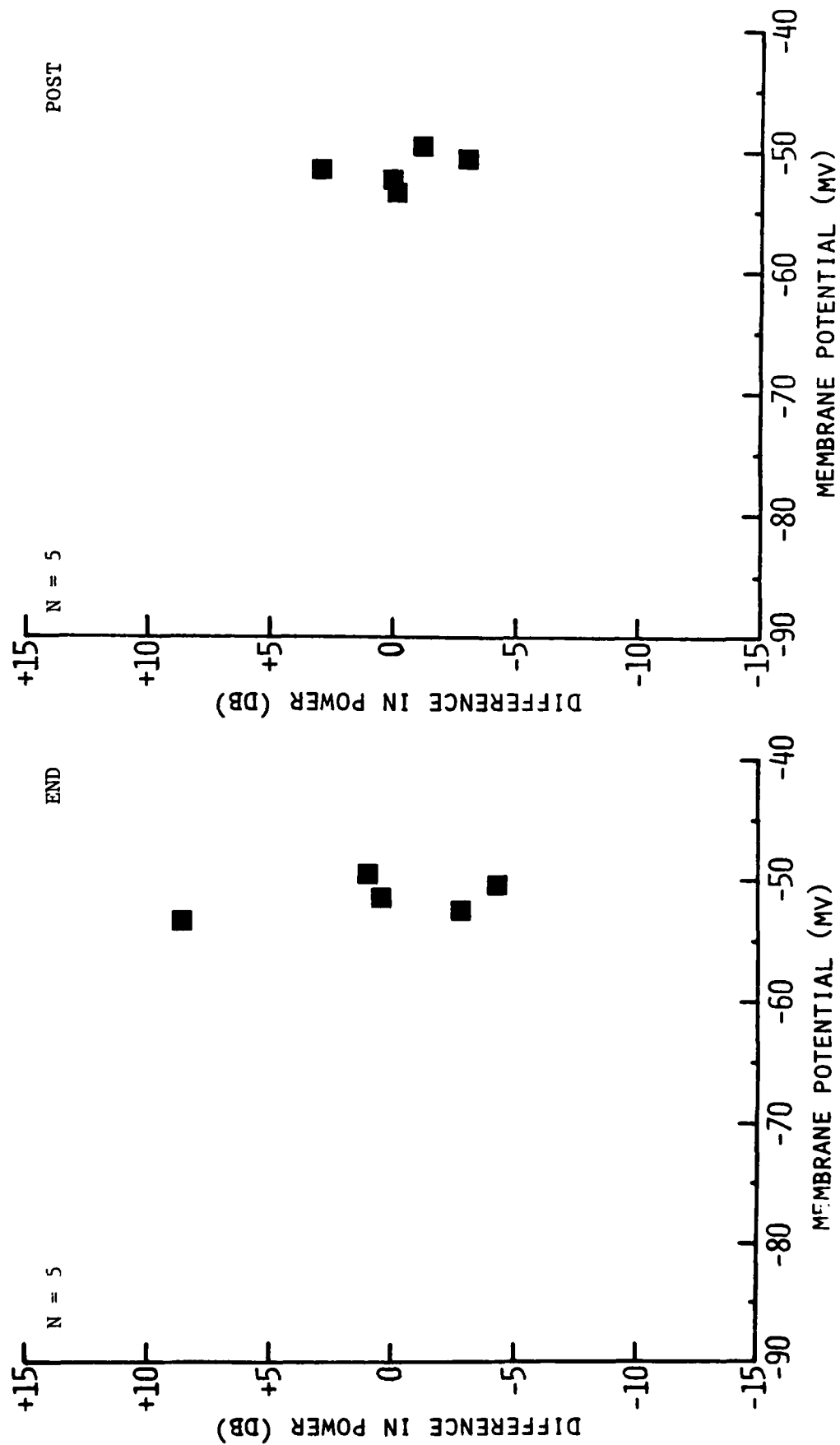
Figure 42B. DIFF analysis of membrane voltage noise power for 2-min SHAM exposures.

Figure 43A. CHANGE analysis of membrane voltage noise power for 2-min 5-15 mW/g CW RFR exposures.
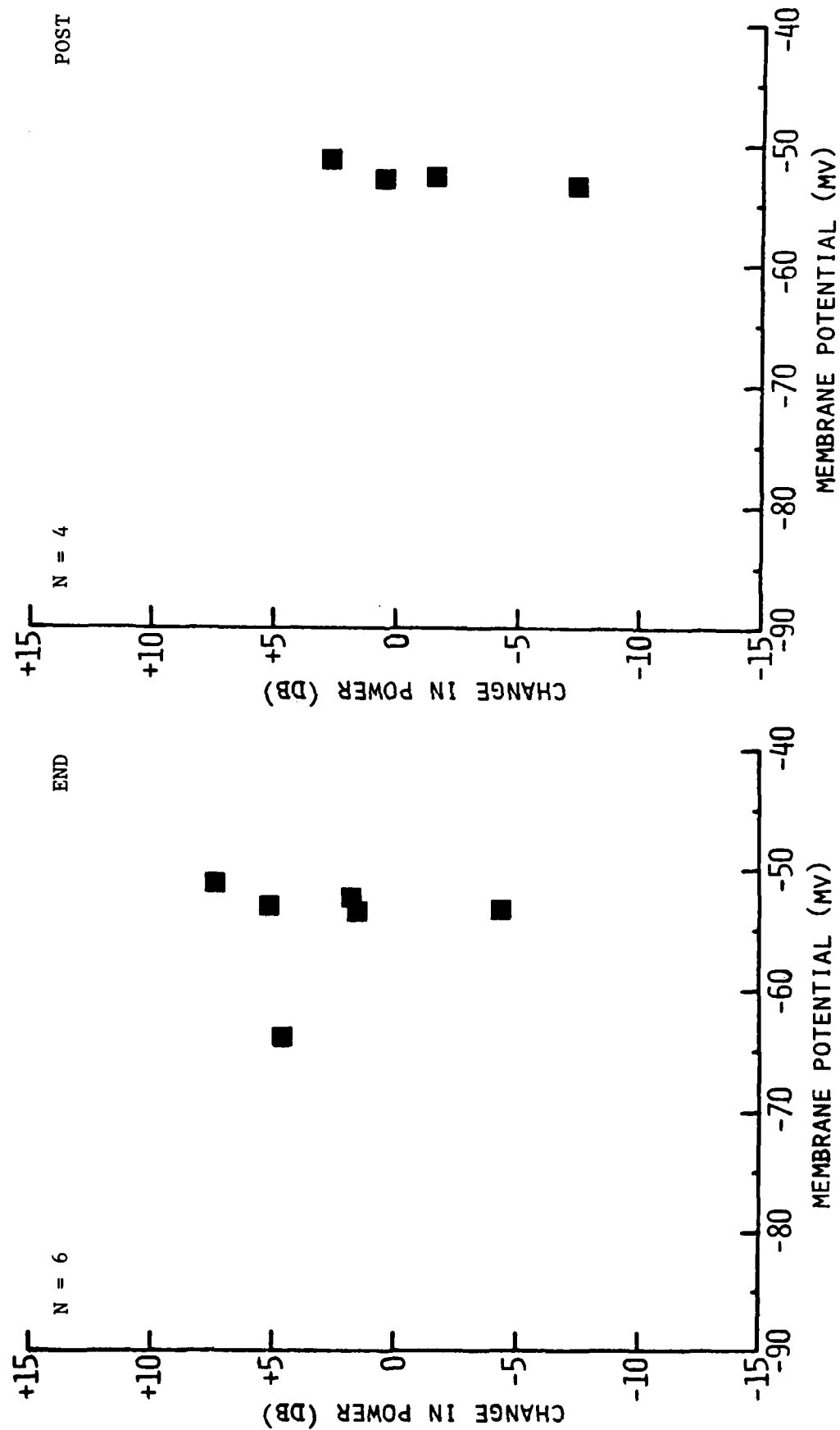
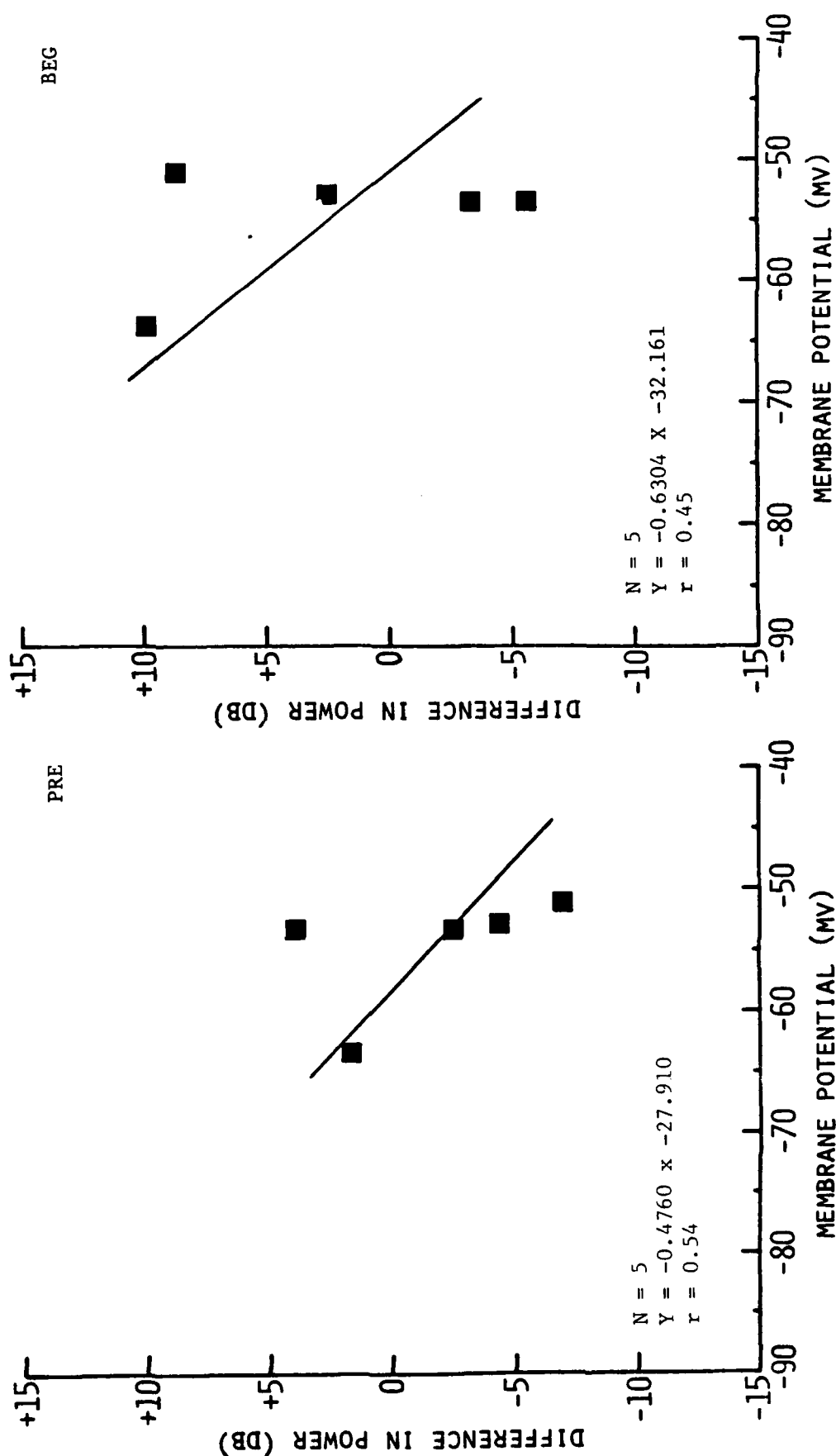Figure 43B. CHANGE analysis of membrane voltage noise power for 2-min 5-15 mW/g CW RFR exposures.
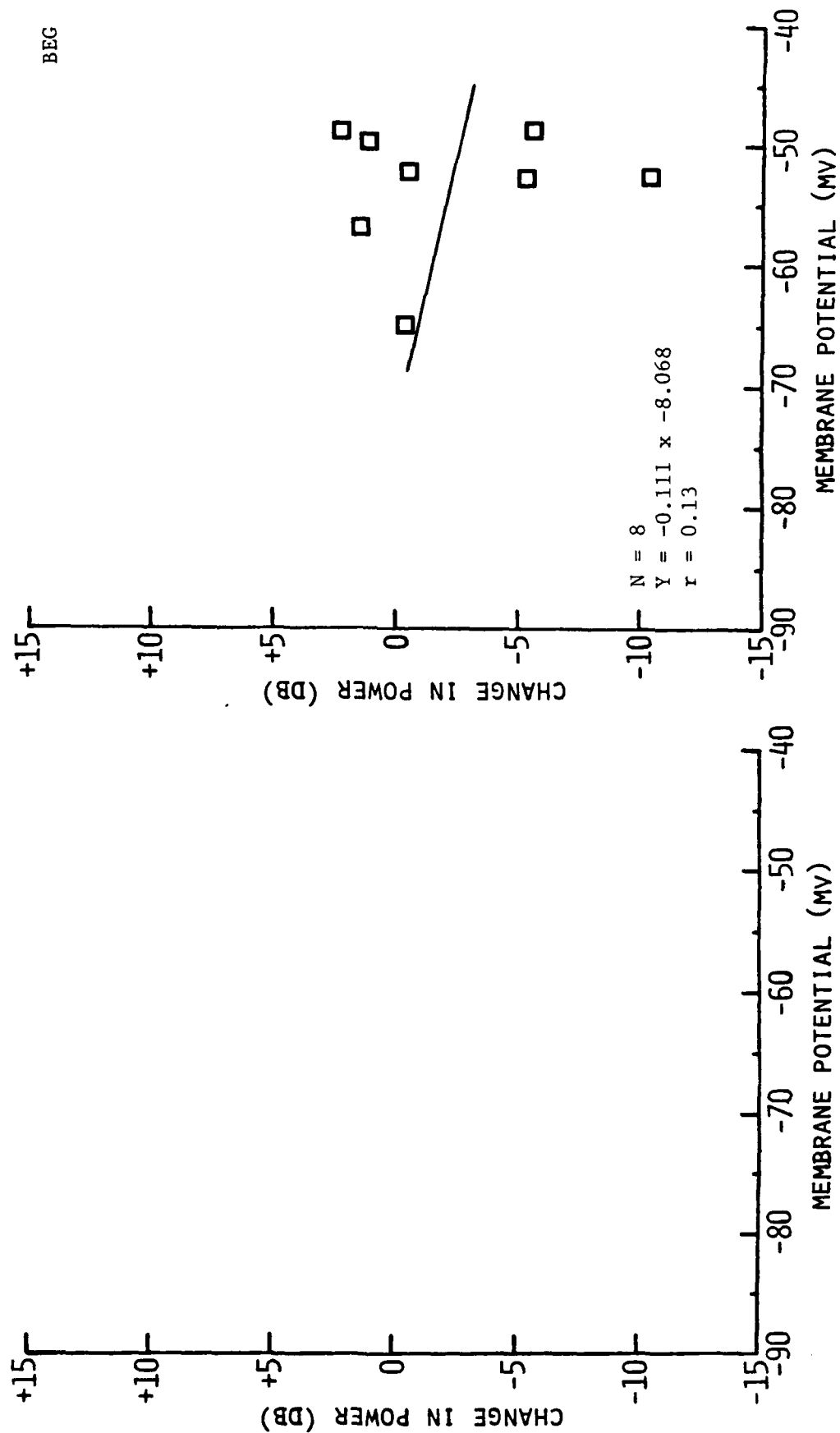
Figure 44A. CHANGE analysis of membrane voltage noise power for 2-min 5-15 mW/g PW RFR exposures.
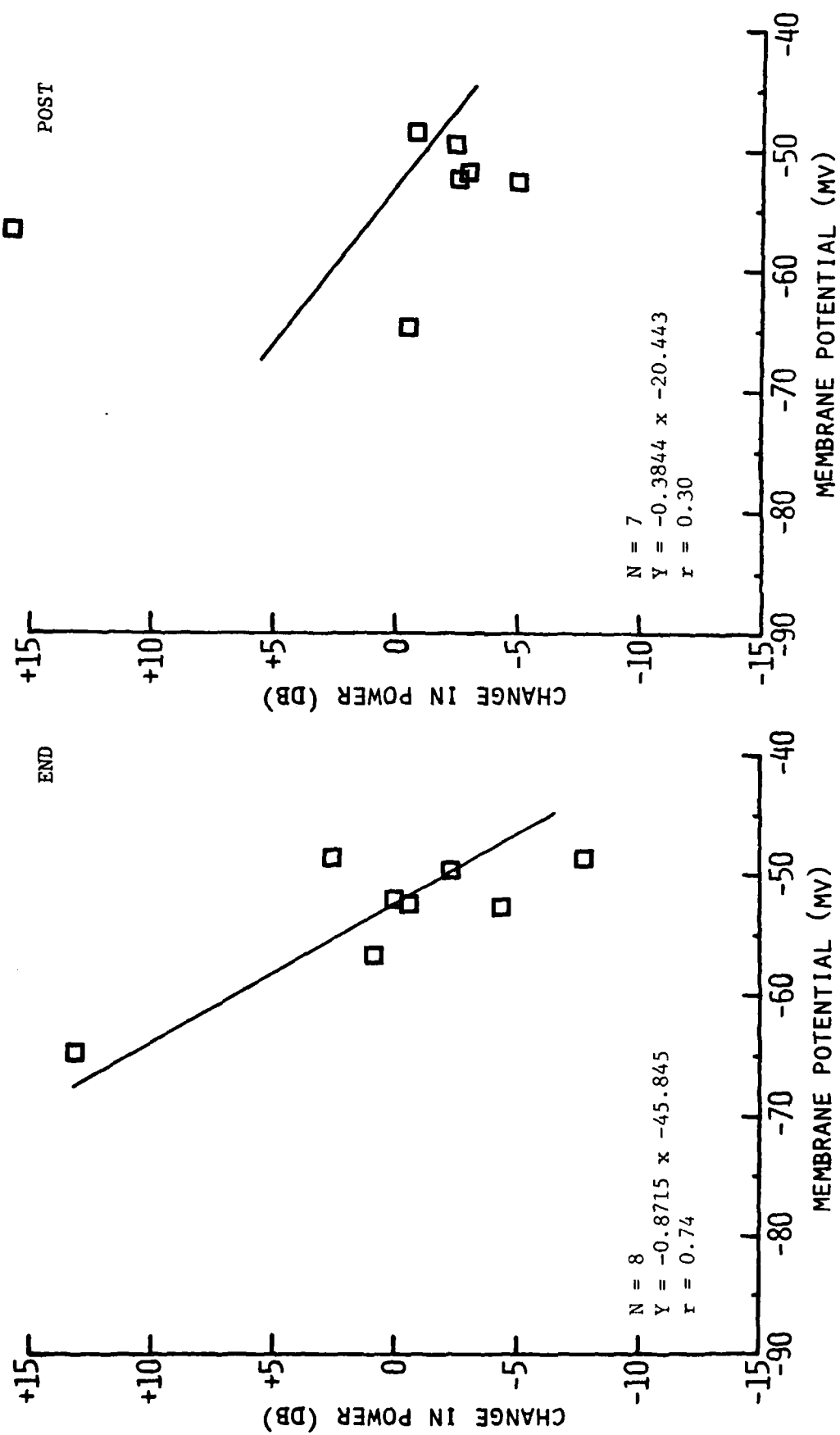
Figure 44B. CHANGE analysis of membrane voltage noise power for 2-min 5-15 mW/g PW RFR exposures.

POST

N = 7
Y = -0.3844 x -20.443
r = 0.30

END

N = 8
Y = -0.8715 x -45.845
r = 0.74

Figure 45A. CHANCE analysis of membrane voltage noise power for 2-min 15-30 mW/g PW RFR exposures.

85
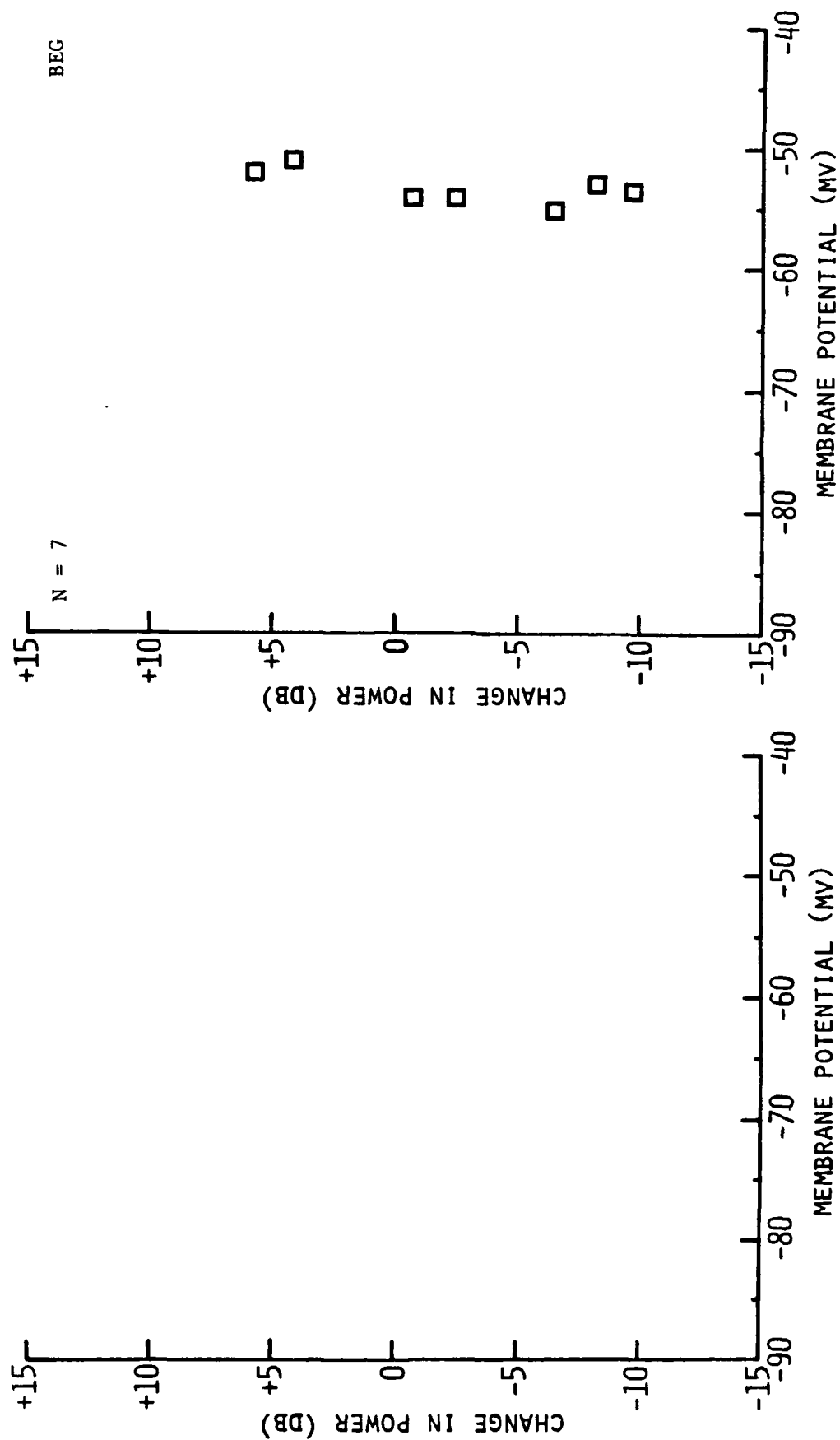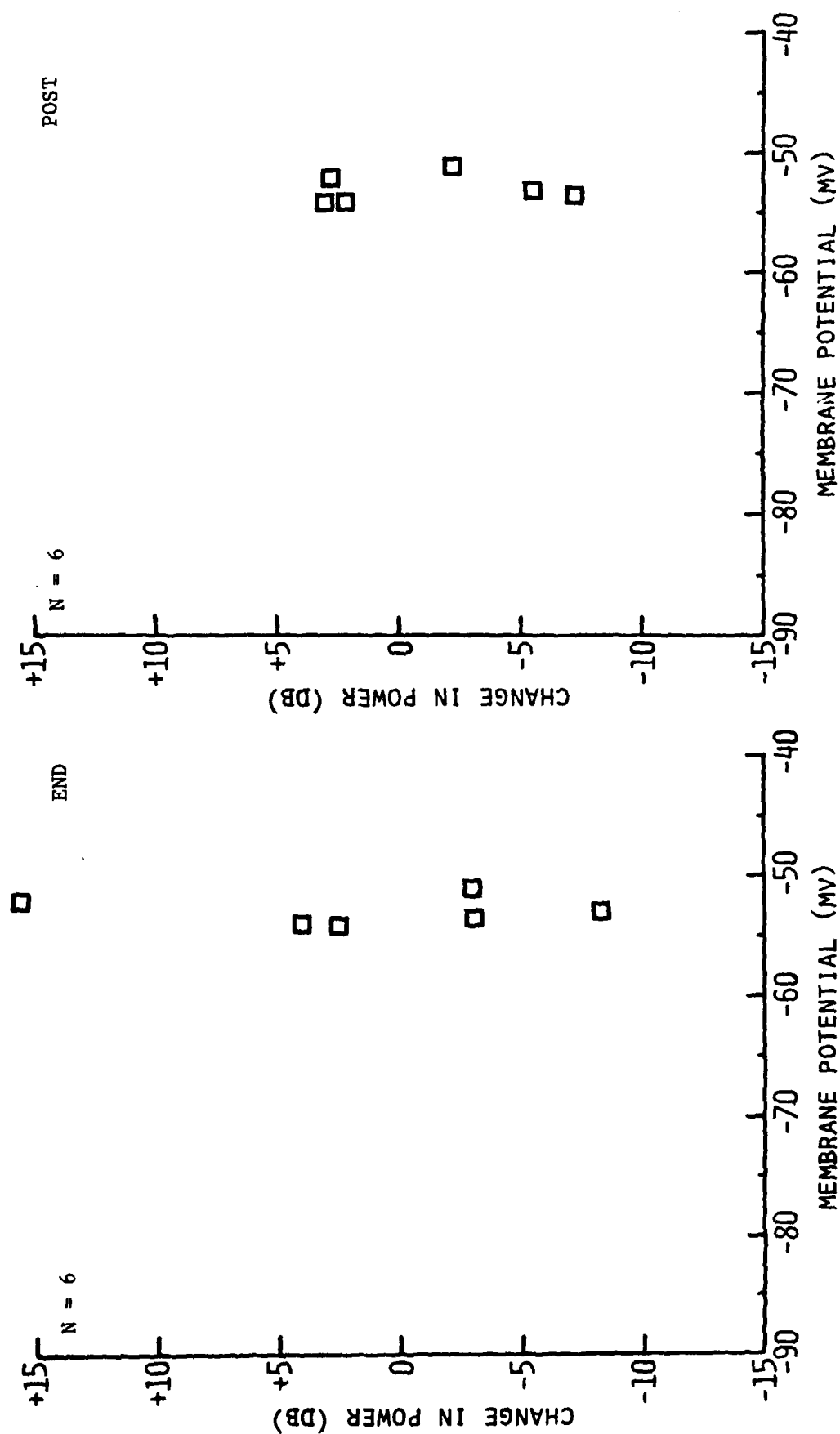
Figure 45B. CHANGE analysis of membrane voltage noise power for 2-min 15-30 mW/g PW RFR exposures.
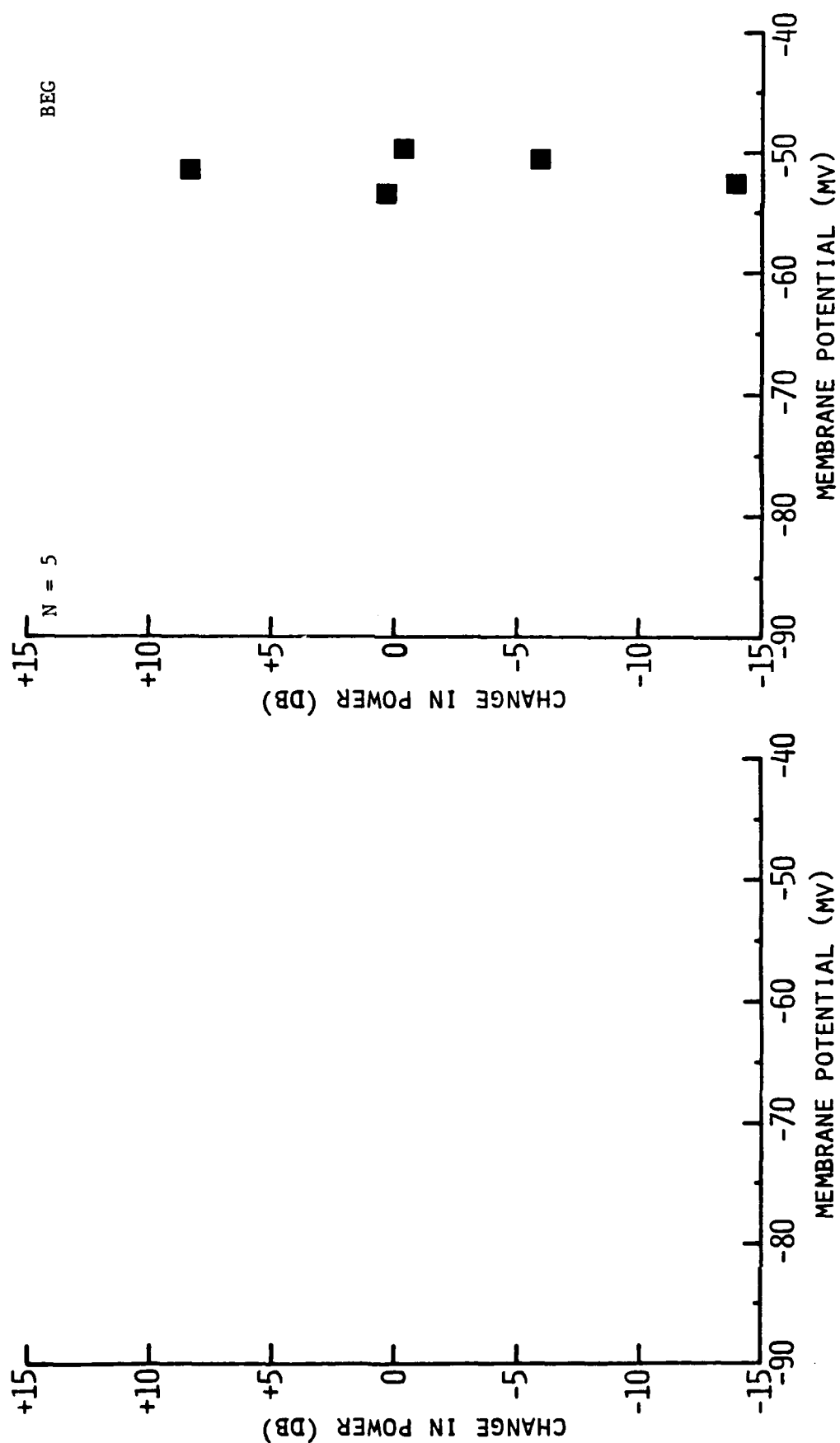
Figure 46A. CHANGE analysis of membrane voltage noise power for 2-min SHAM exposures.
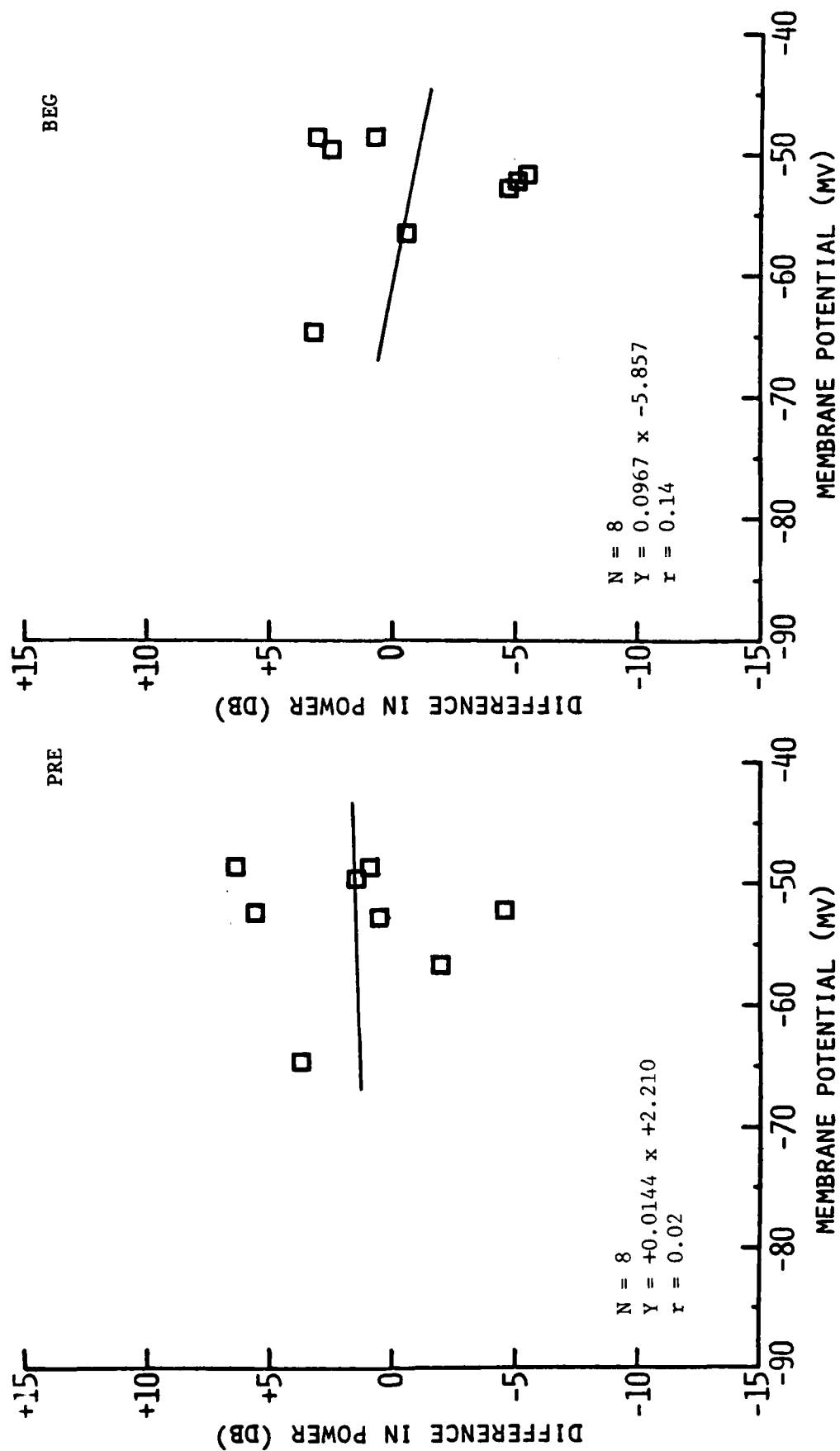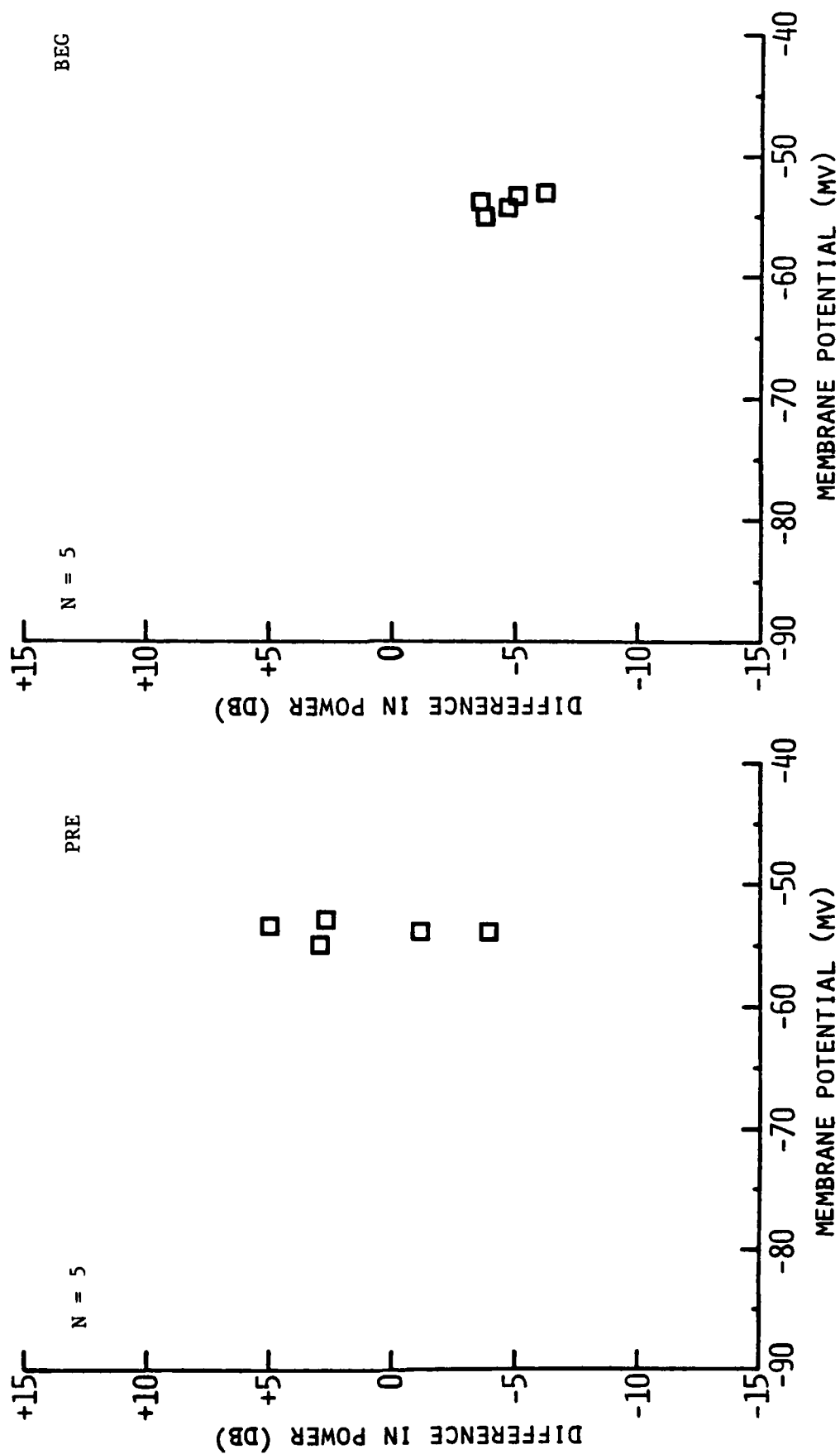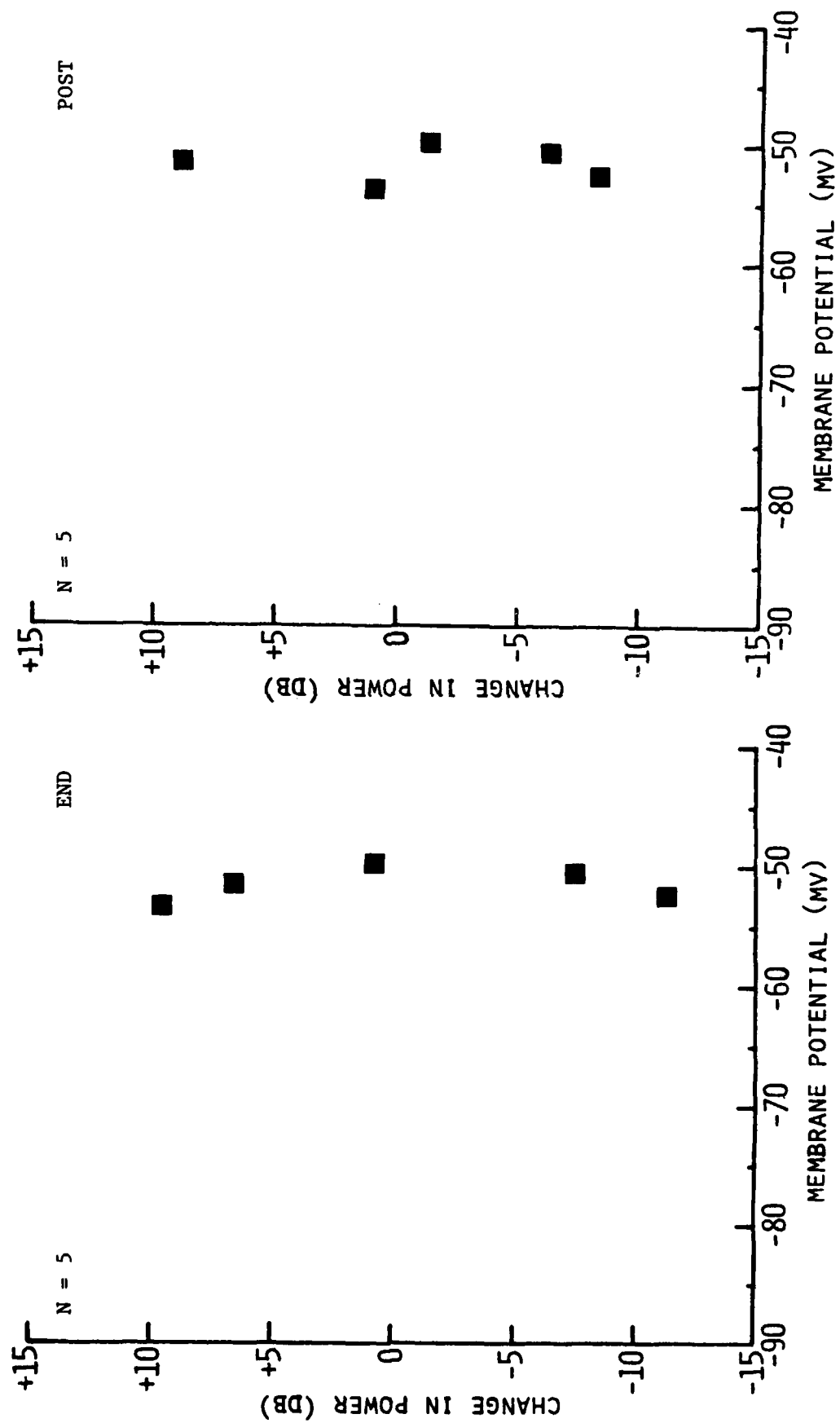
Figure 46B. CHANGE analysis of membrane voltage noise power for 2-min SHAM exposures.

Figure 47A. DIFF analysis of membrane voltage noise power for 2-min 5-15 mW/g CW (solid symbols) and PW (open symbols) RFR exposures.
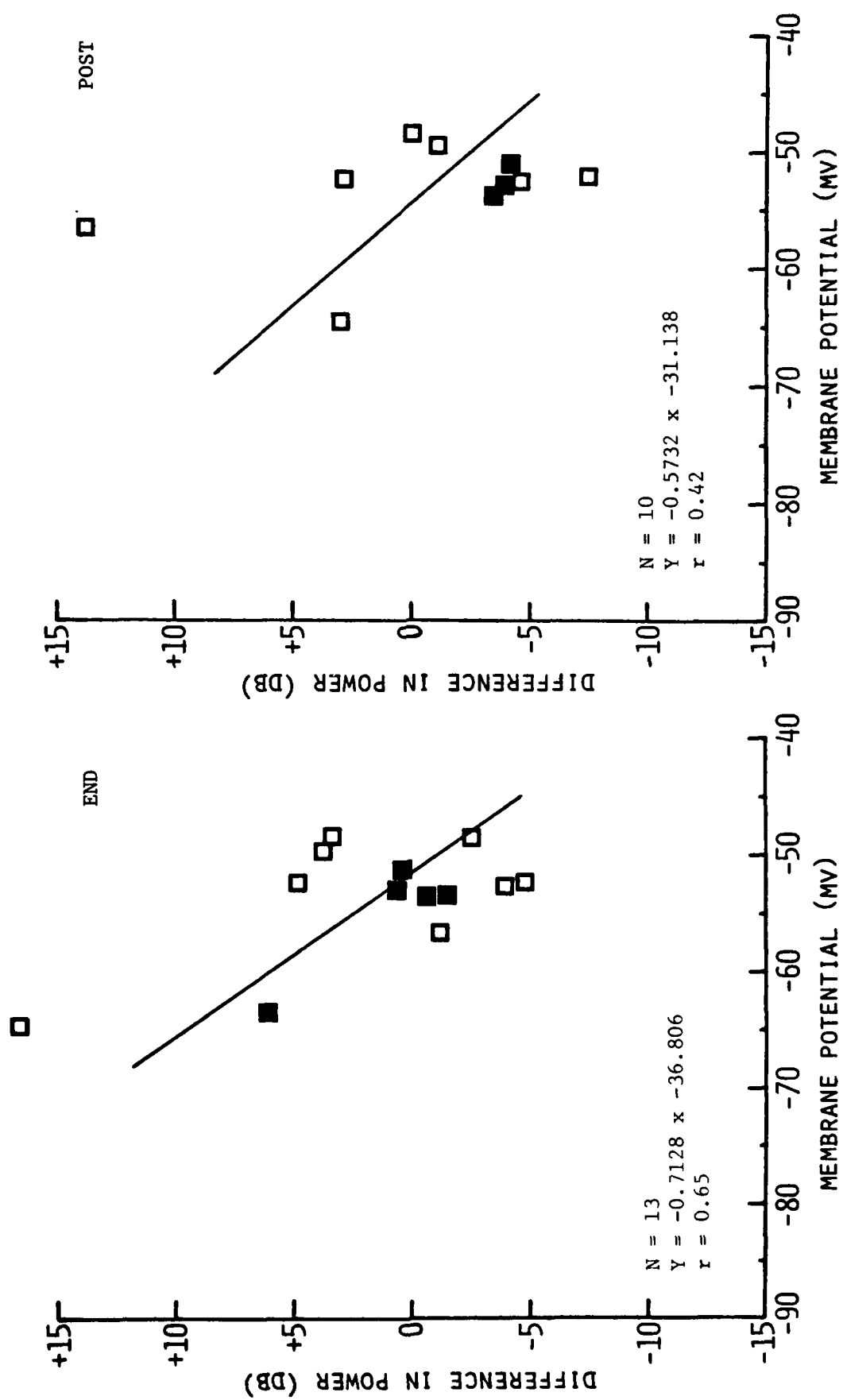
Figure 47B. DIFF analysis of membrane voltage noise power for 2-min 5-15 mW/g CW (solid symbols) and PW (open symbols) RFR exposures.
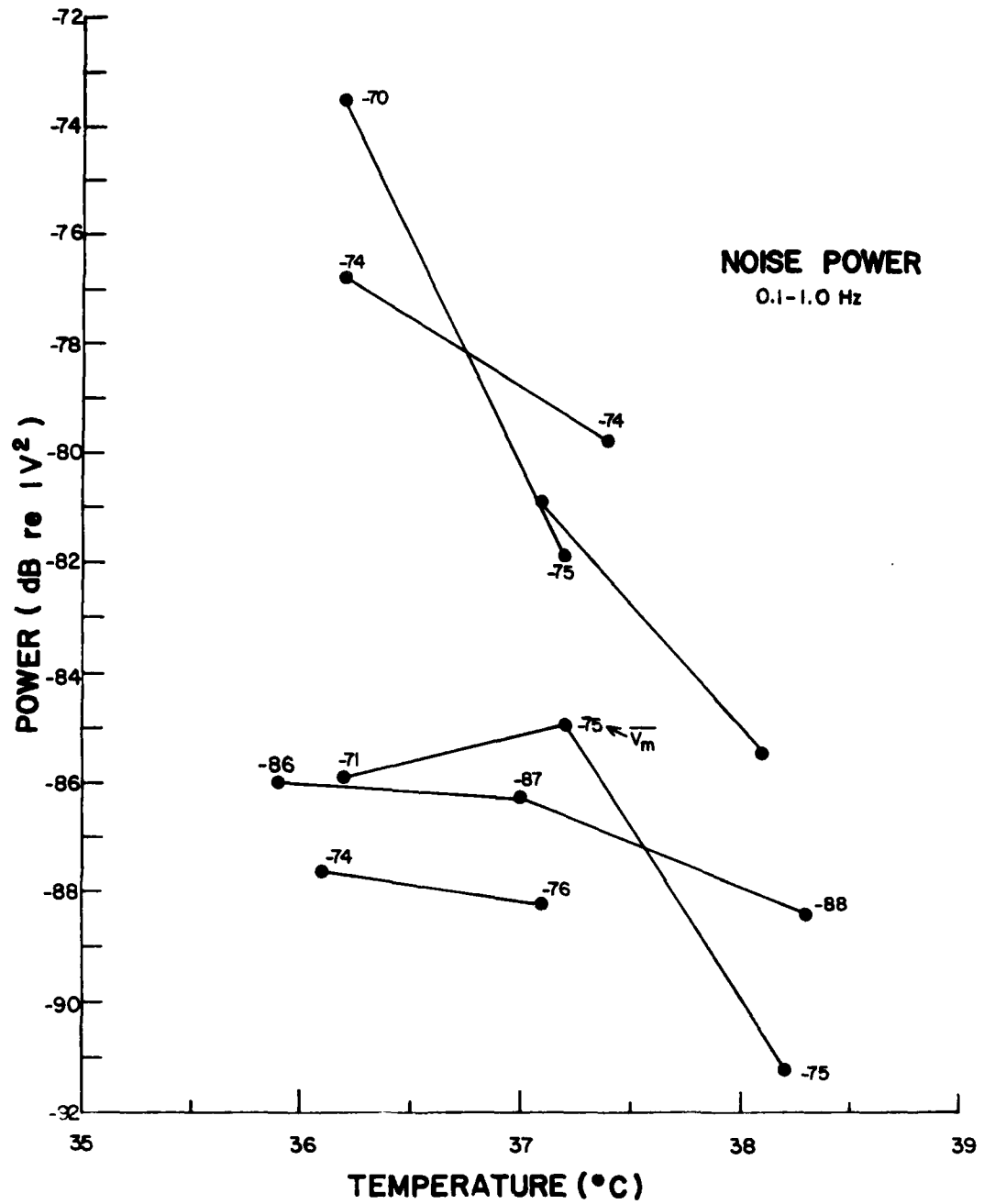
Figure 48. Membrane voltage noise power versus temperature. Lines connect data from one aggregate. Numbers by data points are average membrane potential in millivolts.

C. Microspikes

In detailed examinations of high-gain membrane potential records, transient depolarizing events occurred in random fashion without RFR. These events, termed "microspikes," had been previously described for this preparation [23,24]. Microspike amplitudes ranged from 0.2 to 8 mV, and their durations were from 0.2 s to more than 10 s. Figures 49 through 51 show examples of microspikes recorded from different aggregates. These examples were chosen to illustrate the diversity of microspike shapes; although some were taken from RFR exposures, no shape change with RFR was determined. Microspikes from an aggregate were recorded with both microelectrodes simultaneously and isopotentially, and multiple occurrences were occasionally observed (Figs. 50 and 51). Their characteristic shape included a "fast" onset of a few hundred milliseconds and a much slower return to baseline which often included an undershoot of the original testing membrane potential. Some longer microspikes seemed to be the temporal summation of shorter events. Since more or larger microspikes (or both) would cause an increase in measured membrane voltage noise, these events were investigated as a possible response to RFR exposure and a cause of the noise increases already seen.

In the first experiments to test for possible RFR effects on microspikes, large microspikes occurred within the first minute of exposure. Figure 52 shows this type of response in three different aggregates exposed to 10- to 30-mW/g CW RFR. Figure 53 shows records from another aggregate exposed to different RFR levels. Here the response was strongest for 20.9-mW/g PW; 23.4-mW/g CW and 7.9-mW/g PW were ineffective. These results were consistent with the membrane voltage noise results that indicated a noise increase during BEG of exposures in the 15- to 30-mW/g range.

To investigate microspike responses to RFR more fully, microspikes greater than 0.2 mV were counted during 1-min epochs (BEG, MID, and END) of 3-min RFR exposures. Frequencies of occurrence were determined for 1 min before RFR exposure (PRE), for each of the three 1-min epochs during exposure, and for 1 min after exposure (P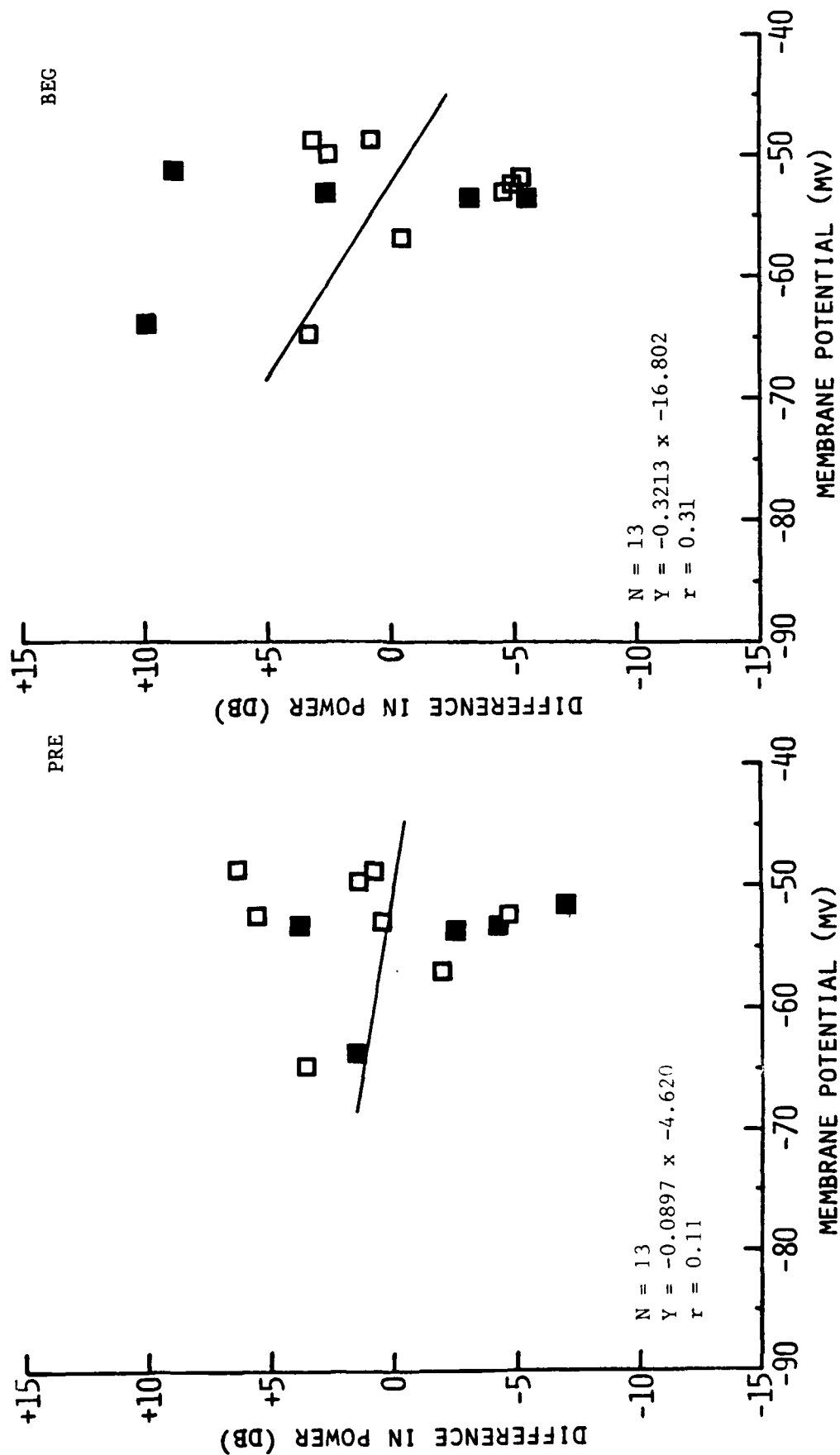OST). The data were pooled according to SAR and modulation, and then a mean frequency of occurrence and its variance for each condition were calculated. A two-tailed t-test was used for differences in means relative to the PRE mean to test these statistics. For membrane voltage noise data, differences were considered to be significant at the 0.05 level.

Figures 54 through 56 show the mean frequencies with standard error bars and the number of epochs for each data point. The only significant difference in means was between PRE and POST in pseudo SHAM. This type of SHAM was done to augment SHAM data and resulted from analysis of data in long periods without RFR exposures. No significant differences were seen in microspike frequency of occurrence with RFR exposure.

92
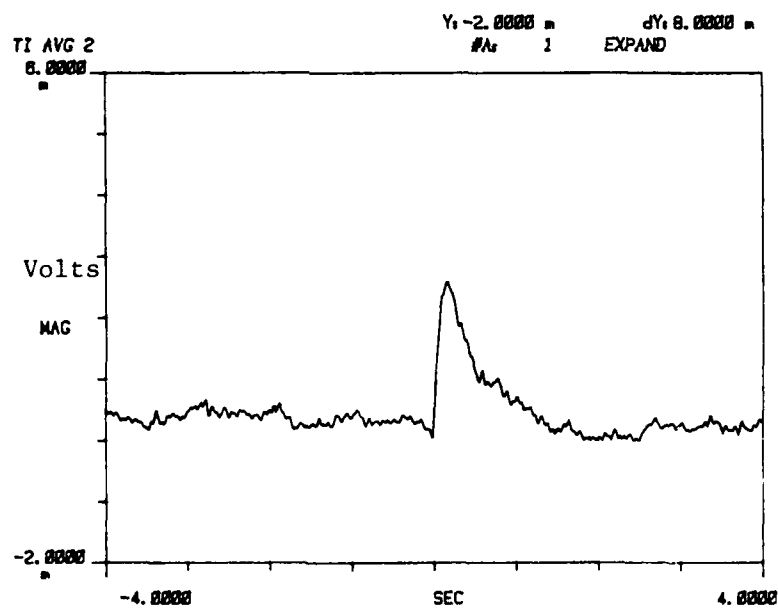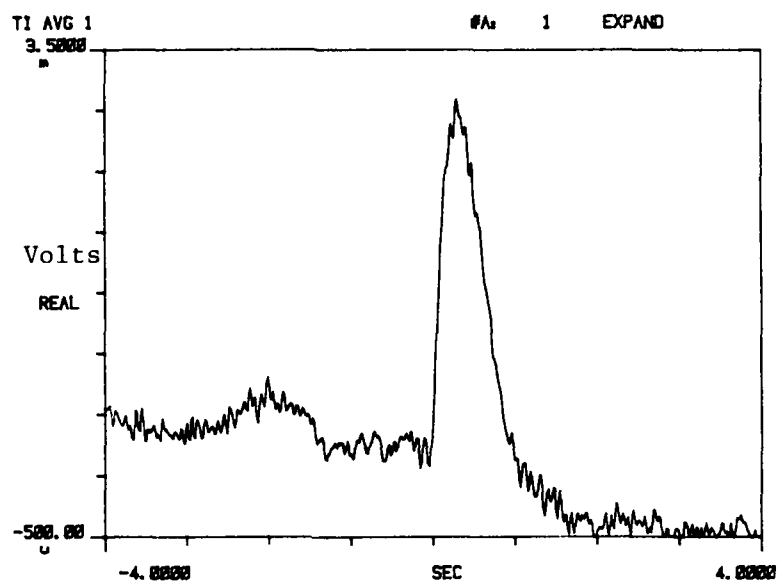
Figure 49. Microspike examples. Top: 4-mV full scale, no RFR. Bottom: 8-mV
full scale, during 21.8-mW/g CW RFR exposure. Both: 1-s time division.
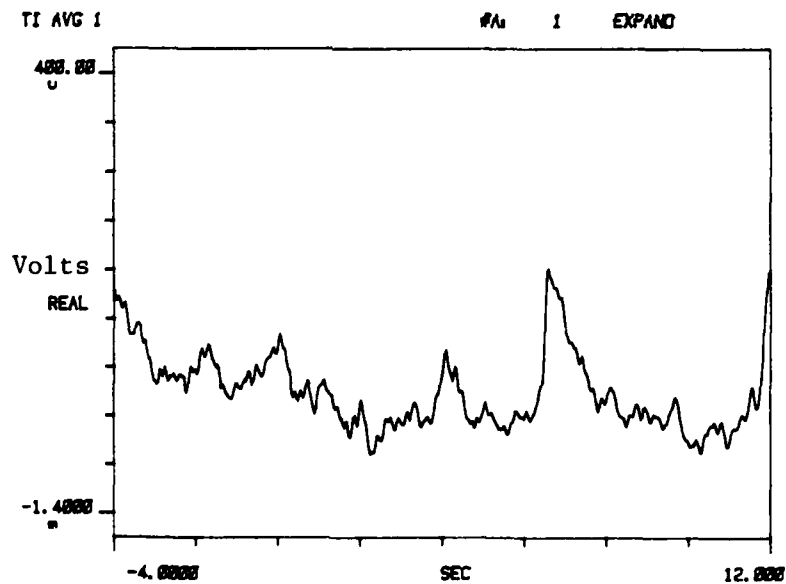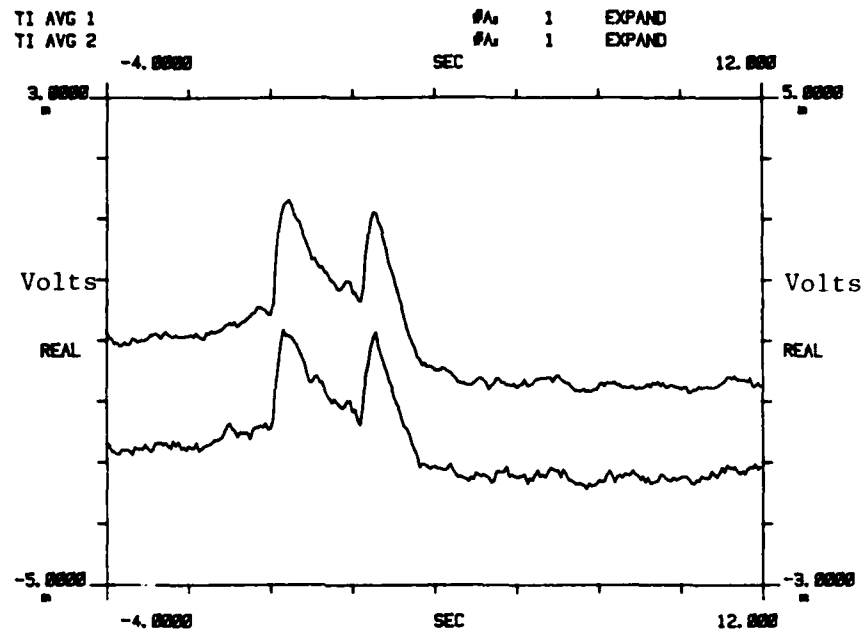
Figure 50. Microspike examples. Top: double microspike, 8-mV full scale with both microelectrode signals (offset), no RFR. Bottom: small microspikes, 2-mV full scale, no RFR. Both: 2-s time division.
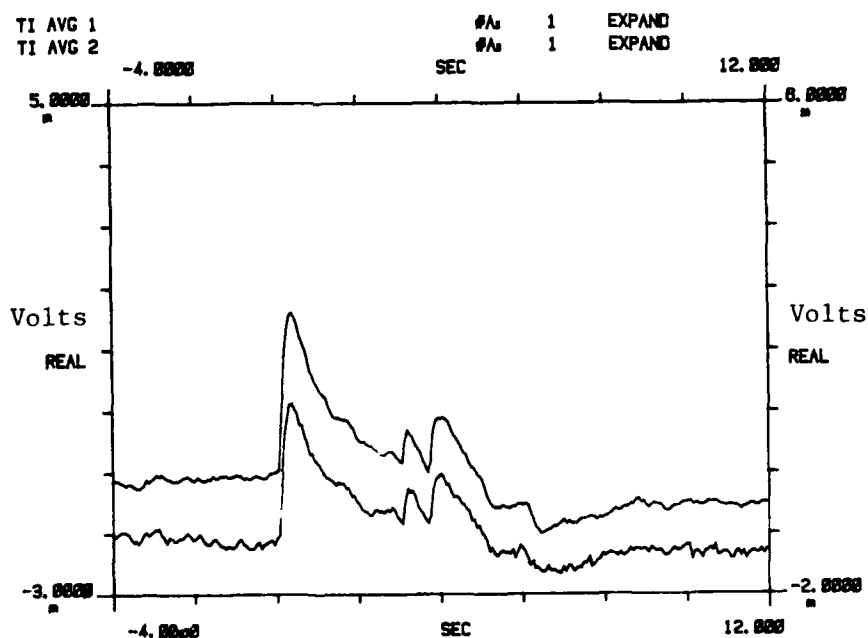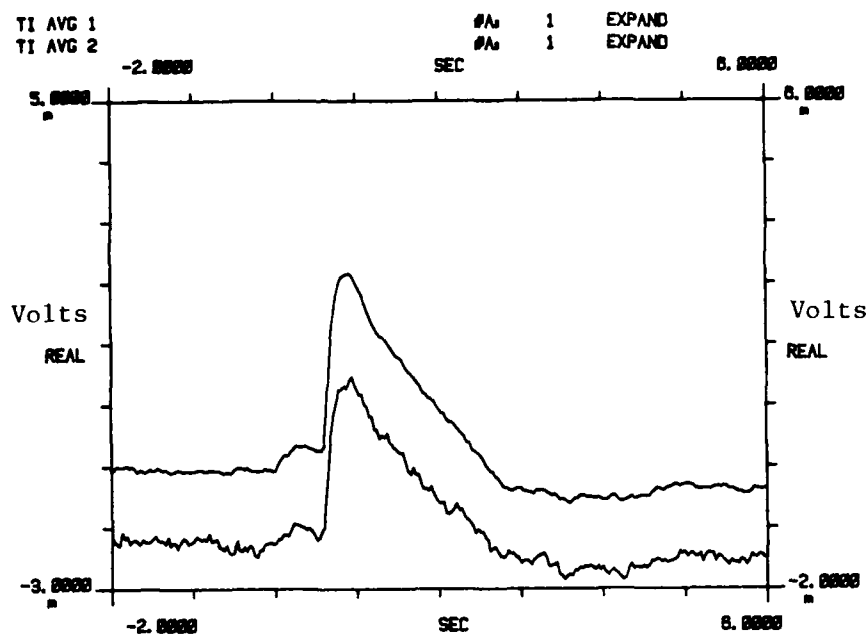
Figure 51. Microspike examples. Both: 8-mV full scale with both microelectrode signals (offset). Top: single microspike during BEG of 7.7-mW/g CW RFR exposure, 1-s time division. Bottom: multiple microspikes during END of same exposure, 2-s time division.
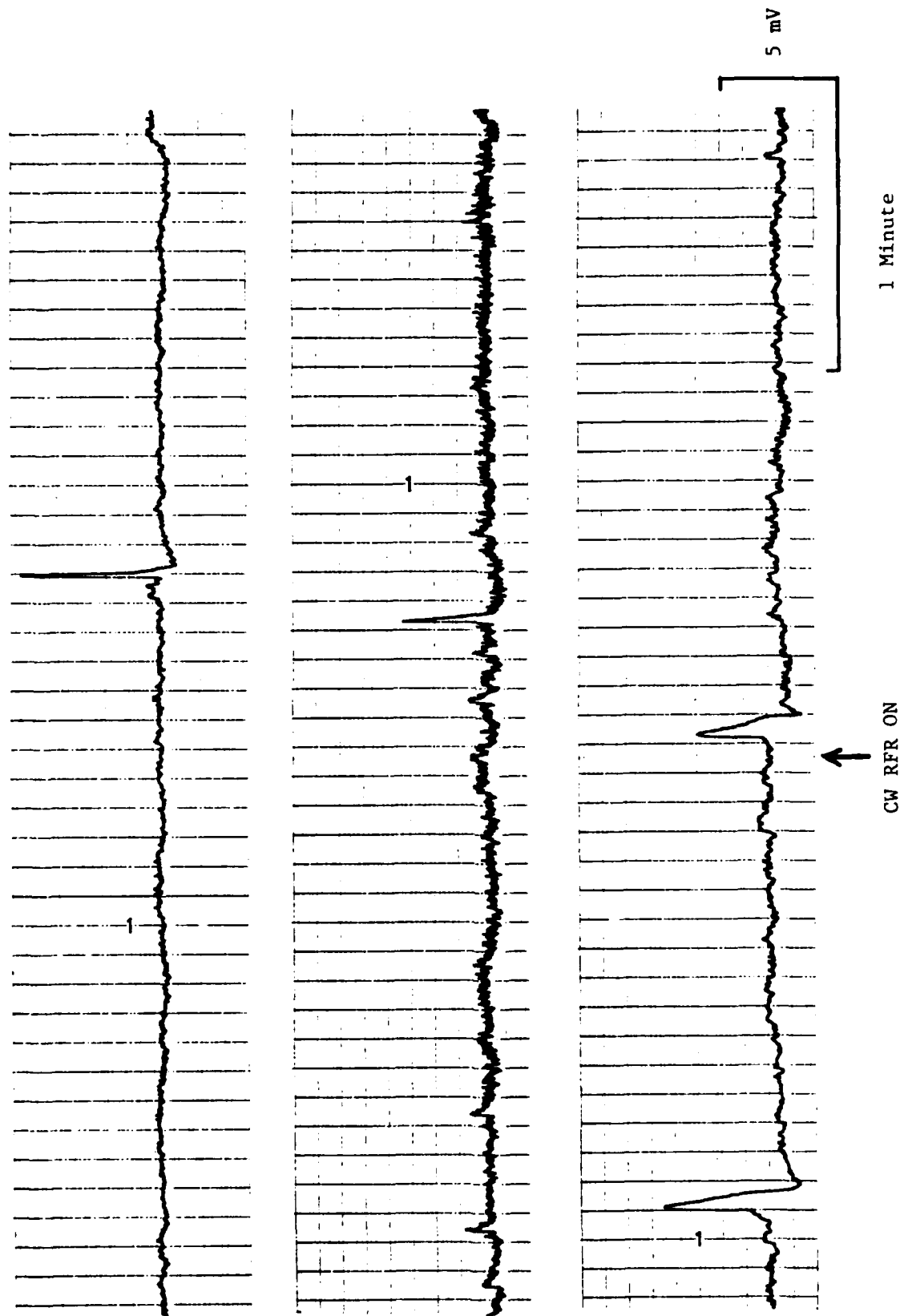
Figure 52. Microspike responses in three aggregates with different background microspike activity. CW RFR onset is indicated by the arrow. The first 133 s of 3-min exposures are shown.
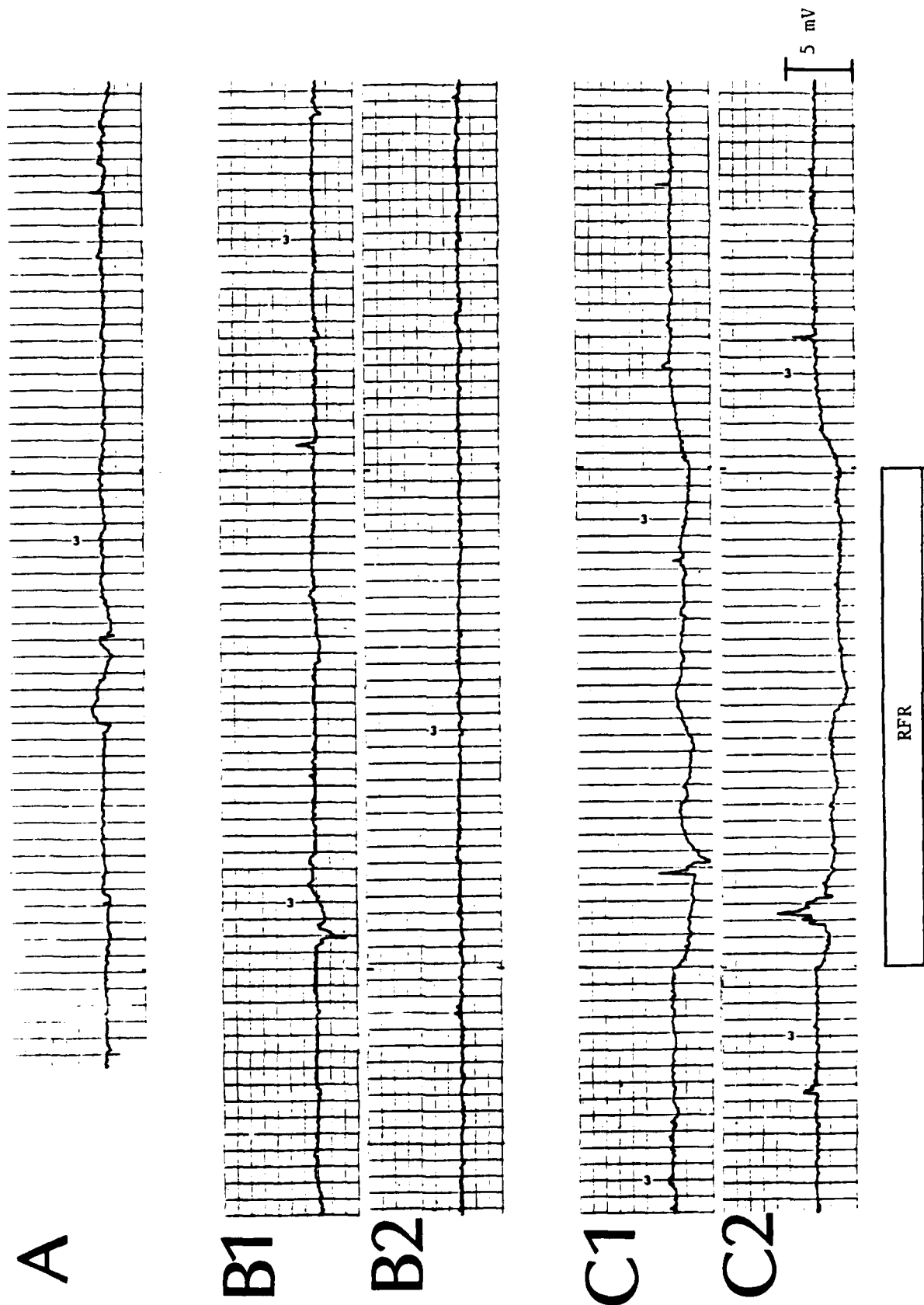
Figure 53. High-gain recordings of the membrane potential of one aggregate during successive 3-min RFR exposures to A, 23.4-mW/g CW; B, 7.9-mW/g PW; C, 20.9-mW/g PW. Pulses were 5 μs at 100 PPs. Scale bar is for all records.
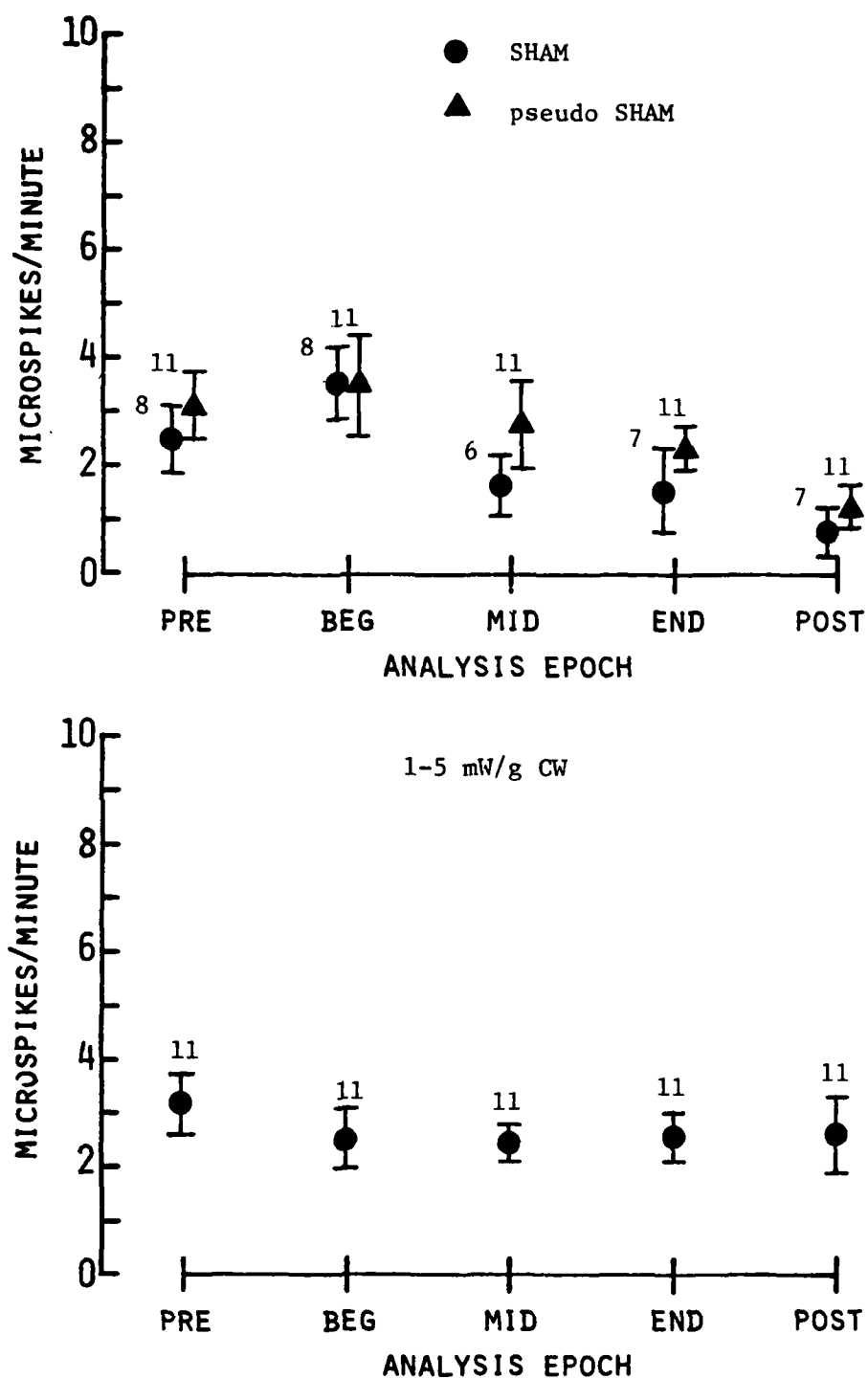
Figure 54. Microspike frequency of occurrence, SHAM and 1-5 mW/g CW. Means +/- standard errors. Number of epochs averaged is shown above each point.
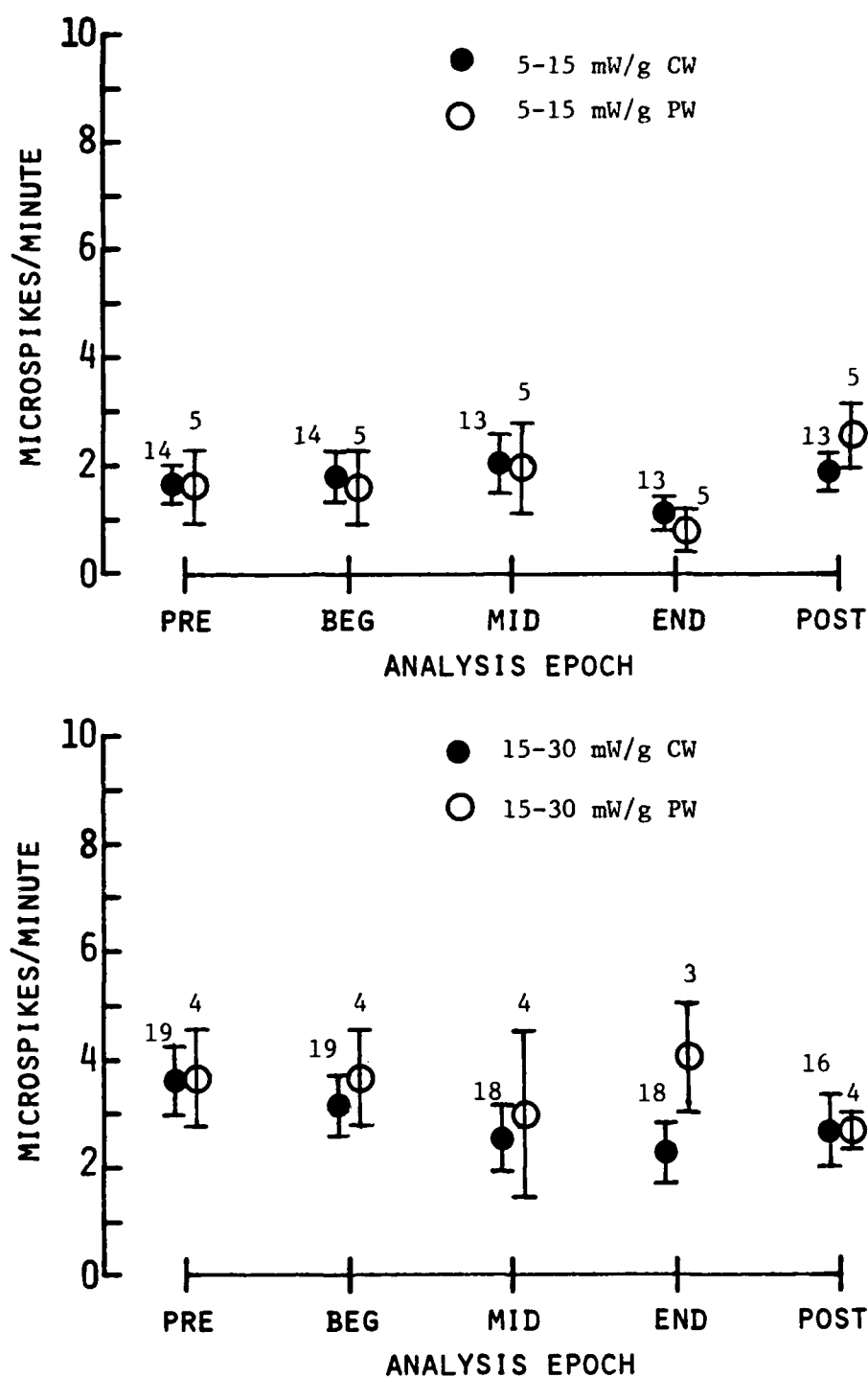
Figure 55. Microspike frequency of occurrence, 5-15 mW/g CW and PW and 15-30 mW/g CW and PW. Means +/- standard errors. Number of epochs averaged is shown above each point.
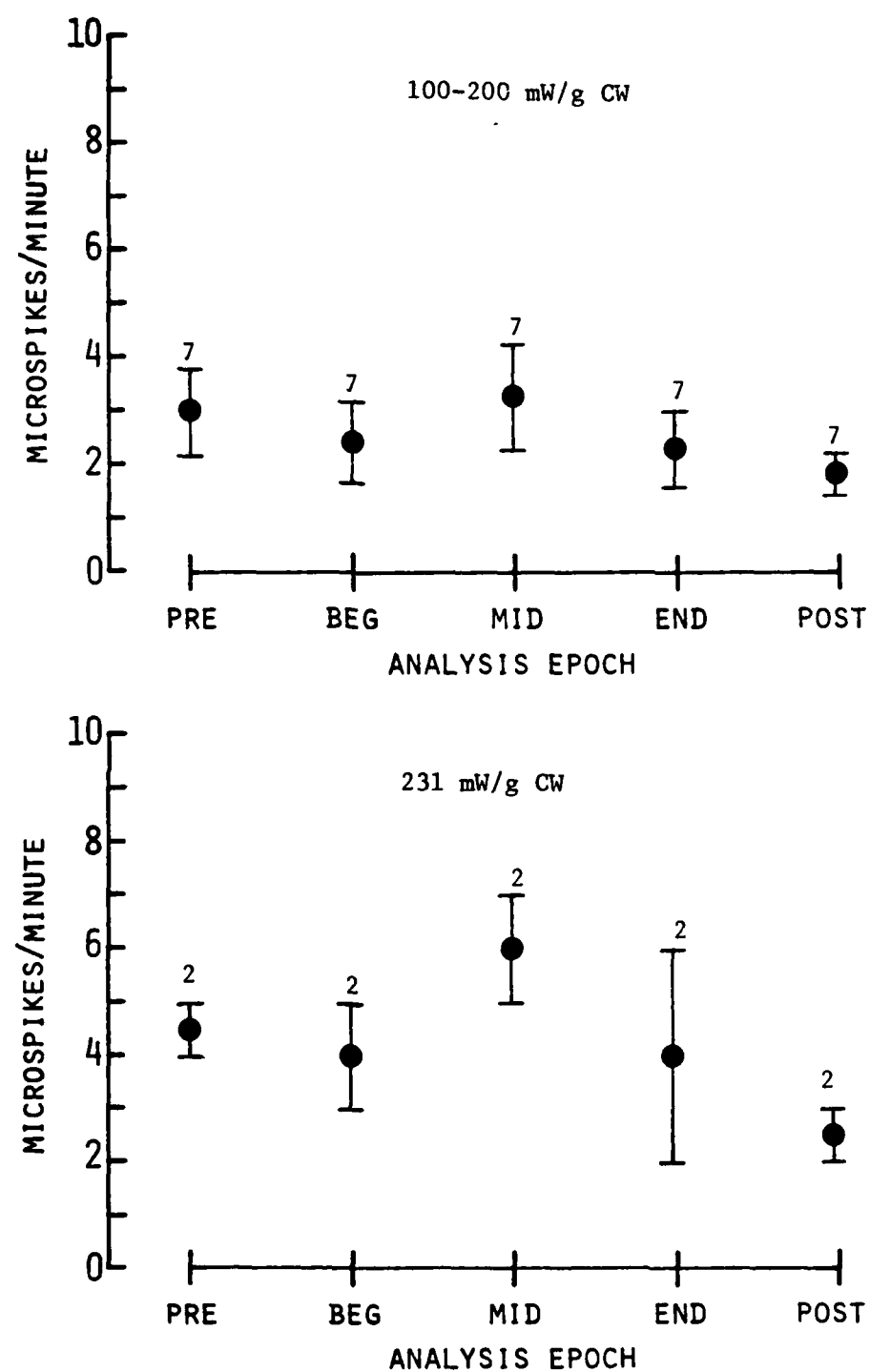
Figure 56. Microspike frequency of occurrence, 100-200 mW/g CW and
231 mW/g CW. Means +/- standard errors. Number of epochs
averaged is shown above each point.

It was surprising to find no significant difference in average microspike frequency of occurrence after the initial experiments had shown obvious microspike responses to RFR (as in Figs. 52 and 53). A millivolt microspike represented a transmembrane inward current of 1-2 nA, depending on aggregate size and experimental conditions, which was capable of modulating the normal beating of aggregates. In the analysis of aggregate beat rate reported in the previous FTR, brief beat-rate increases, called flurries, occurred [50, p. 11]. These flurries occurred with the frequency of microspikes and had the durations of the large microspikes seen more recently. Thus, it was highly likely that microspike events were responsible for the beat rate flurries. This is important because differences in mean beat rate with RFR were often discounted in the earlier work as not significant because of the large variations caused by flurries. Based on the recent microspike data with RFR, it is probably more correct to consider the occurrence of flurries as a possible RFR effect. The large coefficients of variation previously seen in beat rate with RFR SARs from 8.4 to 43.8 mW/g [50] may have been caused by the same mechanism causing microspikes. This observation may also be relevant to previous studies using frog, turtle, and rat hearts in which beat rates were observed [17,25,26,33,34,43,47,53].

Microspikes may be related to fluctuations of intracellular free calcium, as indicated by other experiments, which have been linked to membrane potential fluctuations in this [9,19] and other cardiac preparations [19,29,30,39]. In this regard, the microspikes could be used to study RFR effects on calcium exchange in cardiac cells which involves the glycoproteins and glycolipids of the cell coat [32]. A better understanding of microspike mechanisms would contribute directly to the interpretation of results obtained in such a study.

IV. CONCLUSIONS AND RECOMMENDATIONS

During this program, cardiac-cell aggregates exposed to CW and pulsed 2450-MHz RFR by an open-ended coaxial exposure device provided data on RFR effects on the excitable membranes of living cardiac tissue. Because the well-studied aggregate has representative excitable properties, this information is applicable not only to cardiac cells but also to other excitable cells exposed to similar RFR levels. In this section, conclusions based on the results are given and recommendations are made for further research.

Data were obtained for 2- and 3-min RFR exposures, so results pertain directly to exposures of these acute durations. No effect on membrane resistance and capacitance was observed for exposures to CW RFR from 2 to 142 mW/g. Significant differences in the relation of membrane voltage noise to membrane potential occurred for the following RFR conditions:

1. beginning of 1-5 mW/g CW 3-min exposures

2. beginning of 15-30 mW/g CW 3-min exposures

3. beginning of 15-30 mW/g combined CW and PW 3-min exposures

4. beginning of 15-30 mW/g PW 3-min exposures.

All significant differences were for the beginning analysis epoch (first 1 to 1.5 min) of exposure and most occurred for the 15- to 30-mW/g SAR range. As explained in Section III.B., the 2-min PW and 3-min CW effects were opposite in direction, indicating a possible difference in interaction of the pulsed RFR (5 μs at 100 pps) and CW RFR. Although the initial experiments indicated an RFR effect on the occurrence of microspike potentials, SARs from 1 to 200 mW/g showed no significant differences when results were averaged across experiments.

The following recommendations for further research are based on the experiences with RFR exposure of cardiac-cell aggregates in this program and on the conclusions reached from the results of several experiments:

o   Investigate RFR effects on membrane noise for SARs of 30 mW/g and smaller. This will define the smallest SAR effective in causing changes in noise. These studies should be done using voltage clamp techniques to remove membrane potential as an uncontrolled variable.

o   Conduct experiments with RFR exposures lasting for many minutes (an hour or more). This will provide information on effects of chronic long-term exposure on cardiac cell membranes. Long-term effects have already been reported for frog sciatic nerve [37], snail neurons [2], and plant cells [7].

o   Use microspikes and other membrane properties to study the RFR effects on calcium transport systems in cardiac cells.

V. REFERENCES

1. Adey, W. R. Tissue interactions with nonionizing electromagnetic fields. Physiol Rev 61:435-514 (1981).

2. Arber, S. L. The effects of microwave radiation on passive membrane properties of snail neurons. J Microwave Power 16:15-20 (1981).

3. Baranski, S., and P. Czerski. Biological effects of microwaves. Stroudsburg, Pa.: Dowden, Hutchinson and Ross, 1976.

4. Barnes, F. S., and C. L. Hu. Model for some nonthermal effects of radio and microwave fields on biological membranes. IEEE Trans Microwave Theory Tech MTT-25:742-746 (1977).

5. Barsoum, Y. H., and W. F. Pickard. Radio-frequency rectification in electrogenic and nonelectrogenic cells of Chara and Nitella. J Membrane Biol 65:81-87 (1982).

6. Barsoum, Y. H., and W. F. Pickard. Effects of electromagnetic radiation in the range 20-300 MHz on the vacuolar potential of Characean cells. Bioelectromagnetics 3:193-201 (1982).

7. Barsoum, Y. H., and W. F. Pickard. The vacuolar potential of Characean cells subjected to electromagnetic radiation in the range 200-8,000 MHz. Bioelectromagnetics 3:393-400 (1982).

8. Berkowitz, G. C., and F. S. Barnes. The effects of nonlinear membrane capacity on the interaction of microwave and radio frequencies with biological materials. IEEE Trans Microwave Theory Tech MTT-27:204-207 (1979).

9. Bhattacharyya, M. L., R. D. Nathan, and V. L. Shelton. Release of sialic acid alters the stability of the membrane potential in cardiac muscle. Life Sci 29:1071-1078 (1981).

10. Birenbaum, L., I. T. Kaplan, W. Metlay, S. R. Rosenthal, and M. M. Zaret. Microwave and infra-red effects on heart rate, respiration rate and subcutaneous temperature of the rabbit. J Microwave Power 10:3-18 (1975).

11. Brown, P.V.K., and L.E. Larsen. Differing effects of pulsed and CW microwave energy upon nerve function as detected by birefringence measurement. IEEE Trans Microwave Theory Tech MTT-28:1126-1133 (1980).

12. Burdette, E. C., R. L. Seaman, and D. L. DeHaan. Investigation of radiofrequency radiation effects on excitable tissues. Annual Tech Rep No. 1. Contract F49620-79-C-0055, Georgia Tech Project A-2335, July 1981.

13. Cain, C. A. A theoretical basis for microwave and RF field effects on excitable cellular membranes. IEEE Trans Microwave Theory Tech MTT-28:142-147 (1980).

14. Chou, C. K., L. F. Han, and A. W. Guy. Microwave radiation and heartbeat rate of rabbits. J Microwave Power 15:87-93 (1980).

15. Chou, C. K., and A. W. Guy. Effects of electromagnetic fields on isolated nerve and muscle preparations. IEEE Trans Microwave Theory Tech MTT-26:141-147 (1978).

16. Clapham, D. E., A. Shrier, and R. L. DeHaan. Junctional resistance ʰd action potential delay between embryonic heart cell aggregates J Gen Physiol 75:633-654 (1980).

17. Clapman, R. M., and C. A. Cain. Absence of heart-rate effects in isc ed frog heart irradiated with pulse modulated microwave energ, Microwave Power 10(4):411-419 (1975).

18. Clay, J. R., L. J. DeFelice, and R. L. DeHaan. Current noise parameters derived from voltage noise and impedance in embryonic heart cell aggregates. Biophys J 28:169-184 (1979).

19. Clusin, W. T., M. R. Bristow, H. S. Karagueuzian, B. G. Katzung, and J. S. Schroeder. Do calcium-dependent ionic currents mediate ischemic ventricular fibrillation? Am J Cardiol 49:606-612 (1982).

20. Courtney, K. R., J. C. Lin, A. W. Guy, and C. K. Chou. Microwave effect on rabbit superior cervical ganglion. IEEE Trans Microwave Theory Tech MTT-23:809-813 (1975).

21. DeFelice L. J., and R. L. DeHaan. Membrane noise and intercellular communication. Proc IEEE 65:796-799 (1977).

22. DeFelice, L. J. Introduction to membrane noise. New York: Plenum Press, 1981.

23. DeHann, R. L., and L. J. DeFelice. Electrical noise and rhythmic properties of embryonic heart cell aggregates. Fed Proc 37:2132-2138 (1978).

24. DeHaan, R. L., and L. J. DeFelice. Oscillatory properties and excitability of the heart cell membrane. Theoretical chemistry, Vol. 4, pp. 181-233. New York: Academic Press, 1978.

25. Frey, A. H, and E. Seifert. Pulse modulated UHF energy illumination of the heart associated with change in heart rate. Life Sci, Part I, 7:505-512 (1968).

26. Galvin, M. J., M. S. Dutton, and D. I. McRee. Influence of 2.45-GHz CW microwave radiation on spontaneously beating rat atria. Bioelectromagnetics 3:219-226 (1982).

27. Kamenskii, Yu. I. Effect of microwaves on the functional state of the nerve. Biophysics 9:758-764 (1964).

28. Kaplan, I. T., W. Metlay, M. M. Zaret, L. Birenbaum, and S. W. Rosenthal. Absence of heart-rate effects in rabbits during low-level microwave irradiation. IEEE Trans Microwave Theory Tech MTT-19:168-173 (1971).

29. Karagueuzian, H. S., and B. G. Katzung. Voltage clamp studies of transient inward current and mechanical oscillations induced by ouabain in ferret papillary muscle. J Physiol (Lond) 327:255-271 (1982).

30. Kass, S. R., and R. W. Tsien. Fluctuations in membrane current driven by intracellular calcium in cardiac Purkinje fibers. Biophys J 38:259-269 (1982).

31. Kleinbaum, D. G., and L. L. Kupper. Applied regression analysis and other multivariable methods. North Scituate, Mass.: Duxbury Press, 1978.

32. Langer, G. A., J. S. Frank, L. M. Nudd, and K. Seraydarian. Sialic acid: Effect of removal of calcium exchange on cultured heart cells. Science 193:1013-1015 (1976).

33. Liu, L. M., F. J. Rosenbaum, and W. F. Pickard. The insensitivity of frog heart rate to pulse modulated microwave energy. J Microwave Power 11(3):225-232 (1976).

34. Lords, J. L., C. H. Durney, A. M. Borg, and C. E. Tinnery. Rate effects in isolated hearts induced by microwave irradiation. IEEE Trans Microwave Theory Tech MTT-21:834-836 (1973).

35. MacGregor, R. J. A possible mechanism for the influence of electromagnetic radiation on neuroelectric potentials. IEEE Trans Microwave Theory Tech MTT-27:914-921 (1979).

36. McDonald, T. F., H. G. Sachs, and R. L. DeHaan. Development of sensitivity to tetrodotoxin in beating chick embryo hearts, single cell and aggregates. Science 176:1248-1250 (1972).

37. McRee, D. I., and H. Wachtel. The effects of microwave radiation on the vitality of isolated frog sciatic nerves. Radiat Res 82:536-546 (1980).

38. McRee, D. I., and H. Wachtel. Elimination of microwave effects on the vitality of nerves after active transport has been blocked. Bioelectromagnetics Society First Annual Meeting, Seattle, Washington, 1979.

39. Matsuda, H., A. Noma, Y. Kurachi, and M. Irisawa. Transient depolarization and spontaneous voltage fluctuations in isolated cells from guinea pig ventricles. Circ Res 51:142-151 (1982).

40. Myers, R. D., and D. H. Ross. Radiation and brain calcium: A review and critique. Neurosc Biobehav Rev 5:503-543 (1981).

41. Nathan, R. D., and R. L. DeHaan. In-vitro differentiation of a fast Na^+ conductance in embryonic heart cell aggregates. Proc Natl Acad Sci 75:2776-2780 (1978).

42. Nathan, R. D., and R. L. DeHaan. Voltage clamp analysis of embryonic heart cell aggregates. J Gen Physiol 73:175-198 (1979).

43. Olsen, R. G., J. L. Lords, and C. H. Durney. Microwave-induced chronotropic effects in the isolated rat heart. Ann Biomed Eng 5:395-409 (1977).

44. Pickard, W. F., and Y. H. Barsoum. Radio-frequency bioeffects at the membrane level: Separation of thermal and athermal contributions in the characeae. J Membrane Biol 61:39-54 (1981).

45. Pickard, W. F., and R. J. Rosenbaum. Biological effects of microwaves at the membrane level: Two possible athermal electrophysiological mechanisms and a proposed experimental test. Math Biosci 39:235-253 (1978).

46. Pressman, A. S. Electromagnetic fields and life. New York: Plenum Press, 1970.

47. Reed, J. R., J. L. Lords, and C. H. Durney. Microwave irradiation of the isolated rat heart after treatment with ANS blocking agents. Radio Sci 12(6S):161-165 (1977).

48. Sachs, H. G., and R. L. DeHaan. Embryonic myocardial cell aggregates: volume and pulsation rate. Dev Biol 30:233-240 (1973).

49. Seaman, R. L., and H. Wachtel. Slow and rapid responses to CW and pulsed microwave radiation by individual Aplysia pacemakers. J Microwave Power 13(1):77-86 (1978).

50. Seaman, R. L., E. C. Burdette, and R. L. DeHaan. Investigation of radio-frequency radiation effects on excitable tissues. Final Tech Rep, Contract F49620-79-C-0055, Georgia Tech Project A-2335, July 1981.

51. Spiegel, R. J., and W. T. Joines. A semiclassical theory for nerve excitation by a low intensity electromagnetic field. Bull Math Biol 35:591-605 (1973).

52. Studwell, M. L., and C. C. Davis. Energy absorption for small radiating coaxial probes in lossy media. IEEE Trans Microwave Theory Tech MTT-29:1198-1205 (1981).

53. Tinney, C. E., J. L. Lords, and C. H. Durney. Rate effects in isolated turtle hearts induced by microwave radiation. IEEE Trans Microwave Theory Tech MTT-24:1-18 (1976).

54. Wachtel, H., R. Seaman, and W. Joines. Effects of low-intensity microwaves on isolated neurons. Ann NY Acad Sci 247:46-61 (1975).

55.   Williams, E. H., and R. L. DeHaan. Electrical coupling among heart cells
       in the absence of ultrastructurally defined gap junctions. J Membrane
       Biol 60:237-248 (1981).

56.   Ypey, D. L., D. E. Clapham, and R. L. DeHaan. Development of electrical
       coupling and action potential synchrony between paired aggregates of
       embryonic heart cells. Membrane Biol 51:75-96 (1979).

VI. LIST OF SYMBOLS AND ABBREVIATIONS

BEG
95-s analysis epoch at beginning of 3-min RFR exposure
60-s analysis epoch at beginning of 2-min RFR exposure

CHANGE
analysis of membrane voltage noise in which PRE power was subtracted from powers of subsequent analysis epochs of an exposure

CW
continuous wave

df
degrees of freedom in statistical tests

DIFF
analysis of membrane voltage noise in which averaged noise power from SHAM exposures for an aggregate was subtracted from RFR analysis epochs

END
95-s analysis epoch at end of 3-min RFR exposure
60-s analysis epoch at end of 2-min RFR exposure

IBI
interbeat interval in milliseconds

PW
pulsed (wave) modulation

POST
95-s analysis epoch after 3-min RFR exposure
60-s analysis epoch after 2-min RFR exposure

POSTPOST
second 95-s analysis epoch after 3-min RFR exposure
second 60-s analysis epoch after 2-min RFR exposure

PRE
95-s analysis epoch prior to 3-min RFR exposure
60-s analysis epoch prior to 2-min RFR exposure

Pseudo
SHAM
control exposure during which RFR generator was not energized

r
Pearson's correlation coefficient

RFR
radiofrequency radiation

SAR
specific absorption rate in mW/g

SHAM
control exposure during which RFR generator was energized but output level was zero

t
test statistic used for sample size less than 25

z
test statistic used for sample size greater than 25

μm
micrometer $= 10^{-6}$ meter